Power Management for Microbial Fuel Cells

Nicolas Degrenne

N° d'ordre : 2012-32 Année 2012

THÈSE

présentée devant

l'Ecole Centrale de Lyon

pour obtenir le grade de

Docteur

dans le cadre de

L'école doctorale Électronique Électrotechnique Automatique

par

Nicolas DEGRENNE
Ingénieur INSA

Gestion de l'énergie des piles à combustible microbiennes

Soutenue devant la commission d'examen

le 18 Octobre 2012

Membres du jury :

Ioannis Ieropoulos, Professeur (Bristol Robotics Laboratory)
Sven Kerzenmacher, Docteur (IMTEK)
Yves Lembeye, Professeur (G2Elab)
Paolo Pavan, Professeur (Unimore)
Bruno Allard, Professeur (INSA de Lyon) - Encadrant de thèse
François Buret, Professeur (Ecole Centrale de Lyon) - Directeur de thèse

Thèse ministérielle préparée dans les départements bioingénierie et énergie électrique du laboratoire Ampère de Lyon
UMR CNRS 5005, 36 avenue Guy de Collongue, 69130 Ecully, France

Résumé

Les Piles à Combustible Microbiennes (PCMs) mettent en oeuvre le métabolisme de micro-organismes et utilisent de la matière organique pour générer de l'énergie électrique. Les applications potentielles incluent le traitement d'eau usée autonome en énergie, les bio-batteries, et le grappillage d'énergie ambiante. Les PCMs sont des équipements basse-tension et basse-puissance dont le comportement est influencé par la vitesse à laquelle l'énergie électrique est récupérée. Dans cette thèse, on étudie des méthodes pour récupérer l'énergie électrique de façon efficace.

La tension à laquelle l'énergie est récupérée des PCMs influence leur fonctionnement et leurs performances électriques. La puissance délivrée est maximum pour une tension spécifique (environ 1/3 de la tension en circuit-ouvert). Les PCMs ont été testées à ce point en utilisant une charge contrôlée automatiquement qui inclut un algorithme de recherche de puissance maximale. Un tel outil a été utilisé pour évaluer la puissance maximum, la vitesse de consommation du combustible, le rendement Coulombic et le rendement de conversion de 10 PCMs à chambre unique de 1.3 L, construites de façon similaire. Bien que d'autres choix structurels et opératoires peuvent permettre d'améliorer ces performances, ces résultats ont étudié pour la première fois les performances des PCMs en condition de production d'énergie de point de puissance maximal et les PCMs ont été testées avec des conditions de récupération d'énergie réalistes.

Récupérer un maximum d'énergie des PCMs est la ligne directrice de ce rapport. Cela est rendu possible par des circuits dédiés de gestion de l'énergie qui embarquent un contrôle contre-réactif pour réguler la tension des PCMs à une valeur de référence qui est égale à une fraction de leur tension en circuit ouvert. Deux scénarios typiques sont développés dans la suite.

Une application critique des PCMs concerne le grappillage autonome de petites énergies, pour alimenter des équipements électroniques basse-puissance (e.g. capteurs sans fil). Dans ce cas, les contraintes basse-puissance et basse-tension imposées par les PCMs nécessitent des fonctionnalités de démarrage autonomes. L'oscillateur d'Armstrong, composé d'inductances couplées à fort rapport d'enroulement et d'un interrupteur normalement-fermé permet d'élever des tensions de façon autonome à partir de sources basse-tension continues comme les PCMs. Ce circuit a été associé à des convertisseurs d'électronique de puissance AC/DC et DC/DC pour réaliser respectivement un élévateur-de-tension et une unité de gestion de l'énergie (UGE) auto-démarrante basée sur une architecture flyback. La première est adaptée pour les puissances inférieures à 1 mW, alors que la seconde peut être dimensionnée pour des niveaux de puissance de quelques mW et permet de mettre en oeuvre une commande qui recherche le point de puissance maximal du générateur.

Une seconde application d'intérêt concerne le cas où de l'énergie est récupérée depuis plusieurs PCMs. L'association série peut être utilisée pour élever la tension de sortie mais elle peut avoir des conséquences négatives en terme de performances à cause des non-uniformités entre cellules. Cet aspect peut être résolu avec des circuits d'équilibrage de tension. Trois de ces circuits ont été analysés et évalués.

Le circuit “complete disconnection” déconnecte une cellule défectueuse de l’association pour s’assurer qu’elle ne diminue pas le rendement global. Le circuit “switched-capacitor” transfère de l’énergie depuis les MFCs fortes vers les faibles pour équilibrer les tensions de toutes les cellules de l’association. Le circuit “switched-MFCs” connecte les PCMs en parallèle et en série de façon alternée. Chacune des trois méthodes peut être mise en oeuvre à bas prix et à haut rendement, la plus efficace étant la “switched-capacitor” qui permet de récupérer plus de 85 % de la puissance maximum idéale d’une association très largement non uniforme.

Mots clés : Piles à combustible microbiennes ; récupération d’énergie ; gestion de l’énergie ; convertisseur DC/DC ; équilibrage de tension.

Abstract

Microbial fuel cells (MFCs) harness the metabolism of micro-organisms and utilize organic matter to generate electrical energy. They are interesting because they accept a wide range of organic matter as a fuel. Potential applications include autonomous wastewater treatment, bio-batteries, and ambient energy scavenging. MFCs are low-voltage, low-power devices that are influenced by the rate at which electrical energy is harvested at their output. In this thesis, we study methods to harvest electrical energy efficiently.

The voltage at which energy is harvested from MFCs influences their operation and electrical performance. The output power is maximum for a certain voltage value (approx. $1/3^{rd}$ the open-circuit voltage). This noteworthy operating point is favorable in some applications where MFCs are used as a power supply. MFCs can be tested at this point using an automatic load adjuster which includes a maximum power point tracking algorithm. Such a tool was used to evaluate the maximum power, the fuel consumption rate, the Coulombic efficiency and the energy conversion efficiency of ten similarly built 1.3 L single-chamber MFCs. Although structural and operating condition choices will lead to improved performance, these results investigate for the first time the performance of MFCs in continuous maximum power point condition and characterize MFCs in realistic energy harvesting conditions.

Harvesting energy at maximum power point is the main thread of the manuscript. This is made possible with dedicated energy processing circuits embedding control feedback to regulate the MFC voltage to a fraction of its open-circuit voltage. Two typical scenarios are developed as outlined below.

One critical application concerns autonomous low-power energy scavenging, to supply remote low-power electronic devices (e.g. wireless sensors). In this case, the low-power and low-voltage constraints imposed by MFCs require dedicated self start-up features. The Armstrong oscillator, composed of high turn-ratio coupled inductors and of a normally-on switch, permits to autonomously step-up voltages from a low DC source like MFCs. Although the circuit requires few components, its operation is not trivial because it partly relies on the parasitic elements of the inductors and the switch. Proper sizing of the inductors enables an optimized operation. This circuit can be associated with power electronic AC/DC and DC/DC converters to realize a voltage-lifter and a flyback-based self-starting Power Management Unit (PMU) respectively. The former is suitable for powering levels below 1 mW, while the latter can be scaled for power levels of a few units of mW and facilitates implementation of maximum power point control.

A second application of interest concerns the case where energy is harvested from several MFCs. Serial association can be used to step-up voltage but may lead to detrimental consequences in terms of performances because of hydraulic couplings between MFCs sharing the same electrolyte (e.g. if the MFCs are running in continuous flow) or because of electrical non-uniformities between cells. Whereas the former issue can be addressed with galvanically insulated PMUs, the latter can be solved with voltage balancing circuits. Three of these latter circuits were analyzed and evaluated. The "complete disconnection" circuit isolates a faulty cell from the configuration to ensure it does not impede the overall efficiency.

The “switched-capacitor” circuit transfers energy from the strong to the weak MFCs to equilibrate the voltages of the individual cells in the stack. The “switched-MFC” circuit alternatively connects MFCs in parallel and in series. Each of the three methods can be implemented at low-cost and at high efficiency, the most efficient one being the “switched-capacitor”, that permits to harvest more that 85 % of the ideal maximum energy of a strongly-non-uniform MFC association.

Keywords: Microbial fuel cell; energy harvesting; power management; DC/DC converter; voltage balancing.

Contents

Résumé i

Abstract iii

List of acronyms and symbols x

1 Introduction 1

1.1 Microbial fuel cells use biomass to generate electricity . . . 1

1.1.1 Biomass to electricity conversion pathways . . . 1

1.1.2 Biofuel cells . . . 2

1.1.3 Researches on MFCs . . . 3

1.2 Applications of Microbial fuel cells as energy generators . . . 4

1.2.1 Energy-autonomous wastewater treatment . . . 4

1.2.1.1 Wastewater treatment . . . 4

1.2.1.2 Advantages of MFCs . . . 5

1.2.1.3 Power management strategies . . . 5

1.2.2 Bio-batteries . . . 6

1.2.2.1 The need to develop environmentally-friendly batteries . . . 6

1.2.2.2 Advantages of MFCs . . . 6

1.2.2.3 Power management strategies . . . 6

1.2.3 MFC-based ambient energy scavenging . . . 7

1.2.3.1 Ambient energy scavenging . . . 7

1.2.3.2 Advantages of MFCs . . . 7

1.2.3.3 Electrical energy harvesting strategies . . . 7

1.3 Power management for MFCs . . . 8

1.3.1 Power management unit for one MFC . . . 9

1.3.2 Power management unit for a large number of MFCs . . . 9

1.4 Scope of the thesis . . . 9

1.4.1 Getting to know MFCs better . . . 10

1.4.2 Designing PMUs for a single MFC . . . 10

1.4.3 Dealing with the configuration of a large number of MFCs . . . 11

I Microbial fuel cells as electricity generators 12

2 Literature review 13
2.1 What are microbial fuel cells . . . 13
2.1.1 The energy metabolism of bacteria . . . 13
2.1.2 Microbial fuel cell principle of operation . . . 14
2.1.3 Types of Microbial fuel cell . . . 14
2.2 Internal mechanisms within microbial fuel cells . . . 15
2.2.1 Energy mechanisms of an ideal MFC . . . 15
2.2.2 Losses within a microbial fuel cell . . . 16
2.2.2.1 Voltage losses . . . 16
2.2.2.2 Current losses . . . 17
2.2.2.3 Loss dependencies on the electrical operating point . . . 17
2.3 MFCs seen as a black box . . . 18
2.3.1 Energy conversion efficiency . . . 19
2.3.2 Static electrical characteristics . . . 19
2.3.3 Dynamic electrical characteristics . . . 20
2.4 Electrical characteristics versus MFC design and operational parameters . . . 21
2.4.1 Impact of the reactor design . . . 22
2.4.2 Impact of the operational parameters . . . 22
2.5 Relations between MFCs and the electrical load . . . 23
2.5.1 Load and biofilm initial growth . . . 23
2.5.2 How electrical load determines the power generation . . . 24
2.6 Configuration of a large number of MFCs . . . 24
2.6.1 Issues relative to MFC scaling-up . . . 24
2.6.2 Electrical connection in series . . . 25
2.6.3 Fluidic connection . . . 25

3 Scientific contribution 26
3.1 Materials and methods . . . 26
3.1.1 Construction of lab-scale MFCs . . . 26
3.1.2 Automatic resistorstat . . . 27
3.1.3 Operational environment . . . 29
3.2 Modeling of a MFC . . . 29
3.2.1 Analytical model of losses . . . 30
3.2.2 Identification protocol . . . 31
3.2.3 Results and discussion . . . 32
3.3 Electrical performances of a large number of MFCs at MPP . . . 33
3.3.1 Protocol . . . 33
3.3.2 Biofilm development . . . 33
3.3.3 Maximum power curves . . . 33
3.3.4 Electrical performances of MFCs at maximum power point . . . 34
3.3.5 Analysis of the non-uniformities . . . 35
3.3.6 Conclusions . . . 36
3.4 Test of a FOCV MPPT algorithm for MFCs . . . 37

3.4.1 Protocol . . . 37
3.4.2 Comparison of MPPT algorithms . . . 37
3.4.3 Conclusions . . . 39

4 Summary of the results and perspectives **41**
4.1 Electrical characteristics of MFCs . . . 41
4.2 Scientific conclusions . . . 42
4.3 Specifications for the power electronics . . . 43

II Low-voltage power management unit for microbial fuel cells **45**

5 Introduction and literature review **46**
5.1 Low-voltage self-starting circuits . . . 47
5.1.1 Limitation of the threshold voltage of transistors . . . 47
5.1.2 Self-starting techniques . . . 48
5.2 Maximum power point control . . . 51
5.2.1 Maximum power point of an energy source . . . 51
5.2.2 Importance of maximum power point control . . . 52
5.2.3 Generic implementation of MPPT methods . . . 53
5.2.4 Low-power implementation of quasi-MPPT techniques . . . 55
5.3 State-of-the-art . . . 56
5.4 Conclusion . . . 57

6 Transformer-based low-voltage start-up circuit **58**
6.1 Theoretical study of the oscillator . . . 59
6.1.1 Equivalent circuit of the oscillator . . . 59
6.1.2 Analytical behavior of the oscillator . . . 60
6.1.3 Simulation of the equivalent circuit . . . 61
6.2 Theoretical study of the voltage doubler . . . 62
6.2.1 Transient analysis . . . 63
6.2.2 Load current and equivalent resistance analysis . . . 64
6.2.3 Efficiency analysis . . . 65
6.3 Theoretical study of the full voltage-lifter . . . 67
6.3.1 Voltage-lifter supplied by an ideal voltage source . . . 67
6.3.2 Voltage-lifter supplied by the basic equivalent circuit of a low-power MFC . . . 68
6.4 Experimental results . . . 68
6.4.1 Sizing of the voltage-lifter circuit . . . 68
6.4.2 Testing of the experimental voltage-lifter . . . 69

7 Self-starting DC/DC converters **77**
7.1 Design and theoretical study of a self-starting flyback converter . . . 78
7.1.1 Specifications . . . 78
7.1.2 Circuit description . . . 78
7.1.3 Specifications for the coupled inductances . . . 79
7.1.4 Design of the coupled inductances . . . 80

7.2 Performances of the self-starting flyback converter . . . 80
7.2.1 Single converter . . . 80
7.2.2 Series association of converters . . . 82

8 Scientific conclusions and perspectives 84
8.1 Conclusions . . . 84
8.2 Perspectives . . . 85

III Efficient serial association of non-uniform microbial fuel cells 86

9 Introduction 87
9.1 Concept of MFC-based energy grid . . . 87
9.2 Energy management of serially connected MFCs . . . 88
9.3 Voltage balancing circuits for MFCs . . . 88

10 Literature review 90
10.1 Methods to prevent voltage reversal of serially connected cells . . . 91
10.1.1 Passive method . . . 91
10.1.2 Active methods . . . 91
10.2 Methods to equalize the voltage of serially connected cells . . . 92
10.2.1 Dissipative shunting methods . . . 92
10.2.2 Shuttling active balancing methods . . . 93
10.3 Conclusion of the review . . . 95

11 MFC association in series without voltage balancing circuit 98
11.1 Operation of a two-stage MFC association . . . 98
11.2 Operation of an n-stage MFC association . . . 101

12 MFC association with a complete disconnection circuit 103
12.1 Theoretical study of a two-stage MFC association . . . 103
12.2 Operation of an n-stage MFC association . . . 105

13 MFC association with a switched-capacitor circuit 107
13.1 Theoretical study of a two-stage MFC association . . . 107
13.2 Loss analysis and performance study of a two-stage circuit . . . 109
13.3 Performance study for an n-stage MFC association . . . 111

14 Switched-MFC circuit 113
14.1 Theoretical analysis of a two-stage switched-MFC circuit . . . 114
14.2 Loss analysis and performance study of a two-stage circuit . . . 115
14.3 Generalization to an n-stage switched-MFC circuit . . . 117

15 Scientific conclusions and discussions 119
15.1 Comparison of the voltage balancing circuits . . . 119
15.2 Perspectives . . . 120

16 General conclusions **122**
16.1 Scientific contribution of the thesis 122
16.2 Answers to questions from the introduction 123
16.3 Scientific perspectives 124
16.4 Personal view 125

Bibliography **126**

List of acronyms and symbols

ACFC	Abiotically catalyzed fuel cell
ACFC	Enzymatic fuel cell
ASIC	Application specific integrated circuit
ATD	Adenosine triphosphate
BFC	Biofuel cell
BOD	Biological oxygen demand (mg/liter)
CD	Complete disconnection
CE	Coulombic efficiency
COD	Chemical oxygen demand
CoTMPP	Cobalt tetramethylphenylporphyrin
ECE	Energy conversion efficiency
EIS	Electrical impedance spectroscopy
EMF	Electromotive Force
FOCV	Fractional open-circuit voltage
FSCC	Fractional short-circuit current
GFC	Glucose fuel cell
HFC	Hydrogen fuel cell
IC	Integrated circuit
IEM	Ion exchange membrane
LED	Light emitting diode
LTC	Linear Technology
LV	Liquid volume
MFC	Microbial fuel cell
MPP	Maximum power point
MPPT	Maximum power point tracking

NaCl	Sodium Chloride
OCV	Open-circuit voltage
P&O	Perturbation and observation
PE	Potential efficiency
PMU	Power management unit
Pt	Platinum
PTFE	Polytetrafluoroethylene
PWM	Pulse width modulation
RF	Radio frequency
SA	Serial association
SC	Switch capacitor
SMD	Surface mount device
SMFC	Switched microbial fuel cell
SOC	System on chip
ST	STMicroelectronics
Std	Standard deviation
SWC	Switched capacitor
TCSA	Total cathode surface area
TEG	Thermoelectric generator
Tx	Transformer
WSN	Wireless sensor network
α	Duty-cycle
η	Efficiency (%)
η_{act}	Activation voltage drop (V)
η_{con}	Concentration voltage drop (V)
η_G	Global efficiency (%)
η_{Ohm}	Ohmic voltage drop (V)
λ	Channel-length modulation (V^{-1})
μ_R	Relative permittivity
ω	Pulsation (rad/s)
ε_{ox}	Oxide permittivity (F.m)

ε_{si}	Permittivity of Silicium (F.m)
φ_f	Surface potential (V)
B_{sat}	Saturation magnetic field of a ferrite (T)
C_d	Depletion capacitance (F)
C_{eq}	Equivalent capacitance (F)
C_{GD}	Gate-drain capacitance (F)
C_{GS}	Gate-source capacitance (F)
C_J	Equivalent gate capacitance of a JFET (F)
C_{NL}	Non-linear equivalent capacitance of an MFC (F)
C_{ox}	Oxide capacitance (F)
CO_2	Carbon dioxide
D_J	Equivalent gate-source diode of a JFET
E_{ox}	Standard potential of the oxidator (V)
E_{red}	Standard potential of the reductor (V)
F	Faraday's constant (C/mol)
f_S	Switching frequency (Hz)
G	Gibbs free energy (J)
I	Current (A)
I_{DS}	Drain-source current (A)
I_{L0}	Zero-bias leakage current (A)
I_L	Leakage current (A)
I_{MPP}	Maximum power point current (A)
I_{OUT}	Output current (A)
I_q	Quenched current (A)
J_1	JFET
k	Turn-ratio between two coupled inductances
k_{MPP}	Proportional step ratio for MPPT algorithms
L_1	Inductance of the primary winding of a coupled inductance (H)
L_2	Inductance of the secondary winding of a coupled inductance (H)
n	Number of electrons (mol)
n_1	Number of turns of the primary winding of coupled inductors
n_2	Number of turns of the secondary winding of coupled inductors

n_3	Number of turns of the tertiary winding of coupled inductors
N_a	Doping concentration (m^{-3})
O_2	Dioxygen
q	Charge of an electron (1.602 10^{-19} F.m)
$Q_{effective}$	Amount of charges transfered to the anode (C)
Q_{total}	Total amount of charges produced by the oxidation reaction (C)
R	Perfect gas constant (8.314 J/(mol.K))
R_{eq}	Equivalent output resistance of a DC/DC converter (Ω)
R_{input}	Input resistance of a DC/DC converter (Ω)
R_{int}	Internal resistance of an MFC (Ω)
R_J	Drain-source resistance of a JFET (Ω)
R_{NL}	Non-linear resistance of an MFC, includes the activation and concentration losses (Ω)
R_{Ohm}	Ohmic resistance of an MFC (Ω)
R_{OUT}	Output resistance (Ω)
R_{SW}	Switch on-resistance (Ω)
t_{ox}	Oxide thickness (m)
V_1	Voltage across the primary winding of a coupled inductor (V)
V_2	Voltage across the secondary winding of a coupled inductor (V)
V_{bac}	Voltage drop by the bacteria for their metabolism (V)
$V_{C\varphi 1}$	Voltage across capacitor C at the end of phase φ_1 (V)
$V_{C\varphi 2}$	Voltage across capacitor C at the end of phase φ_2 (V)
V_{diff}	Difference between the maximum and the actual output voltage V_{OUT} (V)
V_D	Diode threshold voltage (V)
V_{GS}	Gate-source voltage (V)
V_{IN}	Input voltage (V)
V_J	Gate-source voltage of a JFET (V)
V_{MPP}	Maximum power point voltage (V)
V_{out}	Output voltage (V)
V_P	Peak voltage (V)
V_{SB}	Source-bulk voltage (V)
V_{start}	Self start-up voltage (V)

V_S	Voltage swing (V)
V_{t0}	Zero-bias threshold voltage (V)
V_{TH}	Threshold voltage (V)
V_T	Thermal voltage (V)

Chapter 1

Introduction

Contents

1.1 Microbial fuel cells use biomass to generate electricity 1
1.2 Applications of Microbial fuel cells as energy generators 4
1.3 Power management for MFCs 8
1.4 Scope of the thesis 9

1.1 Microbial fuel cells use biomass to generate electricity

1.1.1 Biomass to electricity conversion pathways

Fossil fuels are still today the major source of energy worldwide [IEA, 2011]. Although they are not exhausted yet, the pressure on their availability is already in excess, and materializes in a global cost increase. Most countries anticipate the exhaustion of fossil fuels and are developing alternative sources of energy (e.g. based on sun, wind or biomass).

Biomass is biological material derived from living or dead organisms. The present form of biomass (i.e. first generation biomass) used for energy is the same that is traditionally used for food (e.g. sugar cane, corn). Even if it is the easiest biomass to valorize, it causes an issue as to worldwide food availability. Second and third generations of biomass are expected to replace it in the future. Second generation biomass is composed of industrial, agricultural or domestic residues and wastes. Third generation biomass is specially engineered for the purpose of energy production. It is based on low-cost, high-energy and entirely renewable crops. A promising example of third generation biomass is algae.

Biomass can be used to produce heat or electrical energy. The conversion pathways to electrical energy are detailed in Figure 1.1. They are undertaken using two main process technologies: thermo-chemical and bio-chemical/biological [McKendry, 2002]. Within thermo-chemical conversion, four process options are available: combustion, gasification, pyrolysis and liquefaction. Biochemical conversion encompasses two process options: digestion and fermentation. These conversion processes either lead to the production of biogas (e.g. methane) or to the production of biofuel (e.g. ethanol). These are easily transformed into electrical energy using either a combustion-based process (e.g. gas turbines), or a fuel cell based process, named biofuel cells and described in next section. Alternatively, biofuel and biogas can be converted to hydrogen with either a chemical (reforming) or a biological process [Larminie and Dicks, 2003]. This hydrogen can next be converted into electrical energy using a hydrogen fuel cell.

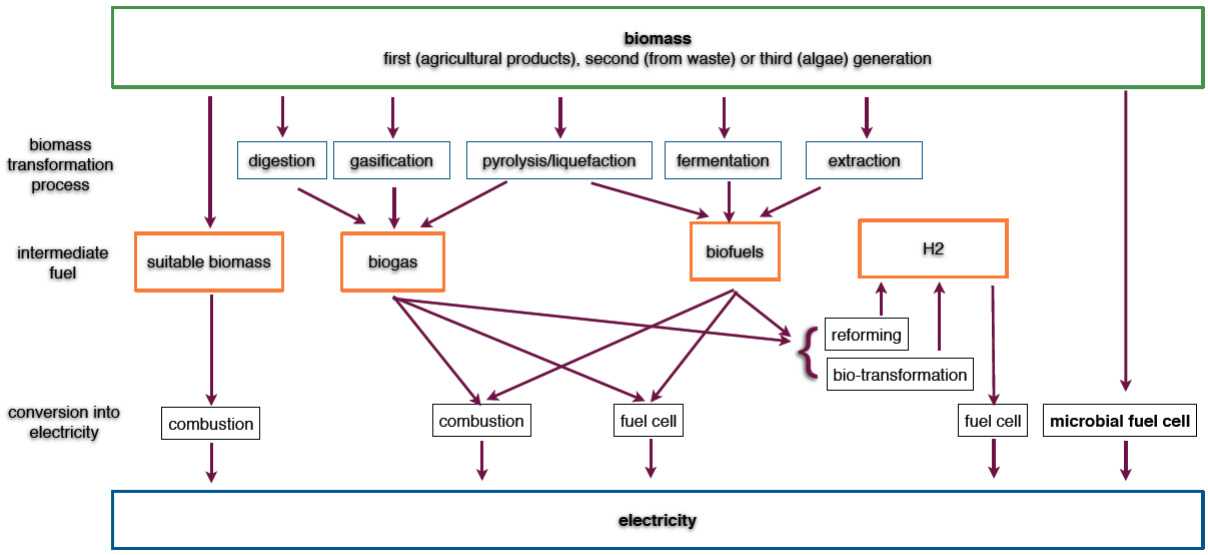

Figure 1.1: Main biomass conversion pathways into electricity

Microbial fuel cells (MFCs), by accepting a wide range of organic matter as a fuel, are a valuable candidate to valorize liquid biomass without a pre-transformation process. They are the unique transducer that enable direct conversion of any type of biomass (i.e. first-, second- and third-generation) into electrical energy (Figure 1.1).

1.1.2 Biofuel cells

Biofuel cells (BFCs) use catalysts (chemical, enzymatic or microbial) to electrochemically convert organic fuels into electrical energy [Bullen et al., 2006]. BFCs are classified into three groups according to the nature of their catalyst:

1. **Abiotically catalyzed fuel cells** (ACFCs) [Kerzenmacher et al., 2008] are exploit chemicals or metals as catalyst. These tolerate only specific organic matter such as glucose. Power densities normalized to electrode surface area of few tens of $\mu W.cm^{-2}$ were reported so far. The high cost of their catalyst limits their applications to low-power energy production. Their bio-compatibility and long-term stability permit to foresee *in vivo* applications such as powering medical implants.

2. **Enzymatic fuel cells** (EFCs) [Osman et al., 2011] offer higher power densities than their abiotically catalyzed counterparts (around 1 $mW.cm^{-2}$ as in [Sakai et al., 2009]), but the limited enzyme stability prevents long-term application. In *in vivo* applications, the enzymes may be inhibited by compounds present in extra-cellular fluids [Cinquin et al., 2010].

3. **Microbial fuel cells** (MFCs) employ whole micro-organisms as catalysts [Du et al., 2007]. They reach power densities of few hundreds of $\mu W.cm^{-2}$ and their main advantage is that they accept a wide range of organic matter as fuel (e.g. domestic and industrial wastewater). In addition, MFCs have been reported to operate for years [Habermann and Pommer, 1991] and are known for their longevity. For this reason, MFCs are expected to be useful in applications such as wastewater treat-

ment [Monier et al., 2008] or ambient energy scavenging to supply low-power devices [Donovan et al., 2010].

1.1.3 Researches on MFCs

Historically, the first actual demonstration of a microbial fuel cell was performed in 1911 by M.C. Potter, professor of Botany at the University of Durham, UK [Potter, 1911]. These results gained increased interest in 1931 when B. Cohen of John Hopkins School of Medicine, USA, demonstrated a voltage source larger than 35 V from serially connected MFCs [Cohen, 1931]. In the 1960's, the NASA studied the opportunity to recycle human waste during space flights [Canfield et al., 1963]. It was in 1976 that further developments were reported by Karube and his team from the National Institute of Agricultural Science in Tokyo, Japan [Karube et al., 1977]. They used hydrogen produced by the fermentation of glucose as the reactant at the anode of a hydrogen fuel cell. Then, a few years later, M.J. Allen and H. Bennetto, both from King's College in London, UK, were the first to study the way microbial fuel cells operated and to use the electricity generated by their MFCs to energize real applications [Allen and Bennetto, 1993, Bennetto et al., 1983]. It was in 1991 that Habermann and Pommer first used domestic wastewater as a fuel in a MFC [Habermann and Pommer, 1991].

Research strengthened in the last decade and new applications emerged in addition to electrical energy production [Kim et al., 2008]. These applications all share a common microbial anode and are commonly named MXCs, the X standing for different types and applications. They include MFC-based biological sensors [Chang et al., 2004], biohydrogen production in microbial electrolysis cells (MECs) [Tartakovsky et al., 2011], and microbial desalination cells (MDCs) [Cao et al., 2009]. Other possible applications include the production of chemicals and the reduction of pollutants (bioremediation) [Lovley and Nevin, 2011].

As far as energy production and wastewater treatment are considered, MFCs offer potential for waste management, green energy production and water availability, which are key challenges of the 21$^{st.}$ century. This assessment explains probably why the research community is so active on this topic as shown in Figure 1.2.

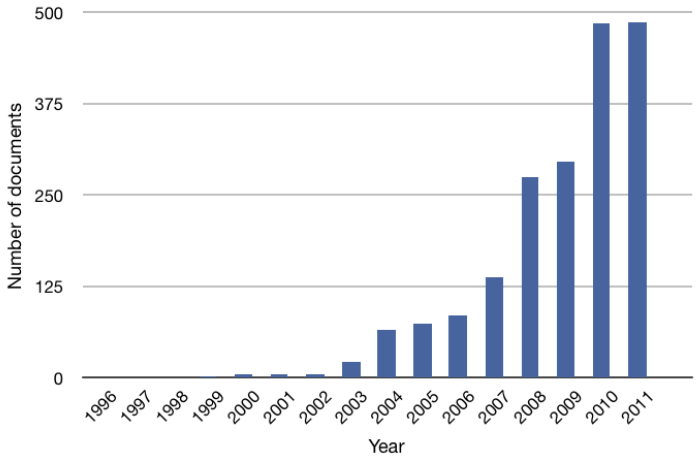

Figure 1.2: Annual number of scientific papers on the topic of microbial fuel cells (reference: Scopus).

1.2 Applications of Microbial fuel cells as energy generators

MFCs are candidates for a number of applications related to energy generation, as outlined in the following.

1.2.1 Energy-autonomous wastewater treatment

1.2.1.1 Wastewater treatment

Typically, sewage treatment is organized as in Figure 1.3 and so, it involves several stages. In the pretreatment, materials that can be easily collected are removed from the raw sewage to prevent damage of the clarifiers; this is a first step. The second step involves temporarily holding the wastewater in a large basin so as to remove both settled and floating materials and fetch the remaining liquid, which can then be treated. In the next stage, micro-organisms are used to clear the water by removing dissolved and suspended biological matter. In this process, the plant needs to drain off the micro-organisms from the treated water. All the sludge resulting from the treatment is then assessed and disposed.

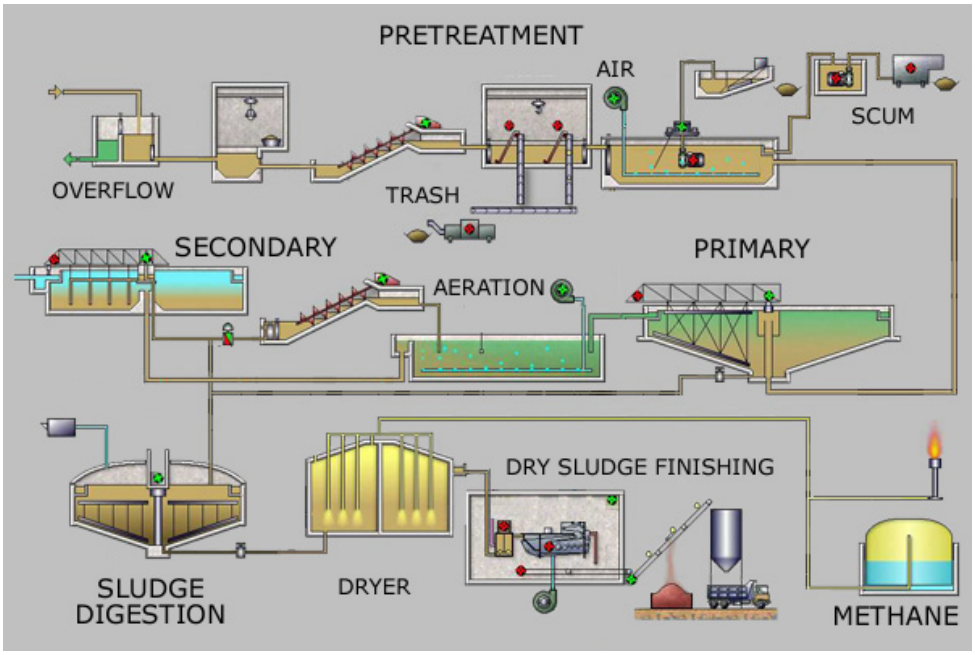

Figure 1.3: Process flow diagram for a typical large scale treatment plant (source: wikipedia, licensed under the *Creative Commons Attribution-ShareAlike 2.5 License*)

A majority of municipal plants use aerobic processes in the secondary treatment. These are based on micro-organisms, which require both oxygen and food to gain their energy to live. Oxygen is introduced at a high cost through aeration and food consists in biodegradable soluble organic contaminants (e.g. sugars, fats, etc.).

1.2.1.2 Advantages of MFCs

Microbial fuel cells are engineered devices that facilitate the partial harvesting of the energy involved in the metabolism of micro-organisms when they consume food. Domestic or industrial wastewater can be used as the source of food, concurrently leading to their treatment. The micro-organisms naturally found in an aerobic wastewater treatment plant are suitable for energy production when placed in a MFC.

Even if the MFC technology is currently pursued at laboratory scale only, the scientific community believes that these reactors can be scaled-up and multiplied to realize full scale MFC-based wastewater treatment plants. These would combine wastewater treatment and energy production in such a way that wastewater treatment becomes energetically favorable with the potential for considerable energy saving. In the US only, it is estimated that public wastewater treatment, accounts for an energy consumption of about 21 billion kWh a year [Oh et al., 2010].

A recent study in Germany estimated that a 10.000 population equivalent MFC-based wastewater treatment plant could continuously produce 20 kW [Sievers et al., 2010]. The main limitation to its feasibility is the electrode/membrane surface area estimated to be 10.000 m^2 (assuming a power density of 2 $W.m^{-2}$) and the resulting size and cost. In order to be economically viable, the electrode/membrane price should be below 7.5 €.m^{-2}.

To date, only a very limited amount of on-site pilot demonstrators have been reported in literature. One of the most significant experiment was performed in Australia, using industrial wastewater from a Foster brewery as a fuel source [Logan, 2010]. This reactor consisted of 12 tubular modules, each 3 m high with a total volume of about 1 m^3, but little is known on its performances. Some industries like *Emefcy* in Israel recently established as an MFC company. This start-up has the project of a spiral aerobic biofim-reactor but, once again, little is known on its performances [Emefcy, 2012].

1.2.1.3 Power management strategies

If a technological breakthrough gives a visible expression to MFC-based wastewater treatment, it will very likely be composed by a large number of split-up reactors. These constitute as many individual energy sources. The electrical energy generated can be consumed locally by a number of equipments (e.g. to supply pumps) and/or to be delivered to the grid.

The electrical architecture of a MFC-based treatment plant therefore involves a large number of participants (suppliers and consumers) and subsequently offers a large number of possible power management strategies to gather, distribute, and act on information about the behavior of all participants in order to improve the efficiency, importance, reliability, economics, and sustainability of electricity service. This raises general questions like:

How to decrease the cost of MFCs?
What size should each individual reactor be?
How to configure a large number of split-up energy generators?
How to manage one or several faulty MFCs?
How many electrical energy converters are required, and what are their functions?
How to ensure high quality wastewater treatment while maximizing power production?

1.2.2 Bio-batteries

Apart from being used in combination with wastewater treatment, MFCs can be used with a reservoir of high-density organic fuel, as portable power sources. In this case, they can potentially be used as a complement or as an alternative to chemical batteries to supply mobile electronic systems.

1.2.2.1 The need to develop environmentally-friendly batteries

The number of mobile consumer electronics is increasing at a fast pace. For example, the iPhone from Apple was first commercialized in 2005, and it is estimated that in 2009, more than 6 million devices were active in the US alone [The Nielsen Company, 2009]. Almost all mobile applications rely on Lithium-ion batteries for their energy supply. These chemical batteries have several disadvantages including limited cell life and toxicity of constituent chemicals. In addition, these batteries only store energy and rely on outer electrical energy availability, that is itself becoming a major concern.

The emerging research themes of biofuel cells could lead to the development of bio-batteries. Bio-batteries would not only rely on a reservoir of biomass as a primary energy source, but would ideally also be constructed from fully biodegradable, non-toxic, and low-price materials. These would be intended as power sources for mobile devices as an alternative to today's chemical batteries. Because organic matter, such as glucose, has an energy density approx. 20 times higher than the one of Li-ion batteries, bio-batteries also offer the promise for extended life-time.

Even-though biofuel cells demonstrated the ability to generate electricity from organic matter, these are presently not constructed from biodegradable, and low-price materials. Furthermore, the presently achieved power densities are orders of magnitude lower than those of their lithium counterparts.

1.2.2.2 Advantages of MFCs

The main strength of MFCs compared to other biofuel cells is that they can be fueled with a wide range of organic matter and that they have an extended life-time. They can potentially be associated with a reservoir of high-density organic fuel (e.g. sugar) to construct bio-batteries. MFCs have the following advantages:

- they rely on bacteria to catalyze electrochemical reactions, and thus permit to avoid the use of expensive metals like platinum
- electrodes for MFCs can be constructed with carbon-based materials and membrane with earthen-based materials, which are both fully biodegradable without environmental damage and low-cost
- the life-span of MFCs is theoretically infinite as far as micro-organisms are fed with appropriate fuel.

The major disadvantages of MFCs to replace Li-ion batteries in mobile applications is their low power density [Ren et al., 2012].

1.2.2.3 Power management strategies

A bio-battery would most probably be composed of a small number of individual reactors laid out in a stack structure. Mobile consumer electronic devices such as smart-phones consume electrical energy very irregularly. They alternate between off, stand-by and active modes. In order to optimize the battery

life-time, the stack should consume very little fuel in off and stand-by modes. In active mode, it should provide energy to the load at the best energy-conversion efficiency (ECE).

Other than energy consumption rate, there is a possible mismatch between the DC voltage required by mobile electronics (around 3.6 V for Li-ion supplied devices) and the voltage available at the output of the stack. When connected to a load, it must be able to provide the required power at a given DC output voltage. This raises questions such as:

How to increase the power density of MFCs?
How can energy conversion efficiency of the stack be maximized?
How does a stack evolve if no energy is drawn during a long time?
How does a stack behave if one of its elements is faulty?
How can a fixed stack output voltage be harvested whatever the output current?

1.2.3 MFC-based ambient energy scavenging

1.2.3.1 Ambient energy scavenging

Wireless sensor networks (WSN) is presently a popular topic in research. A WSN consists of spatially distributed autonomous sensors to monitor physical or environmental conditions and to cooperatively pass their data through the network to a main location. These can be used in a number of applications such as environmental monitoring (e.g. fire detection, air pollution monitoring and others), industrial monitoring (e.g. machine health monitoring) or agricultural monitoring (e.g. sun exposure times). Each WSN has typically several parts: one or several sensors, a radio transceiver, a micro-controller, an energy source (usually a battery or an embedded form of energy harvesting) and a power management circuit to interface the energy source and the other parts.

Ambient energy scavenging is an appealing alternative to batteries as a supply for WSN. Indeed, batteries have limited lifetime and can be toxic to the environment. Research in energy scavenging is very active. A large number of transducers are proposed as an alternative to batteries [Roundy et al., 2004]. These are most of the time solar, thermal, vibrational or electromagnetic transducers. But in certain environments where none of these energy sources are present and where organic matter is available, MFCs could also be possible transducers [Donovan et al., 2010].

1.2.3.2 Advantages of MFCs

MFCs can be used to supply low-power electronic devices intermittently. They can offer a maintenance-free alternative to the use of environmentally harmful batteries. MFCs are particularly interesting at sediment levels of lakes or seas or in sewers where solar, thermal and vibrational transducers are inefficient or inoperable. Some research studies demonstrated the ability of so-called benthic MFCs to supply sensors at the bottom of lakes or oceans [Donovan et al., 2010]. In the future, the development of micro-scale MFCs will permit to integrate them as an embedded power supply for heterogenous micro-systems [Siu and Chiao, 2008].

1.2.3.3 Electrical energy harvesting strategies

In energy scavenging applications, electrical energy is provided intermittently in bursts of power to the load (e.g. wireless sensor). These bursts correspond to the acquisition and the transmission of a set

of data and can occur every few seconds to every few minutes depending on the required acquisition sampling time. The power consumption profile during the burst is irregular as presented in Figure 1.4. The burst is initiated by a short consumption of current corresponding to the wake-up. Then, data are acquired, processed and finally transmitted wirelessly. This last phase is the most demanding in terms of current consumption (13.3 mA for chipcon CC2500). The whole duration of a burst is typically of few milli-seconds, corresponding to a typical energy consumption in the order of 50 µJ.

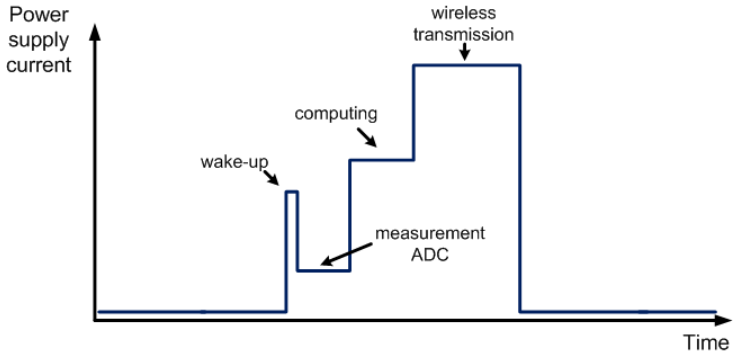

Figure 1.4: Typical wireless sensor consumption profile (inspired by MSP430 [Ivey, 2009] and CC2500 [TI, 2011a])

The power management strategy adopted in this kind of application is to harvest energy at maximum power from the source, and to store it in advance of the burst of power. If the sampling rate is low, one small-scale MFC can be sufficient to provide the necessary energy. The voltage, at which micro-organisms produce electrical energy in a MFC, is very low (few hundreds of mV), thus causing a voltage mismatch between the source and the load. The utilization of MFCs to scavenge energy from the environment leads to the following questions:

How can energy be harvested at maximum power?
How does a MFC constantly operate and develop at maximum power in the long term?
How does a power management unit self-supply if it is supplied by a MFC with a very low voltage?
How to design an efficient power management unit when input power is in the order of 1 mW only?

1.3 Power management for MFCs

As previously outlined, specific energy harvesting strategies will be required to capture, store and distribute the energy in order to improve the efficiency, reliability and sustainability of the electricity service. These strategies are made possible by a Power Management Unit (PMU). The PMU intelligently interfaces the energy generators and the energy consumers. It can be composed of sensors, power electronics converters, control systems and digital processing devices.

In the case of energy production from MFCs, the number of micro-generators can be very different depending on the considered application. One MFC is sufficient to supply a wireless sensor whereas hundreds or thousands of individual units can be used in the case of a large-scale MFC-based wastewater treatment plant. The PMU for these applications can therefore reach different levels of complexity.

1.3.1 Power management unit for one MFC

In energy scavenging applications, the load is normally an unique low-power electronic device. In the case where it is a wireless sensor, it is supplied intermittently. A micro-generator generating less than 1 mW continuously is often sufficient. Therefore, the MFC can be a unique small-scale microbial fuel cell.

For this type of application, the PMU needs to: a) define the energy harvesting rate from the MFC(s), b) capture energy at the highest efficiency possible, and c) provide electrical energy in an acceptable form to the final load. The major constraints of this PMU is to operate at low input voltage and at very low power in a completely autonomous way. For this kind of application, the natural ambient fuel is assumed to be unlimited, and therefore the priority is to harvest sufficient electrical energy regardless of the fuel consumption rate. The PMU will favorably harvest energy at maximum power point.

1.3.2 Power management unit for a large number of MFCs

In the case of a MFC-based wastewater treatment plant, the PMU needs to deal with a large number of individual units. A large and diverse consumer base can then be supported. The huge number of energy generators and consumers imply a wide degree of freedom on the power management strategy.

One approach to deal with a high number of micro-generators is to configure them accordingly. This configuration can be realized at different levels ranging from a direct series or parallel connection of MFCs to an association at the load level. In the case of association at the source level, the PMU "sees" a single equivalent source composed of several connected MFCs and operates at high levels of power. In the other case of energy matching at the load level, the PMU is distributed, each MFC has its dedicated sub-PMU and energy is associated at the output of the sub-PMUs. In one case, the PMU has to deal with a substantial energy source and specifications will be similar to the ones for technologies like hydrogen fuel cells or photovoltaic modules. In a different case, the sub-PMUs are designed for a single MFC and are scaled for very low-power and low-voltage (i.e. like in energy scavenging applications).

All of these extreme configurations are probably suboptimal. On the one hand, the direct connection of MFCs leads to the complexity of managing each cell at its optimum, and also creates reliability issues if one or several cells are faulty. On the other hand, a total subdivision of the PMU leads to a huge number of electrical components to manage the network and to a high payload. In addition, constraints imposed by low-power and low-voltage are reported on each PMU, eventually leading to a poor global efficiency. There is a trade-off to be found between both extreme scenarios, which most probably will consist of the configuration of few MFCs into modules, which are managed by dedicated PMUs.

1.4 Scope of the thesis

This work on power management for MFCs is at the boundary of the two scientific communities of microbial fuel cells and power electronics. The thesis focuses on the three most critical issues encountered when designing PMUs for any of the three applications. It is divided in three distinct parts corresponding to the number of issues to be resolved. Each part is included in a different research topic and therefore start with its own literature review before presenting the contribution of the thesis.

1.4.1 Getting to know MFCs better

Because a proper understanding of MFCs is the foundation for the specific conception of performing PMUs, this thesis first addresses the electrical characterization of MFCs.

The literature review in this part describes the operation of MFCs and links their electrical performance to internal physical, electrochemical, and bacterial mechanisms. It also sums-up the research work relating to the connection of MFCs into stacks.

The manuscript then relates a number of experiments, which aimed to develop new tools, methods and to increase the knowledge on MFCs. At first, MFCs are fitted to a simple equivalent electrical model. This model comes into three levels of complexity, which are used in the two subsequent parts to simulate and test PMUs. Secondly, the electrical performance of MFCs is tested under maximum power operation. This was made possible through the development of a dedicated measurement tool, which emulates a PMU with a maximum power point tracking (MPPT) algorithm. Finally, two MPPT algorithms are compared on MFCs with the objective of implementing one of them in a PMU.

This part of the thesis will attempt to answer the following questions:

What limits the maximum power density of MFCs?

How should energy be harvested to improve the power delivered by MFCs?

What are the electrical characteristics of MFCs when they are operated at the maximum power transfer point?

1.4.2 Designing PMUs for a single MFC

Depending on the final load, it is possible that several electrical energy converters are required to interface with the MFC(s). The second part specially focuses on the layer of power electronics directly connected to MFCs (i.e. front-end PMU), which was identified to be the most crucial part because of the low-voltage constraints and the requirement for a specific control (eventually a maximum power transfer point tracking control).

The literature review describes and compares low-voltage self-starting DC/DC converters and MPPT methods. It outlines the lack of circuit suitable to harvest energy from a single low-power MFC.

The manuscript then describes a start-up circuit based on a transformer-JFET configuration. This circuit is then implemented into two different DC/DC converters. The first is designed for a MFC producing less that 1 mW of power. The second is a 10 mW flyback converter with a MPPT control. It includes an insulation between input and output, which enables a large number of configuration scenarios.

In this part of the manuscript, the following questions will be addressed:

How to step-up the voltage of a single MFC?

How does a sub-threshold self-oscillating circuit operate?

How can a start-up strategy be implemented into a low-power DC/DC step-up converter?

How can a low-cost maximum power point tracking be implemented in a low-power DC/DC step-up converter?

1.4.3 Dealing with the configuration of a large number of MFCs

The association of a large number of MFCs is a critical research area, which will lead to the development of efficient stacks. The third part of the thesis addresses this issue.

The literature review introduces state-of-the-art voltage balancing circuits. These circuits usually control the charge and discharge of batteries of supercapacitors, but can be designed to manage the association of MFCs.

A few voltage balancing methods from the literature are evaluated when they are used with MFCs. A new so-called “switched-MFC” method is introduced, which permits the configuration of MFCs at high efficiency. These methods are compared with each other to point out the benefits of each.

In this part of the manuscript, the following questions will be addressed:

How are the performance of a serial association of MFCs quantitatively affected when MFCs have non-uniform electrical characteristics?

How do voltage balancing circuits operate?

Which voltage balancing circuit offers the best performance?

Part I

Microbial fuel cells as electricity generators

Chapter 2

Literature review

Contents

2.1 What are microbial fuel cells 13
2.2 Internal mechanisms within microbial fuel cells 15
2.3 MFCs seen as a black box 18
2.4 Electrical characteristics versus MFC design and operational parameters 21
2.5 Relations between MFCs and the electrical load 23
2.6 Configuration of a large number of MFCs 24

The research community working on MFCs still needs to address a number of issues before successful implementation in practical applications. The main objective is to increase the ratio between power density and cost. This is not only limited to finding new materials for the electrodes or membrane. It is also necessary to gain a better understanding of the different mechanisms behind electrical energy production. Firstly, the electrical characteristics of MFCs as a power source are not well known. Secondly, the influence of static and dynamic electrical output load on MFC power production, and fuel consumption rate, is not well understood and poorly characterized.

Part I on MFCs addresses the following questions:
What is a basic electrical equivalent circuit that best represents the static and dynamic electrical characteristics of MFCs?
How are the electrical performances linked to the reactor structure and to other operational parameters?
What is the performance of MFCs at the special electrical maximum power operating point?

2.1 What are microbial fuel cells

2.1.1 The energy metabolism of bacteria

There is a plethora of metabolic pathways that bacteria can use for their growth and maintenance that were previously summarized in [Aelterman, 2009]. One can classify bacteria based on the type of energy they utilize: a) sunlight (phototrophs) or b) chemical compounds (chemotrophs), which includes both organic (organotrophs) and inorganic (lithotrophs) compounds. Chemotrophs are the bacteria of interest

in microbial fuel cells. They are "respiring organisms" because they oxidize chemical substances and utilize oxygen or other electron acceptors. This catabolic reaction releases energy that can be used to synthesize ATP and drive their metabolism.

Chemotrophs can be classified according to the type of final electron acceptor they use for respiration. Oxygen is the electron acceptor of **aerobic organisms**. Other inorganic compounds, such as nitrate, are the electron acceptors of **anaerobic organisms**. In the absence of possible electron acceptors, chemotrophs may use **fermentation**. In fermentation [Wikipedia, 2012], electrons taken from the reduced substrates are transferred to oxidized intermediates to generate reduced fermentation products (e.g. lactate, ethanol, hydrogen, butyric acid, etc.). In the presence of oxygen, fermentation is generally shut down since the energy gain through fermentation is less than with respiration of oxygen. In fact, oxygen is the electron acceptor with the highest redox potential, and as such, electrons preferably react with it.

2.1.2 Microbial fuel cell principle of operation

A microbial fuel cell is a device engineered to harness the metabolism of chemotrophic bacteria in order to generate electrical energy. The basic principle is to separate the reduction and oxidation reactions involved in the respiratory mechanisms in order to harvest a part of the energy available from these reactions.

In a microbial fuel cell, bacteria are placed in a chamber with organic matter but where the natural terminal electron acceptors necessary for their living are replaced by a solid conductive anode. The latter is electrically connected to a cathode, which lay in the presence of oxygen in some configuration. This way, bacteria (not necessarily aerobic bacteria) are forced to indirectly use oxygen as a final electron acceptor through the circuit composed of the two electrodes and their electrical connection. The electrons generated in the oxidation reaction at the anode are transferred to the cathode for corresponding reduction.

Bacteria that are capable of exocellular electron transfer are defined as exoelectrogens [Logan, 2009]. Three mechanisms of electron transfer were outlined: a) direct contact by outer membrane cytochromes, b) use of excreted mediators (also known as shuttles) and c) through synthesized appendages capable of transferring electrical current called nano-wires.

At the same time as electrons are generated, bacteria also produce protons and degraded organic matter. Like electrons, protons are involved in the reduction reaction at the cathode. The cathode is therefore placed in an adjacent chamber where protons can migrate through an ion selective membrane.

2.1.3 Types of Microbial fuel cell

A double-chamber MFC is composed of two compartments separated by an Ion Exchange Membrane (IEM) which can be either a proton or a cation exchange membrane (Figure 2.1, a). The anodic compartment contains the organic substrate and the bacteria, whereas the cathodic compartment contains an electrolyte rich in electron acceptor (e.g. oxygen).

A single-chamber MFC is composed of an anodic compartment alone (Figure 2.1, b). The cathode is merged with the reactor such that it interfaces the internal electrolyte and the external air. This type of membrane is called air-cathode. A membrane can be placed on the internal side of the cathode to limit the diffusion of oxygen within the reactor. The main advantage of this type of MFC is that it does not require any aeration of the cathodic electrolyte, reducing thus the hydraulic flow.

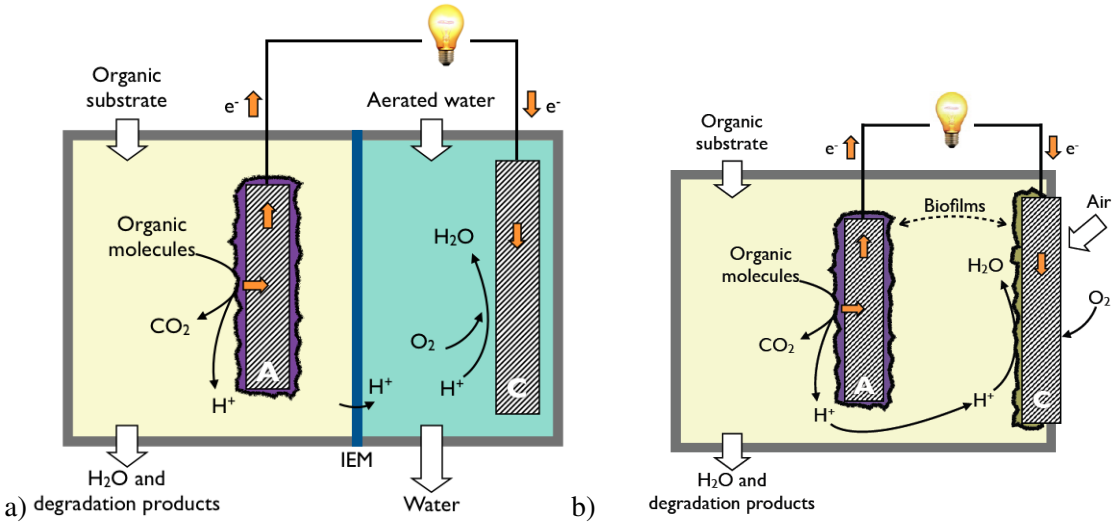

Figure 2.1: Schematic of a double-chamber (a) and single-chamber (b) MFC

2.2 Internal mechanisms within microbial fuel cells

2.2.1 Energy mechanisms of an ideal MFC

Chemotrophs are respiring bacteria which gain their energy for life and growth through the coupled mechanisms of nutrient oxidation and electron donation (i.e. reduction). These mechanisms involve the transformation of reactants (i.e. organic matter and oxygen) into products (i.e. water and carbon dioxide). The theoretical energy available for the bacteria is related to the difference between the energy content of the reactants and the products. The energy content (Gibbs free energy G) can be expressed as the product of the electromotive force (EMF) and the corresponding charge flow nF [Bard and Faulkner, 1981].

$$G = nF(E_{RED} - E_{OX}) \tag{2.1}$$

where n in the number of electrons involved in the reaction (mol), F is the constant of Faraday, and E_{RED} and E_{OX} are the reduction and oxidation potentials respectively which difference corresponds to the EMF.

In laboratory experiments, acetate is often used as a substrate for its great assimilability by bacteria. Acetate often appears as an intermediate product of the degradation of other fuels. When oxidized, acetate is degraded into bicarbonate according to Equation 2.2 which is counterbalanced by Equation 2.3.

$$CH_3COO^- + 4H_2O \rightarrow 2HCO_3^- + 9H^+ + 8e^- \quad (E^0 = 0.187V) \tag{2.2}$$

$$2O_2 + 8H^+ + 8e^- \rightarrow 4H_2O \quad (E^0 = 1.229V) \tag{2.3}$$

The corresponding standard potentials E^0 were determined from the Gibbs free energy data tabulated in [Thauer and Jungermann, 1977] for the acetate/bicarbonate couple and from [Bard and Faulkner, 1981] for the oxygen/water couple. The EMF is therefore 1.042 V in standard conditions. The effective EMF depends on temperature and on local reactant and product concentration according to the Nernst equation as used in [Logan et al., 2006]. A MFC with an acetate oxidizing anode ($HCO_3^- = 5mM$, $CH_3COO^- = 5mM$, pH = 7) and an oxygen reducing cathode (partial pressure $pO_2 = 0.2$, pH = 7) would therefore have an EMF of 0.805-(-0.296) = 1.101 V.

In an ideal microbial fuel cell, the potential difference between the fuel and the terminal electron acceptor is shared between the bacteria and the outer electrical load. The potential difference available for the bacteria corresponds to the one between the anode and the fuel. The potential difference available for the outer electrical load corresponds to the one between the cathode and the anode.

2.2.2 Losses within a microbial fuel cell

The previous energy mechanisms were described for an ideal MFC. Within a real MFC, a number of losses impede the operation of the MFC. These can be divided into voltage drops and current drops as described in [Larminie and Dicks, 2003].

2.2.2.1 Voltage losses

The EMF corresponds to the theoretical maximum voltage of a MFC. Such voltage is never achieved practically by MFCs because of voltage drops as in classical hydrogen fuel cells (HFCs).

Bacterial voltage drop was described in the previous section. Bacteria capture a fraction of the energy content of the substrate for their growth and maintenance. This is done by deducing a certain voltage V_{BAC} from the EMF. Because bacterias are activating the reaction at the anode, the voltage drop V_{BAC} can be included in the more general definition of **activation drop**, that also includes phenomena at the cathode. These are caused by the necessity to have a local potential difference, overcoming energy barriers, before a reaction takes place at the surface of both electrodes. A proportion of the voltage generated is lost in initiating the chemical reactions that transfer the electron to or from the electrode. This voltage drop is highly non-linear.

The **ohmic drop** is the linear resistance to the flow of electrons through the material of the electrodes and the various interconnections, as well as the resistance to the flow of ions through the electrolyte. This voltage drop is essentially proportional to current density (Ohm's low).

The **concentration (or mass transport) drop** results from the change in concentration of the reactants at the surface of the electrodes as the fuel is used. Local concentrations directly affect the electrode potentials according to the Nernst Equation 2.4 [Bard and Faulkner, 1981]. Concentration drops are amplified for high current densities, when the reactants are consumed at high rates at the surface of the electrodes.

$$E = E^0 + \left(\frac{RT}{nF}\right) ln \frac{[reactants]}{[products]} \tag{2.4}$$

where R is perfect gas constant.

For each electron involved in the redox reactions, the total theoretical energy available is shared between the bacteria, the electrical load and the losses. The unit representative of voltage drops is the potential efficiency (PE). The PE is therefore current dependent and decreases for high current densities.

PE is defined in (2.5) as the fraction of the actual output voltage versus the theoretical potential of the involved reaction.

$$PE = \frac{V_{OUT}}{E_{RED} - E_{OX}} \tag{2.5}$$

where V_{OUT} is the MFC output voltage.

2.2.2.2 Current losses

In an ideal MFC, the anode is the unique ultimate electron acceptor available to bacteria for the oxidation of the substrate. In practice however, a fraction of electron may well migrate to the cathode through the electrolyte or react with alternative electron acceptors like oxygen and non-organic oxidants. Firstly because the oxygen eventually diffuses in the anodic compartment, secondly because non-organic electron-accepting molecules like nitrate may be naturally present in the substrate (in particular when the substrate is wastewater). Finally, in the absence of viable electron acceptor, some bacteria are able to develop fermentative metabolism pathways.

The current drops are inversely proportional to the electrophilic attraction of the anode that is itself correlated to its potential. When the MFC is in short-circuit, the potential of the anode is close to the potential at the cathode, and the anode is therefore strongly attractive. Bacteria will mostly use the anode as an electron acceptor. Other comparatively strong alternative electron acceptors such as diffused oxygen will divert electrons. On the contrary, when the MFC is in open-circuit, the anode does not attract any electrons, and bacteria are more likely to select alternative electron acceptors, in the order of diffused oxygen, non-organic acceptors, and eventually also fermentation.

As a practical conclusion, the higher the output voltage V_{OUT}, the less attractive the anode, and the more electrons to be quenched by competitive electron acceptors.

The unit representative of current drops is the Coulombic efficiency (CE) defined in Equation 2.6. It is the fraction of electrons effectively used as current versus the total number of electrons n (mol) involved in the internal reactions.

$$CE = \frac{Q_{effective}}{Q_{total}} = \frac{\int Idt}{n \times F} \tag{2.6}$$

where $Q_{effective}$ corresponds to the amount of charges transferred to the anode and Q_{total} corresponds to the total amount of charge produced by the oxidation reaction. I is the output current. The electrons that are not transferred to the anode are called "quenched electrons" and can be represented as a current I_Q.

2.2.2.3 Loss dependencies on the electrical operating point

The locations of the different voltage drops in an operating MFC are schematically represented in Figure 2.2. The corresponding drops are plotted for various load scenarios ranging from open-circuit to short-circuit. The sub-plot at the right-bottom corner represents the proportion of electrons transferred to the anode or diverted in alternative electron acceptors.

The open-circuit voltage (OCV) is usually in the order of 0.7 V, which is small compared to EMF computed with the standard potential of the reactants (≈ 1.042V). The reason is two-fold: first, the local

concentration of reactants can be very different from the concentration in the substrate, even when the rate of reaction is low. The biofilm itself constitutes a complex structure in which the concentration can be very specific [Lejeune, 2003]. These local concentrations result in an EMF, which is lower than the EMF in standard conditions. Second, when in open-circuit, the proportion of diverted electrons is maximum. These alternative pathways contribute to lower the voltage of the anode.

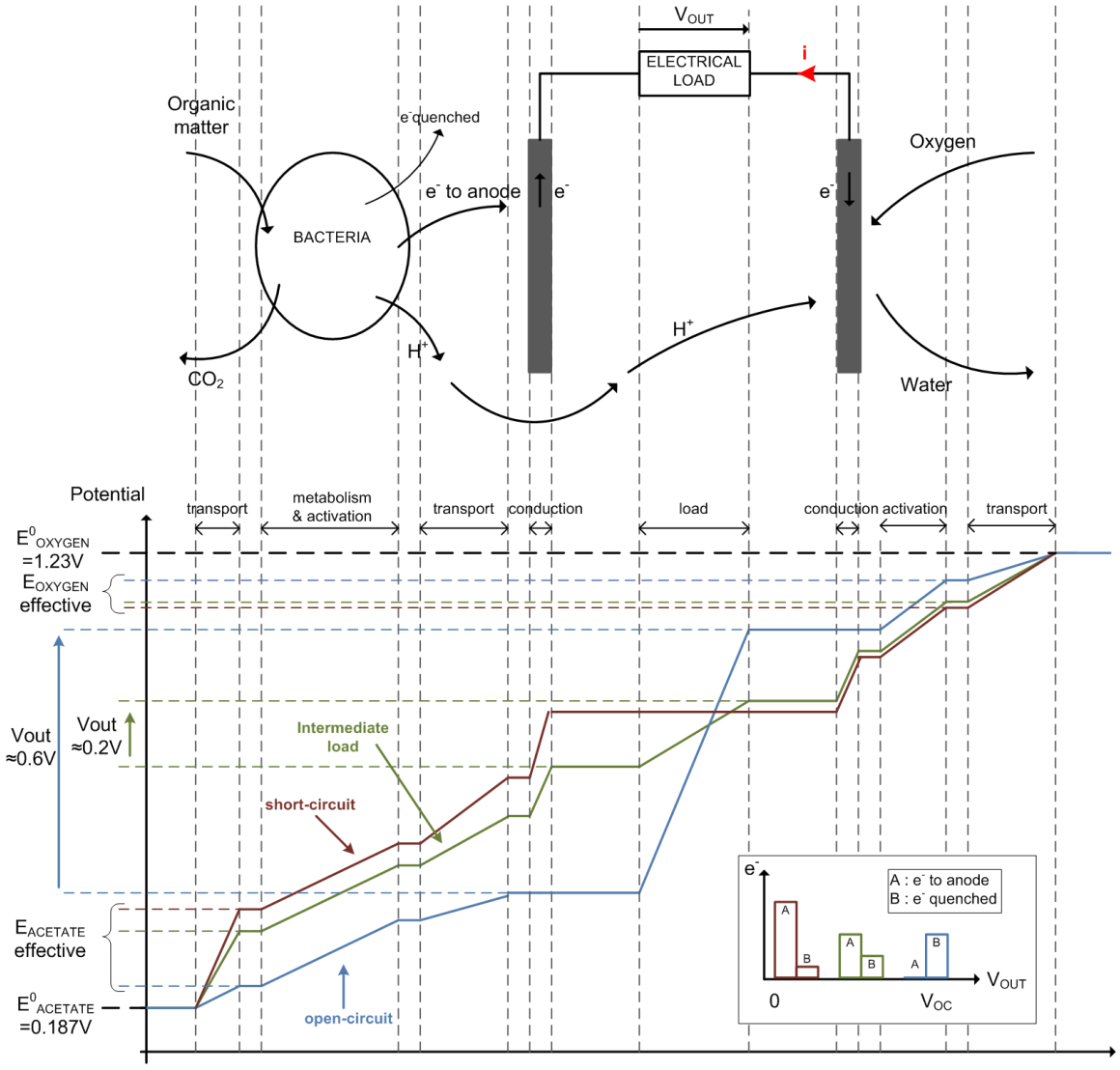

Figure 2.2: Qualitative graph of the voltage drops in the different part of the MFC when the electrical load is varied (effect of pH not taken into account).

2.3 MFCs seen as a black box

Now that the internal mechanisms of MFCs are presented, this section describes a MFC as a black box that converts the chemical energy from the reactants (i.e. organic matter and oxygen) into electrical

energy like in Figure 2.3. This "converter" is studied in terms of energy conversion efficiency, and in terms of static and dynamic electrical characteristics.

2.3.1 Energy conversion efficiency

MFCs, as systems, interact with their external environment in two ways:

1. A chemical flow inputs the reactants (i.e. O_2 and organic matter) and outputs the products (i.e. CO_2 and water).
2. An electrical-load defines the rate at which electrical energy is harvested and as such defines the voltage/current relationship (electrical operating point).

The fraction of the energy actually harvested from the MFC versus the theoretical energy available through the decomposition of substrate is the energy-conversion efficiency (ECE) defined in Equation 2.7:

$$ECE = \frac{\int VIdt}{nF(E_{RED} - E_{OX})} = CE \times PE_{eq} \tag{2.7}$$

where PE_{eq} is the average potential efficiency of an electron transferred to the anode:

$$PE_{eq} = \frac{\int VIdt}{\int Idt \times (E_{RED} - E_{OX})} \tag{2.8}$$

The degradation of substrate can be estimated with the measure the removal rate of either the Chemical Oxygen Demand (COD) or the Biological Oxygen Demand (BOD), which are commonly used to indirectly measure the amount of organic matter in water.

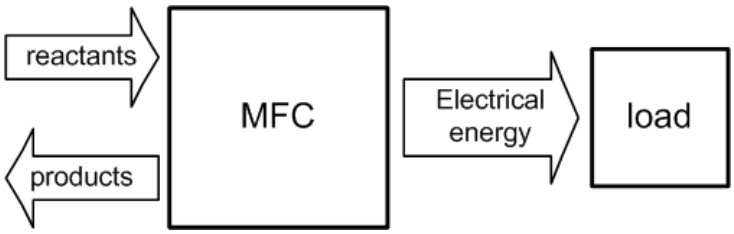

Figure 2.3: A system representation of a MFC

2.3.2 Static electrical characteristics

The static electrical characteristic of a MFC is a representation of its possible output voltage/current relationship in steady-state. Figure 2.4 graphically represents (in blue) the operating points of a lab-scale MFC. This curve is either called a static electrical characteristic curve (or V-I curve) by physicists, or polarization curve by bio-electrochemists.

This curve can be obtained in three different ways: a) imposing a voltage across the MFC and measuring the corresponding output current (potentiostat), b) imposing an output current and measuring

the corresponding voltage (galvanostat) and c) applying a variable resistance at the output of the MFC and monitoring either the voltage or the current (the other value can be computed using the Ohm's law $V = RI$) (resistorstat [**?**][1]). Depending on the method used and the parameters (i.e. sweeping range and sweeping rate), the results can be different. As such, the acquisition method is still debated in the scientific community of MFCs at present.

For a typical MFC like in Figure 2.4, the voltage decreases when the current increases due to the losses described before. OCV or V_{OC} denote the open-circuit voltage. I_{SC} denotes the short-circuit current.

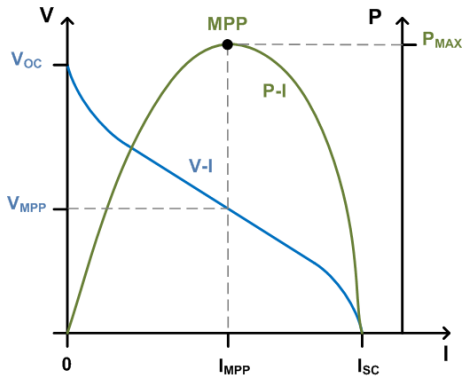

Figure 2.4: Static electrical characteristic of MFCs.

The polarization curve can be represented differently to express the power delivered by the MFC as a function of its output current (e.g. power curve in green in Figure 2.4). The power is null when $V = V_{OC}$ $(I = 0)$ and when $I = I_{SC}$ $(V = 0)$. Between these extreme points, the curve presents a maximum called maximum power point (MPP). The voltage and current at MPP are respectively termed V_{MPP} and I_{MPP}.

The general aspect of these polarization and power curves is similar to the one of chemical fuel cells, except that power levels are a lot lower because of lower current levels. In MFCs, short-circuit current varies from a few μA to few A depending on the size of the cell [Ren et al., 2012]. Normalized surface or volume values are used for current and power densities. In literature, a number of different ways exist to normalize current and power densities and contribute to the difficulty of comparing the static electrical performances of different MFCs [Ieropoulos et al., 2010c]. In this manuscript the normalization is made with respect to the total cathode surface area (TCSA) or to the liquid volume (LV) of the reactor.

The static electrical characteristic curves ideally represent the voltage/current pair that a given MFC can sustain in steady-state, and do not convey information on the dynamic properties of the cell. In practice, these curves are acquired discretely by measuring a limited number of operating points. For each point, the MFC is kept at a given load until its voltage stabilizes and before the point is recorded.

2.3.3 Dynamic electrical characteristics

MFCs have slow dynamic electrical characteristics that can be outlined by the recording of the MFC response to a step of load-resistance like in Figure 2.5. This curve shows the presence of various time-

[1]The paper [Degrenne et al., 2012c] is the result of a scientific collaboration between Laboratoire Ampère and Bristol Robotics Laboratory, UK.

constants. After an immediate voltage decrease corresponding to the instantaneous increase of the ohmic voltage drop, the voltage keeps dropping at a pace similar to that of a first order differential equation, but actually containing different time constants, that relate to various internal mechanisms linked to bacteria (metabolic, physiologic and/or ecologic shifts) and to mass transfer phenomena. These mechanisms are complex and their contribution in the dynamics of MFCs are still not properly understood.

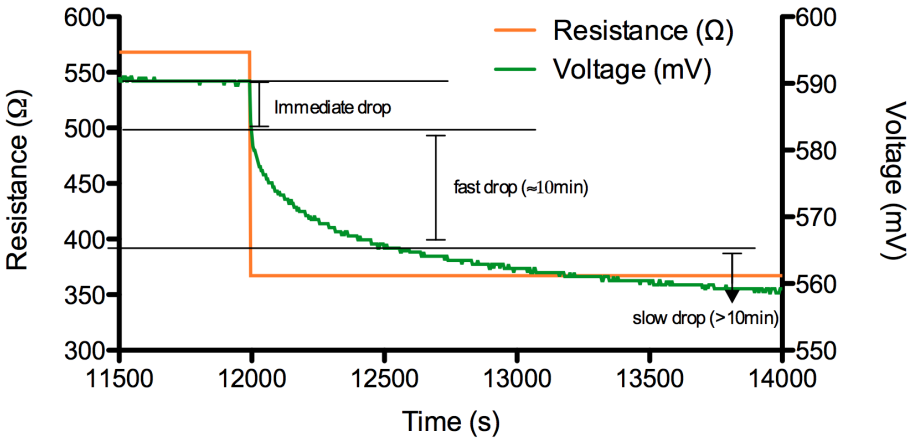

Figure 2.5: Example of MFC response to a load-resistance step (cubic MFC of 4-liters)

The ability of bacteria to store electrons is studied in [Bonanni et al., 2012]. According to the authors, bacteria can store electrons in temporarily reducing iron ions in exocytoplasmic cytochromes. This ability of bacteria to store electrical charges externally and release them later can explain the faster dynamics observed.

Only few research papers were found on the time involved by a metabolic shift because of a change in the electron acceptor. It is probable that bacteria can adapt quickly (in the order of few minutes) to small changes, but that they will take several hours to adapt to a completely different operating point.

The mass-transfer mechanisms are highlighted by experiments on abiotically catalyzed glucose fuel cells (GFC). In [Kerzenmacher et al., 2009], an original galvanostat-based permits to acquire the voltage of GFC for different output currents. At high output current, the time required before stabilization of the voltage can be up to 12 hours, giving an idea of the time-constants related to mass-transport phenomena.

In most research studies, the polarization curves are taken with time steps of few minutes that allow the stabilization of the fastest dynamics but neglect the slow dynamics. The validity of these curves is thus limited, and their analysis must be performed with care.

2.4 Electrical characteristics versus MFC design and operational parameters

The electrical characteristics of MFCs are defined by activation, ohmic and concentration internal phenomena, which are themselves governed by bio-electrochemical and physical mechanisms that can be modified through architectural and operational parameters. The potential to increase the electrical per-

formance of MFCs drive the research community to investigate the influence of a number of these parameters on the MFCs.

Because of the large quantity of scientific references on the subject, the following review is not exhaustive, and only a selection of the most recent works are discussed.

2.4.1 Impact of the reactor design

During the last decade, a systematic experimental survey of materials and architectures was realized, most often as a perspective to increase maximum power, but also to reduce the overall cost [Behera et al., 2010]. The following discussion is a non-exhaustive survey on the recent advances on MFC reactors.

Carbon-based materials in various forms (e.g. paper, cloth, mesh, felt, veil etc) are most commonly used for the **anode** because they are low-cost and bio-compatible conductive materials [Wei et al., 2011]. Graphite fiber brushes with a titanium core were first introduced in [Hasvold et al., 1997] and used in [Logan et al., 2007] to optimize the effective surface area without compromising with the conductivity. Chemical or thermal treatments of anodes can be advantageously used to modify the electrode surface [Cheng and Logan, 2007].

In single-chamber MFCs, the **cathode** is probably the most critical component because it combines the roles of an electrode and of a membrane. Its frame is most often a piece of carbon cloth or carbon paper. On the air side, a diffusion layer is added to ensure water-proofing while enabling diffusion of oxygen. On the internal side, a catalyst (e.g. platinum, or cobalt tetramethylphenylporphyrin (CoTMPP)) layer can be added with a binder (e.g. nafion or polytetrafluoroethylene). In the absence of a catalyst, the reaction at the bio-cathode can be catalyzed by specific microorganisms [He and Angenent, 2009]. The addition of a physical barrier on the internal side decreases the diffusion of oxygen within the substrate and eventually permits to decrease the distance between anode and cathode [Fan et al., 2007].

A number of considerations affect the choice of the **reactor architecture**: a) the materials of the reactor should not be conductive and should be bio-compatible [Ledezma et al., 2010], b) the anode to cathode surface ratio should be optimized such that one of them is not too limiting compared to the other, c) the distance between electrodes compromises between the losses in ion mobility and the diffusion of oxygen and d) the input of substrate should be made at a sufficient rate of supply. The reactor architecture is also influenced by the application that is targeted. In batch mode, as opposed to continuous flow, the supply of fuel is intermittent. For treating wastewater streams are necessarily large and are often made with a tubular design, which facilitates the continuous flow of substrate [Rabaey et al., 2005].

2.4.2 Impact of the operational parameters

Most commonly used substrates in lab experiments are acetate and glucose but a plethora of other **types of organic substrates** were explored in MFCs and were reviewed in [Pant et al., 2010]. More recently, a noticeable experiment showed that urine could be used as a substrate on a previously inoculated MFC [Ieropoulos et al., 2012].

The correlation between **substrate concentration** and power generation was investigated before 2005 by a number of studies [Bennetto et al., 1983, Gil, 2003, Chang et al., 2004, Liu and Ramnarayanan, 2004, Liu et al., 2005a]. More recently, Aelterman in [Aelterman et al., 2008] pointed out that higher substrate concentration mostly reduce the concentration voltage drop at high current densities, having no effect on maximum power which is located in the ohmic region of the polarization curve. Other researches completed this result and showed that at low substrate concentration (i.e. below $1g.L^{-1}$ of acetate), maximum power generation is proportionally linked to substrate concentration [Cheng and

Logan, 2011]. The linear correlation between concentration and maximum current was used in [Di Lorenzo et al., 2009] to realize a biosensor that can measure up to $350 mg.cm^{-3}$ of BOD. Finally, in [Ghoreyshi et al., 2011], an excessive substrate concentration in glucose and date syrup resulted in a decrease of electrical performances.

Temperature changes affect the kinetics (e.g. activation energy, mass transfer mechanisms, solution conductivity, etc.), the thermodynamics (e.g. free Gibbs energy, electrode potentials, etc.) and the nature and distribution of the microbial community. Temperature therefore largely influences electrical characteristics [Larrosa-Guerrero et al., 2010]. Patil in [Patil et al., 2010] showed that an elevated temperature (35 °C) during initial biofilm growth accelerates the biofilm formation process and that biofilms grown at an elevated temperature are more electrochemically active at such temperature than those grown at a lower incubation temperature. Similar results were found in [Larrosa-Guerrero et al., 2010] where MFCs fed with brewery wastewater were tested in batch mode at different temperatures ranging from 4 to 35 °C. At 4 °C, final COD removal was 58% (compared to 94 % at 35°C) and volumetric maximum power was $15.1 mW.m^{-3}$ (compared to $174 mW.m^{-3}$ at 35°C). Other experiences show that the effect of temperature depends on the type of substrate. In [Ahn and Logan, 2010], power generation of identical MFCs was monitored with different substrates at ambient (23 °C) and mesophilic temperatures (30 °C) with various substrates. With acetate and butyrate, there was relatively little effect of temperature on maximum power densities. Howerer, power densities for propionate were 27% higher at mesophilic temperature than under ambient conditions.

The **ionic strength** of substrate has a direct impact on its conductivity for proton transport from anode to cathode and as such on the value of the internal resistance. In [Liu et al., 2005b], ionic strength was increased from 100 to $400 mM$ by adding NaCl and power output consequently increased from 720 to $1330 mW.m^{-2}$.

Finally, the **pH** affects the presence and metabolism of bacteria, affecting the electrical performances [Gil, 2003]. In a batch MFC, the pH evolves depending on the membrane type, eventually leading to poisonous conditions [Rozendal et al., 2007].

2.5 Relations between MFCs and the electrical load

The electrical performances of MFCs are determined by a large number of structural and operational parameters as discussed above. Another parameter that is often neglected by the research community concerns the electrical-load (defining the operating point) at which the MFC is operated both during biofilm maturing and once the biofilm is mature. The electrical operating point is interlinked with the metabolism of bacteria and to other internal mechanisms such as mass transport phenomena and as such it influences the short-term and long-term production of electrical energy and consumption of organic matter.

2.5.1 Load and biofilm initial growth

At present, most published reports use a fixed resistor value as a load both during start-up and steady-state operation. The resistor is usually arbitrarily set to 1 kΩ. Such a load resistance is very impractical and does not mean anything. It may either set the operating point in the activation, ohmic or concentration region, depending on the performance of the studied MFC, and lead to completely different effective loading scenario from one MFC to another.

The effect of different external resistance on the start-up process was investigated in [Lyon et al., 2010] and [Zhang et al., 2011]. While the first paper observes a difference in the biofilm structure only and no difference in electrical performances, the second paper shows that the long-term electrical performances (current and power generation) are also modified. In particular, the MFC started-up with a low resistance can later sustain higher current densities. While both papers outline the impact of electrical-load on the internal mechanisms of MFCs, they are contradictory on whether electrical load impacts future electrical performances or not.

2.5.2 How electrical load determines the power generation

The effect of external resistance on a mature MFC was investigated in [Aelterman et al., 2008]. It was found that when MFCs are operated at low load resistances, the maximum currents observed during polarization are higher because the phenomena associated with mass transfer or kinetic limitations are decreased. In [Katuri et al., 2011], the COD removal rate was investigated for different output resistances. The paper shows that high resistance values (low current densities) reduce COD more slowly and increase the cumulative electrical energy produced by a given amount of organic fuel. The latter observation indicates a better ECE for high resistance value. In [Rismani-Yazdi et al., 2011], a MFC was operated with different load resistances. Maximum power was then estimated with polarization curves. Low load resistance resulted in higher maximum power. In addition, at high resistance value, a difference in bacterial metabolism is observed with an increase in the production of short chain fatty acids.

It is clear from the literature review that the electrical load can provide optimum conditions for maximum power production, bacterial development or substrate consumption.

2.6 Configuration of a large number of MFCs

The association (e.g. series and/or parallel) of a large number of individual MFCs offers very interesting opportunities for electrical energy generation: a) the association of standardized small-scale elementary MFCs permits the conception of a MFC that answers more attractive specifications in output power, b) the series association can advantageously scale-up the low output voltage of an individual cell and c) a system built on numerous elements is more robust against the non-uniformity or deficiency of a fraction of its individual elementary cells. In addition to these three points, several research examples show that higher power-densities can be achieved with small scale MFCs, thus encouraging the association of small-scale elementary MFCs instead of the construction of large-scale devices.

2.6.1 Issues relative to MFC scaling-up

Literature reports the study of MFCs ranging from few μL [Qian et al., 2009] to several liters [Dekker et al., 2009]. The effect of MFC volume on the electrical performance was analyzed in [Clauwaert et al., 2008] through the plot of the volume-based internal resistance as a function of reactor volume for a selection of scientific papers. These papers report on the electrical performance obtained with different MFCs and under different operating conditions, which make it difficult to attribute the results to the volume of MFCs only. A number of other scientific papers outline the decrease in power densities when reactors are scaled-up [Logan, 2010, Dewan et al., 2008]. To explain these results, a number of hypotheses are given in [Liu et al., 2008, Ieropoulos et al., 2008, Dekker et al., 2009]: a) in large MFCs, the electrode surface is larger and the distance between the site where an electron is generated

at the anode and the location where it exits to the external circuit can be large, b) the resistance in the interconnections become significant in large MFCs because of the higher output current levels, c) the substrate is less likely to spread uniformly in large-scale MFCs, resulting in mass-transfer limitation and d) the structure of large-scale MFCs is less controllable, leading to more internal non-uniformities.

There are presently two trends in the research community on MFCs: one addresses the issues related to scaling-up MFCs with the optimization of large-scale designs, and the other focuses on the association of a large number of small-scale MFCs as an alternative to large-scale designs [Ieropoulos et al., 2010a]. For applications such as wastewater treatment, it is most probable that a combination of both approaches will be necessary.

2.6.2 Electrical connection in series

When connection of a large number of MFCs is intended, three main scenarios are conceivable: serial or parallel association, or a combination of both. While parallel connection adds currents and is similar to scaling-up a MFC in volume, serial association adds voltages. The latter configuration steps-up the low input voltage of elementary MFCs, but has its own limits, reported in a number of scientific papers as outlined below.

In [Aelterman et al., 2006], 6 MFCs were connected in series, resulting in an OCV of $4.16V$. The individual voltages of 6 MFC units connected in series diverged at high current densities, some of them even polarized negatively, absorbing energy instead of generating it. This phenomenon is called “cell reversal” and was attributed to either inadequate fuel supply or limiting catalytic substrate conversion of some microbial consortia. The same phenomenon was also observed in an array of μL-sized MFCs [Choi and Chae, 2011]. This time, the result was attributed to the impedance mismatch among cells resulting from the non-uniform manufacturing process. Whether it is caused by fuel supply, microbial or reactor non-uniformities, the impedance mismatch is definitely the reason for voltage reversal, like with other electrical generators such as electromagnetic transducers [Degrenne et al., 2012d]. Voltage reversal is detrimental to power generation because the concerned MFC absorbs the energy produced from the others. To a lesser extent, voltage divergence is also detrimental because it results in operation of MFC units at different operating points. The effect of non-uniformities on MFC serial connection is formally described in Chapter 11.

2.6.3 Fluidic connection

Another phenomenon impacts the electrical performance of serially connected MFCs when they are hydraulically connected. In this configuration, a number of studies show that hydraulic couplings create internal cross-conduction and result in a poor stack efficiency.

These phenomena were first described and discussed in [Zhuang and Zhou, 2009]. The authors also investigated how cross-conduction was minimized through controlling the distance between the electrodes and the cross-sectional area of the substrate flow. Ieropoulos and his team in [Ieropoulos et al., 2008] designed a robot powered by MFCs that are hydraulically connected via a drop-by-drop system that prevents the detrimental consequence of continuous fluidic connection [Ieropoulos et al., 2010b]. The impoverishment of substrate for the last MFCs of the fluidic association was studied in [Winfield et al., 2012]. Its detrimental consequences were avoided with a sufficient initial substrate concentration.

Chapter 3

Scientific contribution

Contents

3.1 Materials and methods 26
3.2 Modeling of a MFC 29
3.3 Electrical performances of a large number of MFCs at MPP 33
3.4 Test of a FOCV MPPT algorithm for MFCs 37

3.1 Materials and methods

The experimental work of this thesis was conducted using lab-scale MFCs and a dedicated testing environment. The MFCs were built based on state-of-the-art processes, but using an original low-cost and highly replicable reactor based on commercially available draining-tubes. The testing environment enables the characterization of MFCs under various electrical-load scenarios. In particular, it permits automatic acquisition of static polarization curves and tests under maximum power point electrical load.

3.1.1 Construction of lab-scale MFCs

Single-chamber MFCs outperform their dual-chamber counterparts for combined energy production and wastewater treatment because they do not require aeration of the cathode chamber. Two sets of single-chamber batch-mode MFCs were designed in the scope of this work:

- The **A-series** are made of a single graphite fiber brush and of a single air-cathode. The brush (Gordon Brushes Inc, USA) has a diameter of 10 cm, a length of 2.5 cm and is twisted on a 5 cm titanium wire. The cathode is composed of a carbon cloth frame on which a PTFE-based diffusion layer was heat-coated on the external side, and a catalyst layer with nafion as a binder ($0.1 mg.cm^{-2}$ Pt) was applied on the internal side. The distance between the edge of the anode and the cathode is 4 cm. This series was replicated in four MFCs each with a different total cathode surface area (TCSA) and referenced A03501, A06401, A08401 and A10901 because the diameter of their cathode is respectively 35, 64, 84 and 109 mm. The test of these MFCs showed that maximum power was proportional to the TCSA (results not shown) and thus suggested that the cathode was limiting the performance.

- The **B-series** are made using two graphite fiber brushes and two air-cathodes for improved performances (Figure 3.1). The two brushes have a diameter of 5 cm and a length of 5 cm and 10 cm respectively and are twisted in the center of a 15 cm titanium wire. The cathode design was unchanged. The anodes were located in the center of a cylindrical reactor with one cathode on each side, at a distance of 4 cm from the edge of the anode. Ten identical MFCs were constructed with the same cathode area and are referenced B10901 to B10910.

Both designs use low-cost PVC draining tubes for the reactor. The internal liquid volume of the A-series was estimated to be $1L$ and the one of the B-series to be $1.3L$. The cathode was fabricated manually, using a paintbrush as described in [Middaugh et al., 2006]. The cathodes are attached to the leads of the tubes by contact pressure and an addition of silicon sealant for water-proofing. Electrical contact with the anode was facilitated by the titanium wires that pass through the reactor, used directly as an electrical contact. At the cathode, a titanium wire was pressed between the internal side of the cathode and the reactor, resulting in a rather less reliable physical contact. This was addressed by the construction of cathodes with improved stainless steal collectors (Paxitech, France), that are out of the scope of the thesis.

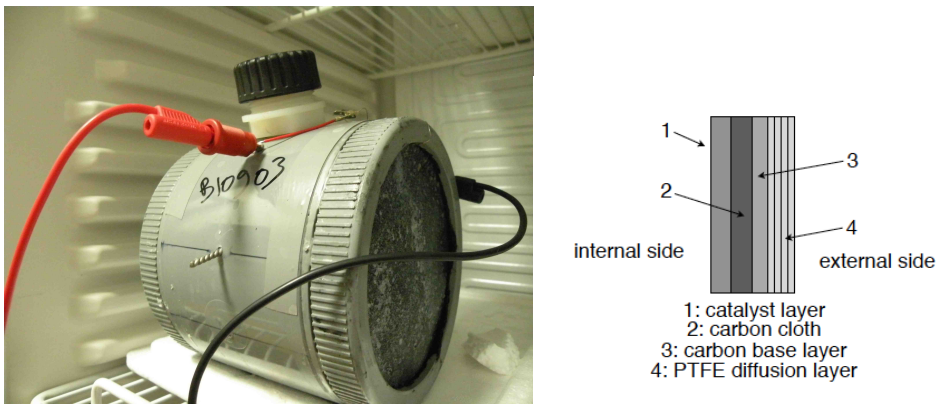

Figure 3.1: Lab-scale single-chamber B-series MFC (left) and schematic representation of the cross-section of the air-cathode (right).

3.1.2 Automatic resistorstat

An original testing environment[1] was developed to test up to ten MFCs simultaneously (Figure 3.3). It controls the output load (resistance) of each MFCs independently. The resistance ranges from 4.7 Ω to 5 kΩ with steps of 4 Ω, plus open-circuit with the voltage recorded at the same time.

One of the system's function allows the operator to automatically sweep a series of resistances. The time-step Δt can be set by the operator to permit stabilization of the voltage (slow MFC dynamics). The load-resistance can be swept from high to low values thus realizing automatic acquisition of polarization and power curves. Other sequences of resistor values can be used to test MFCs with an extensive choice of loading scenarios.

[1] The automatic resistorstat was constructed together with Pascal Bevilacqua, engineer at Laboratoire Ampère.

Another one of the system's functionality permits to control the resistance using a so-called MPPT algorithm and to record the maximum power in real-time. This can be done using a P&O algorithm, or a voltage regulation (FOCV) algorithm which are described now:

- **P&O algorithm** starts with an arbitrary resistance chosen by the operator (e.g. 1 kΩ). After a defined time-step (e.g. 5 min), it records power and modifies the resistance with proportional steps k_{MPP} set by the operator (e.g. $k_{MPP} = 1.2$, the new resistance being therefore 1.2 kΩ). Such a proportional resistor step enables increased sensitivity for low resistance values. After a time-step Δt, the power is recorded again. If it increases, the MPP is for higher resistance values and the algorithm next compares powers for higher resistances (e.g. 1.2 kΩ and 1.44 kΩ). If it decreases, the MPP is for lower resistance values and the algorithm next compares powers for lower resistances (e.g. 0.83 kΩ and 1 kΩ). The operation of this algorithm is illustrated in Figure 3.2 with $k_{MPP} = 2$.

a)

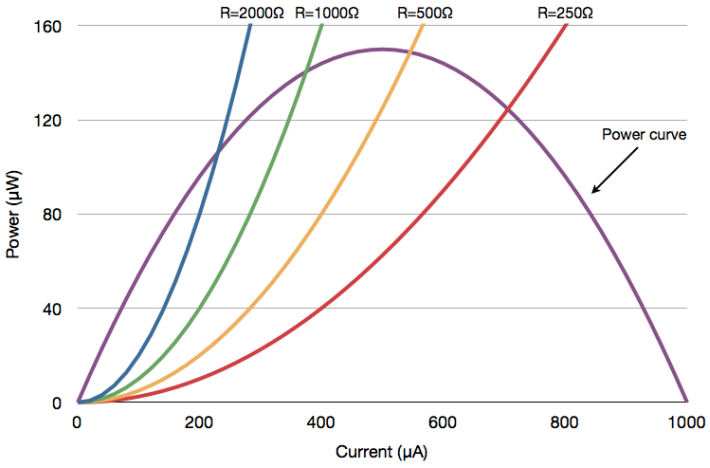

b)

Time (min)	Resistance (Ω)	Power (µW)
5	1000	140
10	2000	105
15	500	145
20	1000	140
25	250	125
30	500	145
35	500	145
40	1000	140
45	250	125
50	500	145

Figure 3.2: Ideal operation of the P&O algorithm with $\Delta t = 5$ min, $k_{MPP} = 2$ and a first resistance value of 1 kΩ. a) represents the P-I curve of a MFC with an internal resistance of 600 Ω and few "equi-resistance" curves, b) represents the time series of the load resistance and the corresponding power.

- **FOCV algorithm** senses the open-circuit voltage every 24 hours and controls the load resistance to impose a voltage equal to one-third of the open-circuit voltage. This ratio approximately corresponds to the MPP voltage like presented in the experimental Figure 3.4. This is because of the

large activation losses with the tested MFCs, but the ratio can be different with other MFCs. If the voltage is higher than one-third of the OCV, it reduces the resistance by 20 %, and if the voltage is lower, it increases the voltage by 20 %.

For both algorithms, a limitation is that the optimal output resistance is approached with 20 % accuracy which impacts the effectiveness of the electrical production. Decreasing the proportional resistor steps adversely affects convergence speed.

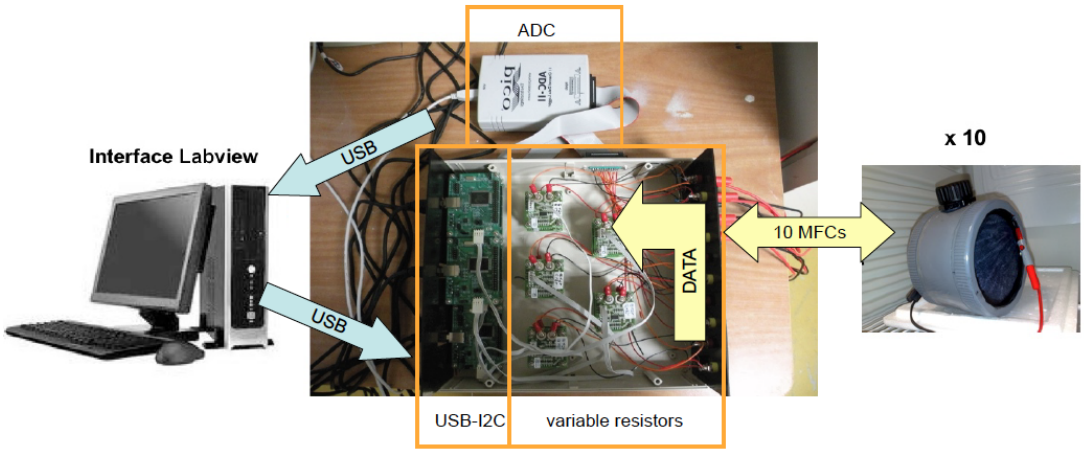

Figure 3.3: Measurement tool

3.1.3 Operational environment

MFCs are operated in batch-mode. They are inoculated with wastewater (Limonest wastewater treatment plant, Grand Lyon, France) and $1g$ of acetate (the initial concentration is therefore $9.4mMol.L^{-1}$ for the B series MFCs). During inoculation, the load is arbitrarily set to 1 kΩ for each cell until the output voltage increases (we attribute this to the development of an electrogenic biofilm at the anode) and then output voltage drops(we attribute this to the consumption of the acetate).

MFCs are kept in a thermostatically controlled incubator which is by default set to 30°C and regularly fed with sodium acetate after the power decreases.

3.2 Modeling of a MFC

The various voltage drops discussed in the literature review correspond to physical phenomena which depend on the current density at which the MFC operates. Previous works on HFCs gave an analytical description of the voltage drops. This section[1] applies the analytical expressions in [Larminie and Dicks, 2003] to MFCs, with the objective to build an analytical model of the electrical characteristics.

[1]This section was realized with the help of Marcelino Seif from Université Libanaise, Beyrouth, Lebanon.

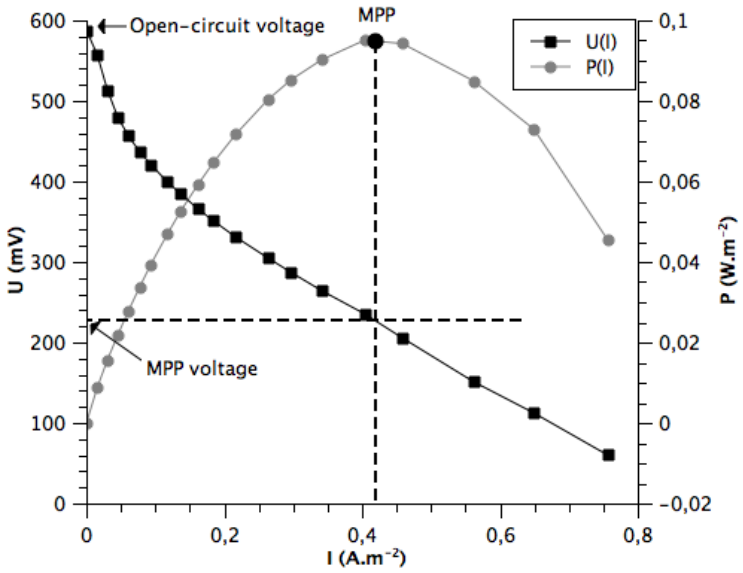

Figure 3.4: Experimental polarization and power density curves normalized to the cathode area (MFC04 during experience 3)

3.2.1 Analytical model of losses

Based on the previous analysis, the output voltage of a MFC is governed by Equation 3.1 :

$$V_{OUT} = EMF - \eta_{act}(I + I_q) - \eta_{Ohm} - \eta_{con} \tag{3.1}$$

where $\eta_{act}(I + I_q)$ is the activation voltage drop related to the sum of the output current, I, and the current lost to alternative electron acceptors, I_q. η_{ohm} is the ohmic voltage drop and η_{con} is the concentration voltage drop. The above equation can be simplified as follow:

$$V_{OUT} = V_{OC} - \eta_{act} - \eta_{Ohm} - \eta_{con} \tag{3.2}$$

In an electrochemical cell such as a hydrogen fuel cell (HFCs), the activation, ohmic and concentration voltage drops can be modeled in detail. The activation drop is usually represented by Tafel's model, the ohmic drop by a Ohm's law, and the concentration drop by the Nernst equation. MFCs are governed by the same mechanisms as HFCs except that they also include bacterial mechanisms. Following the demonstration in [Larminie and Dicks, 2003], the output voltage is expressed by as:

$$V_{OUT} = A - B\ln(I) - R_{Ohm}I - D\exp(E \times I) \tag{3.3}$$

where A, B, D, E and R_{Ohm} are constants to be determined. The expression of the activation losses is valid when $I > 1A$ which is not a valid assumption in the case of MFCs. When currents below 1 A

are considered, it can be modified by an almost equivalent expression. The output voltage is therefore modified as follows for MFCs:

$$V_{OUT} = A - B\ln(\frac{I}{C} + 1) - R_{Ohm}I - D\exp(E \times I) \tag{3.4}$$

where C is a constant. When $I = 0$, A and D are related by the equation $V_{OUT} = V_{OC} = A - D$.

In terms of electrical equivalent circuit, the analytical equations above can be represented by an ideal voltage source and a number of electrical components connected in series and responsible for the different voltage losses. The ohmic losses are represented by a constant resistance while the other losses are non-linear and are represented in Figure 3.5 with variable resistances. The dynamics on the non-immediate mechanisms (i.e. activation and concentration) can be represented using electrical capacitors which behave like reservoirs of charge.

The combination of static and dynamic mechanisms are represented in the equivalent electrical model in Figure 3.5 (right model). This model can be further simplified to merge the activation and concentration losses in a common equivalent resistance, R_{NL}, and capacitance, C_{NL}. When working in the linear region of the MFC, R_{NL} can be considered constant and V_{OC} decreased to V_{OCeq}, like in Figure 3.5 (left model). In this case, one can define the total internal resistance, R_{int}, as the sum of R_{Ohm} and R_{NL}. We therefore have $R_{int} = R_{Ohm} + R_{NL} = R_{Ohm} + R_{act} + R_{con}$.

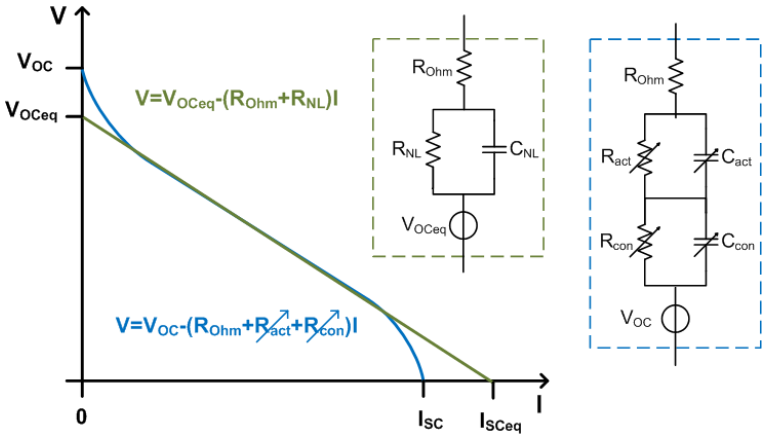

Figure 3.5: Electrical equivalent circuits for a MFC and their static electrical characteristic

3.2.2 Identification protocol

Equation 3.4 defines the analytical expression of a polarization curve with 6 parameters to define. A direct fitting of a polarization curve does not necessarily enable the identification of all parameters accurately because different parameters can affect similar parts on the polarization curve. For example, the voltage drop associated with R_{Ohm} can be hidden by the expression of the activation and concentration drops. The ohmic resistance is therefore primarily determined using electrical impedance spectroscopy (EIS) or current interrupt method like explained in [Zhao et al., 2009]. Other parameters are determined through least square fitting of a polarization curve.

The ohmic resistance R_{Ohm} of MFC B10901 was determined to be 9Ω using EIS. The other parameters were determined through fitting of the experimental polarization curve with the 5-parameters equation (Prism software) as demonstrated in Figure 3.6:

$$V_{OUT} = 0.566 - 0.119\ln(\frac{I}{0.0003} + 1) - 9I - 0.017\exp(318I) \tag{3.5}$$

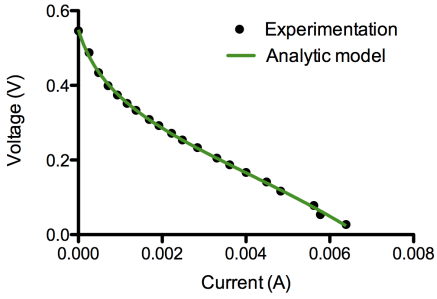

Figure 3.6: Result of the fitting of an experimental curve with the analytical model

The voltage drops associated with the various phenomena, and represented by the above equation are presented in Figure 3.7. This figure outlines the relative importance of the activation losses which are due to the low rate of the reactions taking place at the surface of the electrodes.

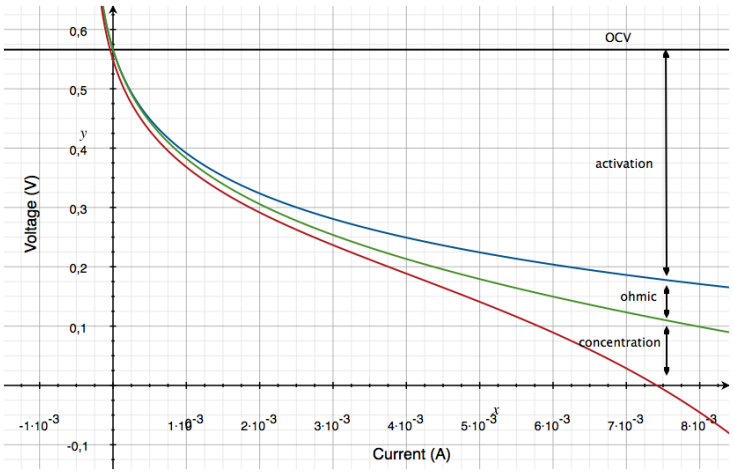

Figure 3.7: Estimation of the activation, ohmic and concentration voltage drops in MFC B10901

3.2.3 Results and discussion

A simple protocol was introduced to perform the analytical modeling of a MFC. The equation developed using Tafel, Ohm and Nernst expressions proved to model sufficiently the static electrical characteristics of a MFC. This modeling permits to estimate the individual share of activation, ohmic and concentration

voltage drops. In the tested MFC, the activation losses were predominant (see Figure 3.7), indicating that the reaction rate at the electrodes were too low. When transposed to the equivalent electrical circuit in Figure 3.5 , $R_{Ohm} = 9\Omega$, $V_{OC} = 0.4V$, $R_{NL} \approx 48\Omega$ but C_{NL} is not defined (a dynamic identification protocol would be required).

Further studies with half-cell MFCs would permit to attribute the activation losses to the bacterially catalysed anode and to the chemically catalyzed cathode.

3.3 Electrical performances of a large number of MFCs at MPP

In this section[1], the MFCs were tested in terms of electrical performances (i.e. maximum power, CE, PE and ECE) at the special operating point corresponding to MPP.

3.3.1 Protocol

The ten identical batch-mode MFCs of the B-series (called MFC01 to MFC10) were simultaneously tested using the resistorstat. Three consecutive experiments were conducted. In experience 1 (EXP1), each MFC was initially new. They were inoculated with wastewater and 1 g of acetate at time t_{1A}. The load was set to be 1 kΩ for each cell. This experiment lasted 40 days until voltage increased and dropped (indicating that an electrogenic biofilm developed at the anode and that acetate was then consumed). In the two next experiments experiences 2 and 3, 1 g of acetate was added at times t_{2A} and t_{3A} respectively and the MFCs were tested using the P&O algorithm until acetate was fully consumed. Between each experiment, water losses were compensated with distilled water. Polarization runs were carried out during experiments.

3.3.2 Biofilm development

During experience 1, the MFCs were inoculated and voltage was recorded during biofilm development as illustrated in Figure 3.8. After 20 days, voltage peaks were visible. The amplitude and the length of these peaks were different from one MFC to another. After 41 days, the voltages of all ten MFCs dropped down to almost 0 V and we assume that the totality of the injected acetate was consumed.

The resistance value of 1 kΩ used during experience 1 is questionable because previous works [Pinto et al., 2011] showed that the proliferation of the anodophilic microorganisms was enhanced with low output resistances (5 Ω). All MFCs produced a voltage peak after more than 20 days in the presence of bacteria and acetate.

3.3.3 Maximum power curves

During experiences 2 and 3 (Figures3.9 and 3.10), most cells showed power increase with time (while substrate was consumed). The substrate concentration and power were not directly related. It appears that MFCs produced almost identical power for any concentration value above a certain threshold (power vs concentration saturation curve). Power then decreased abruptly when concentration was below the threshold. During experience 3, the acquisition was interrupted at times t_{3B} and t_{3C} to realize static polarization curves.

[1] The results of sections 3.3 and 3.4 were published in the Journal of Power Sources [Degrenne et al., 2012b].

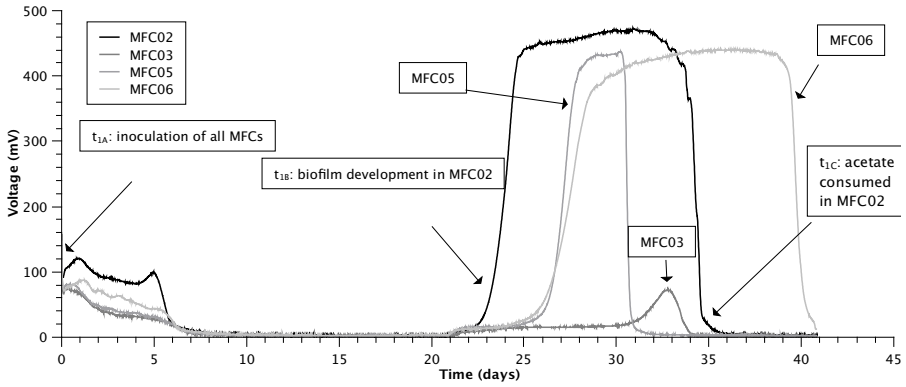

Figure 3.8: Typical voltage curves during EXP1

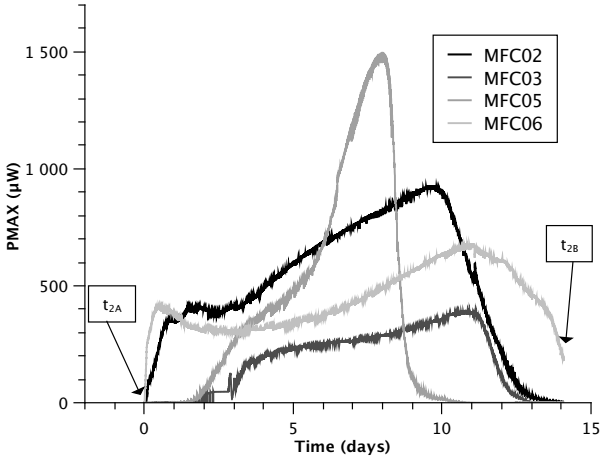

Figure 3.9: Typical power curves during EXP2

In Figure 3.11, the MFC voltage and power and the load-resistance are simultaneously plotted. The load resistance was initially high but quickly decreased to match with the internal resistance of the MFC. When the acetate was consumed at day 7, the load resistance was increased. The MFC output voltage was approx. 200 mV during the energy harvesting time. The curve is wide because the resistance kept toggling between two values, creating a variation in the output voltage (20 % precision because $k_{MPP} = 1.2$). When acetate was consumed at day 7, the MFC voltage stayed in the range of 200 mV but the width of the curve increased, indicating that the MPP tool had more difficulties to track the MPP, probably because of increased time-constants.

3.3.4 Electrical performances of MFCs at maximum power point

Figure 3.12 presents the maximum power achieved during experiences 2 and 3 for all MFCs. Average overall maximum power was about 1.3 mW during experience 3. The peak power value is an indicator that must be dealt with carefully. Indeed, peaks of power can happen after a MFC is temporarily stopped for example to run a polarization acquisition. The low performances during experience 2 show that the

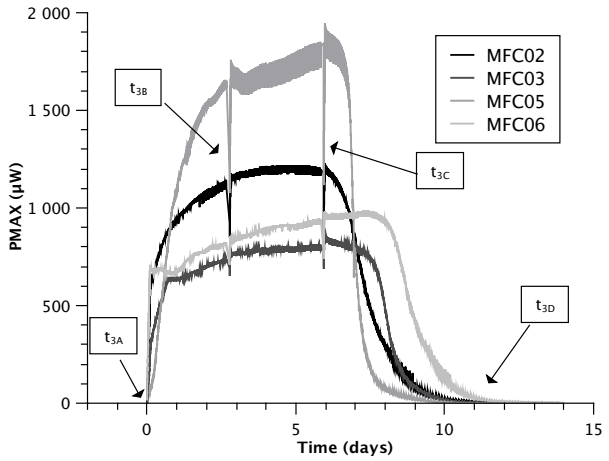

Figure 3.10: Typical maximum power curves for EXP3

biofilm was not fully developed at the end of experience 1. Energy conversion rates are better in EXP3 showing that the biofilm was better developed.

Power was constantly recorded through the consumption of acetate. The integration of the maximum power curve versus time gives the electrical energy harvested from the MFC. These were computed over each experiment (Figure 3.13). The recovered electrical energy can be compared to the theoretical energy available through the full decomposition of 1 g of acetate (i.e. 10364 J) like explained in [Logan et al., 2006, Larminie and Dicks, 2003]. Figure 3.14 gives PE_{eq}, CE, and ECE for all MFCs in experience 3. The average potential efficiency (PE_{eq}) is equal to 18.1 % in average (the minimum value is 16.1 % for MFC08 and the maximum value is 21.1 % for MFC05). Low PE can be explained by the internal multiple voltage losses (activation, resistive, concentration). CE is 38.4% on average (min 30.1 % and max 47.5 %). Low values of CE indicate that only a small fraction of the electrons from the reaction are transferred to the anode. ECE is almost proportional to CE and has an average value of 7.3 % (min 4.9 % and max 9.3 %). The best conversion efficiency of 9.3 % was achieved for MFC09 for CE = 47.5 % and PE_{eq} = 19.5 %. Practically, it means that when 100 % of the organic fuel was consumed, less than 10 % of its energy content was harvested in the form of electrical energy, because of high current drops, but mainly because of high voltage drops.

3.3.5 Analysis of the non-uniformities

Figure 3.15 and 3.16 respectively show the polarization curves and the power curves for four arbitrarily chosen MFCs. The OCV is similar for all curves, but the slope of the curve during the ohmic region is different, leading to short-circuit currents from 6.5 mA for MFC03 to 14 mA for MFC05. Maximum power subsequently also varies between 800 µW for MFC03 and 1800 µW for MFC05.

All MFCs were built identically but were clearly subject to variations due to the lab-scale fabrication process. As can be seen in the Figures 3.12 and 3.13, the maximum power and energy conversion efficiency are wide spread. All experiment conditions being equal, dispersions result from non-uniform manufacturing processes or microbial heterogeneity during inoculation, which is more marked in large-scale, batch-mode systems.

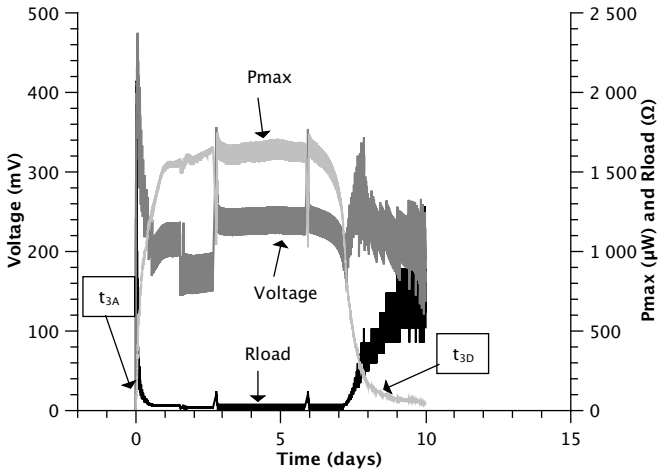

Figure 3.11: Load resistance, voltage, and maximum power for MFC04 in EXP3

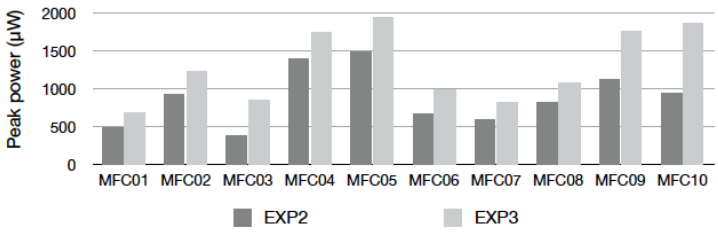

Figure 3.12: Maximum measured power during experiments

3.3.6 Conclusions

The use of MPPT algorithm on ten identical single-chamber 1.3 liter MFCs permitted to impose a realistic load condition and to constantly measure electrical performances of MFCs. Firstly, the CE, PE and ECE were computed and compared with the potential energy input from the injected fuel. Results are summarized in Table 3.1. A best global substrate conversion efficiency of 9.3 % was achieved for the conversion from acetate to electrical energy through microbial fuel cells. Secondly, the presence of variations over identical cells was confirmed. This may be caused either by the non-reproducibility of the construction process, or by the variability of the bacterial systems in large-scale batch-mode systems. The author confirms the necessity to test MFCs in triplicates at least in future research works.

Table 3.1: Key experimental results over experiments 2 and 3, energies are in J and powers in µW

	Min energy	Max energy	Average energy	Min power	Max power	Average power
EXP2	219	633	493	392	1495	888
EXP3	570	974	758	688	1946	1300

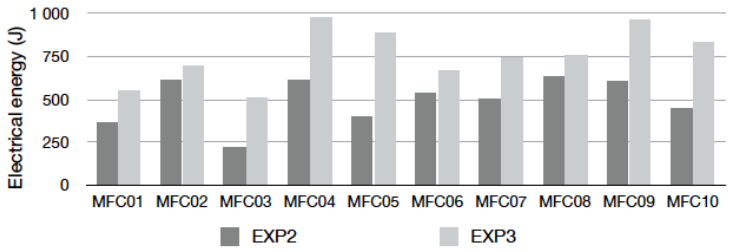

Figure 3.13: Total electrical energy produced from 1 g of acetate

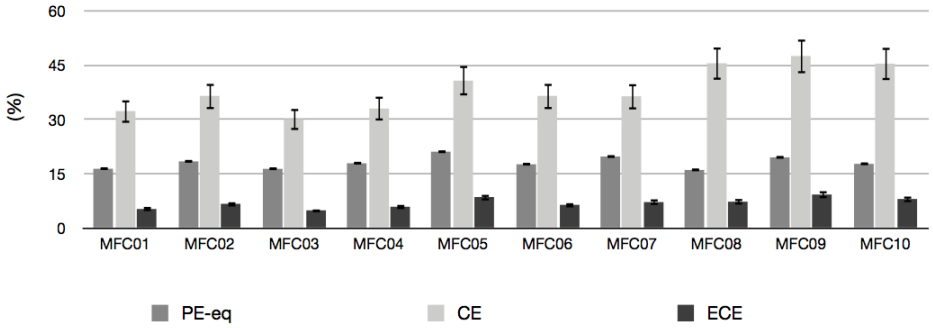

Figure 3.14: PE_{eq}, CE, and ECE for all MFCs for EXP3

3.4 Test of a FOCV MPPT algorithm for MFCs

In this section, a novel algorithm, so-called FOCV, is compared to the previous P&O in terms of energy harvesting performance. These algorithms were presented in the sub-section 3.1.2.

3.4.1 Protocol

The protocol is the same as in Section 3.3. Two additional experiments were carried out immediately after experience 3. In experience 4, the first five MFCs of the B-series (MFC01 to MFC05) were tested using P&O algorithm whereas the last five MFCs (MFC06 to MFC10) were tested using FOCV algorithm. In experience 5, the first five MFCs (MFC01 to MFC05) are tested using FOCV algorithm whereas the last five (MFC06 to MFC10) were tested using P&O algorithm.

3.4.2 Comparison of MPPT algorithms

The objective of experiences 4 and 5 was to compare the ability of P&O and FOCV algorithms to harvest electrical energy from the MFCs. In Figure 3.17, the power curve of MFC05 is plotted for experience 4 (P&O) and experience 5 (FOCV). The curve corresponding to the P&O conforms with the previous experiments. The curve recorded with the FOCV algorithm is interrupted every 24 hours for 20 min in order to re-set the open-circuit voltage. The power level was significantly lower, indicating either that the biofilm was better performing in experience 4 than in the next experiment, or that the FOCV algorithm is less efficient. In Figure 3.18, the power curve of MFC08 is plotted for experience 4 (FOCV)

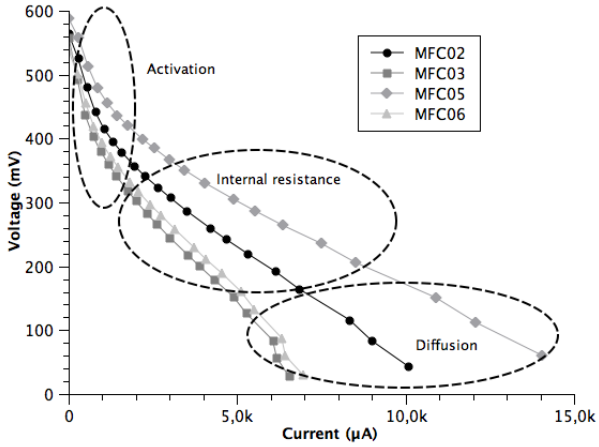

Figure 3.15: Typical polarization curves of MFCs after 6 days of EXP3

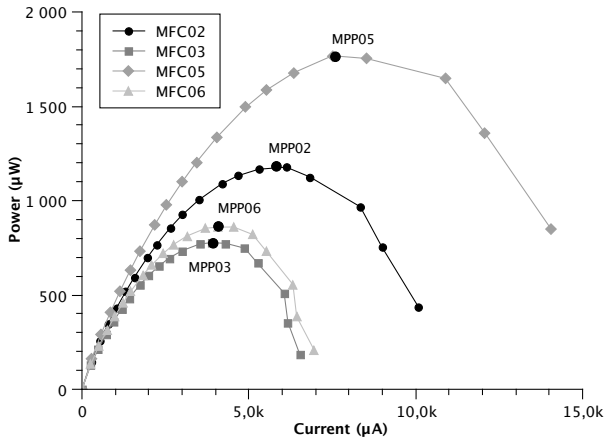

Figure 3.16: Typical power curves of MFCs after 6 days of EXP3

and experience 5 (P&O). The curve recorded with FOCV algorithm indicates this time a rather constant power level over a longer time.

With regards to the differences between the two typical curves under discussion, it is difficult to make valid assumptions on two MFCs only. This is the reason why experiments were largely duplicated. The following discussion considers results of the ten MFCs.

In experience 5, the first set of MFCs produced 20.8 % less energy with the FOCV algorithm than in experience 4 with the P&O algorithm. In contrast, the second set produced 6.8 % less energy in experience 5 with the P&O algorithm than in experience 4 with FOCV algorithm. Experience 5 produced less energy on average than experience 4 (14 %), probably because of batch-mode operation, which is a decaying mode, because the substrate is not regenerated and that the MFC may get self-poisoned in the long-term. Based on this assumption, the P&O algorithm on average produced 6.8 % more electrical energy than FOCV algorithm in average (regardless of the energy decrease in experience 5). The maximum ECE value with FOCV algorithm was achieved with MFC09 in experience 4 and is 8.6 %, compared to a maximum ECE of 9.5 % with P&O algorithm with MFC04 during experience 4.

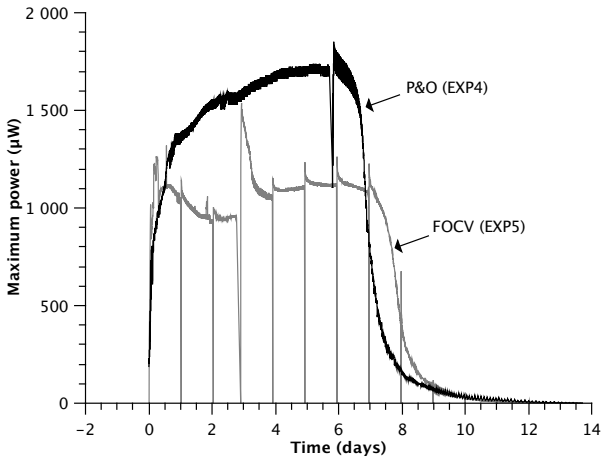

Figure 3.17: Maximum power of MFC05 measured using P&O (experience 4) and FOCV (experience 5) algorithms. The discontinuities on the FOCV curve correspond to the daily sensing of the OCV.

3.4.3 Conclusions

A novel MPPT algorithm was introduced and compared to the state-of-the-art P&O method. Results are summarized in Table 3.2. Best global conversion was 8.6 % with this algorithm. A better tuning (time step, resistance step and reference voltage) of FOCV algorithm would eventually enable to equalize P&O algorithm while easing the implementation of an output DC/DC converter. The advantage of this algorithm being a compromise between the power transfer effectiveness and the implementation efficiency gain compared to its P&O counterpart.

Table 3.2: Key experimental results over experiments 4 and 5, , energies are in J and powers in µW

	Min energy	Max energy	Average energy	Min power	Max power	Average power
EXP4 (P&O)/(FOCV)	560/593	985/888	743/712	675/865	1851/1946	1212/1334
EXP5 (FOCV)/(P&O)	425/411	808/934	588/663	740/642	2265/2566	1290/1384

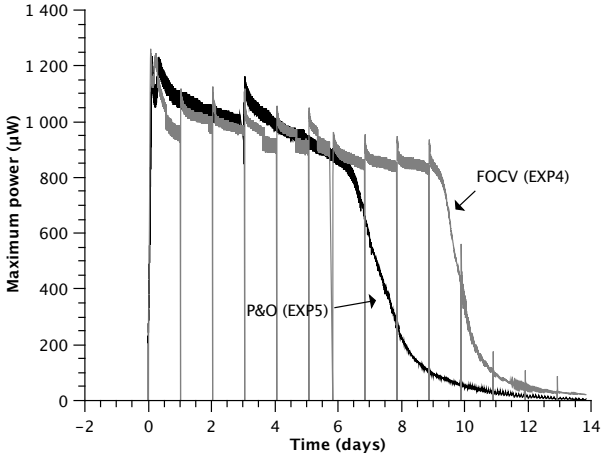

Figure 3.18: Maximum power of MFC08 measured using FOCV (experience 4) and P&O (experience 5) algorithms. The discontinuities on the FOCV curve correspond to the daily sensing of the OCV.

Chapter 4

Summary of the results and perspectives

Contents

4.1 Electrical characteristics of MFCs 41

4.2 Scientific conclusions 42

4.3 Specifications for the power electronics 43

4.1 Electrical characteristics of MFCs

The electrical characteristics of MFCs depend on a number of multi-physical internal phenomena which govern the reactions' rate and the potential at the electrodes.

The **activation voltage drop** is the most significant source of losses in a MFC and results from the large local potential difference necessary to allow a reaction at the electrodes. The dynamics of this phenomenon are diverse and include storage of energy by bacteria, metabolic shifts, and evolution of the microbial community.
The **ohmic voltage drop** is caused by resistance in interconnections and in the electrolyte. This drop is not subject to slow dynamics and is immediate with a change of output current.
The **concentration voltage drop** is caused by the diffusion of reactants and products to and out of the reaction site. The dynamics related to this phenomenon can be very slow.
The **current drops** are caused because of the presence of alternative metabolic pathways other than the anode. They decrease the effective output current and mainly contribute to the activation voltage drop.

When studying MFCs as a power source a number of quality factors need to be considered.

The **maximum power point** can be determined through the polarization curve, or with a MPPT algorithm. Our work proved that the MPP corresponds to an identical voltage, V_{MPP}, and that it can be found by controlling the voltage of the MFC to 1/3rd of its OCV.
The **potential, Coulombic and energy conversion efficiencies** are indicators of how the MFC performs compared to ideality.
The **COD (or BOD) removal rates** are indicators of how fast the organic matter is consumed. It is directly linked to the reaction rate and as such to the output current.

The importance of each of these factors is different depending on the application as reminded in the following:

For **wastewater treatment**, MFCs have to produce maximum power generation while ensuring high COD reduction rate (i.e. wastewater treatment rate).

For **bio-batteries**, the MFC should provide energy to the load at the best energy-conversion efficiency (ECE) to optimize the battery life-time. It should also consume very little fuel when no energy is consumed by the load.

For **ambient energy scavenging**, MFCs capture a certain quantity of electrical energy and provide it intermittently in some bursts of power corresponding to the acquisition and the transmission of a set of data.

In Part I, we considered therefore the performance of MFCs in terms of maximum power, PE, CE, and ECE at the particular electrical operating point called MPP. This operating point is of interest for any application related to energy generation.

4.2 Scientific conclusions

The multi-physical knowledge on the internal mechanisms of MFCs was modeled analytically to elaborate a simple **electrical equivalent model**. This model separates voltage drops that are immediate with a change of current (i.e. ohmic drops) to voltage drops that correspond to time constants (i.e. activation and concentration drops). This was tested and proved to fit adequately with experimental results. This model is a prerequisite to the design of harvesting electrical circuits because it can potentially be used in electrical simulation software packages.

A number of MFCs were constructed based on state-of-the-art technics. Ten MFCs (B-series) were **characterized electrically at MPP** with a novel testing environment that was realized during the thesis. On average they produced about 1.3 mW at 0.23 V in average corresponding to normalized power densities of 1 W.m^{-3}LV or 70 mW.m^{-2} TCSA. At MPP, the best performing MFC with best performances achieved 9.5 % ECE. This low value is the consequence of a low CE (47.5 %) and a low average PE (20 %). Testing ten similar MFCs simultaneously highlighted important non-uniformities in internal resistances that would create detrimental voltage divergence in case of serial associations of several individual MFCs. The differences in performance was such that the weakest MFC produced 688 µW whereas the strongest produced 1946 µW.

Finally, a novel algorithm (FOCV) which senses the OCV and controls the MFC voltage to be a fraction of it (e.g. 1/3rd) was tested and compared to the state-of-the-art P&O algorithm. This algorithm resulted in almost similar performances as the P&O algorithm, while promising much easier implementation in a power management unit (PMU).

The electrical characteristics of MFCs are summarized:
MFC static electrical performances show a MPP averaging 1.3 mW at 0.23 V operating voltage (despite the non-uniformities).
MFC dynamics are complex and the slowest mechanisms can take up to several hours or days.
The dispersion in equivalent internal resistance is very high, causing poor efficiency of MFC association in series.

4.3 Specifications for the power electronics

The three main applications of MFCs (e.g. wastewater treatment, bio-batteries and ambient energy scavenging) imply different final loads as reminded in the following:

For **wastewater treatment**, the final load can either be continuous (DC) to cover the needs of the treatment plant or alternating (AC) if the excess energy is delivered to the grid.

For **bio-batteries**, the MFCs must be able to provide the required power at a given DC output voltage. The energy harvested from the load is again highly non-constant in this configuration.

For **ambient energy scavenging**, the final load is a low-power electronic module composed of sensors and of a wireless data transmission circuit. This circuit has several modes, including a stand-by mode during which it consumes no or very little electrical energy, and a working mode during which it acquires and transmits a set of data. The energy harvested from the load is highly non-constant.

Looking at the form of electrical energy at the output of a MFC, it is clear that an adaptation block (PMU) must be used to interface the MFC and the practical load. The PMU is composed of specifically controlled power electronics. In some applications, where the load profile is highly non-constant, an external energy storage may be necessary to capture energy when the demand of the load is low, and deliver it when the demand of the load is high.

In practice, a DC/DC-based PMU will almost always be used as a front-end interface to MFCs like in Figure 4.1. This first conversion stage can be advantageously complemented by other DC/DC conversion stages to achieve higher step-up ratios, or by DC/AC converters (i.e. inverters) to distribute excessive electrical energy to the grid.

The front-end DC/DC converter modifies the apparent load seen from the MFC such that energy can be harvested at any operating point allowed by the MFC. A special operating point is the MPP which enables energy harvesting at maximum power.

In the case where energy is harvested from a single MFC or several MFCs in parallel, the front-end DC/DC converter requires a specific design because it needs to operate at very low input voltage (0.23 V) and to step-up voltage with a high ratio while operating at high efficiency. This particular configuration in Figure 4.1 will be studied in Part II of this manuscript.

A second approach illustrated in Figure 4.2 is to associate a large number of individual MFCs in series, to remove a constraint on the input voltage of the PMU. However, in this configuration, the non-uniformities will result in voltage divergence between MFCs of the stack. An extra voltage-balancing circuit is required to equalize the voltage of each MFC. The PMU in this case is still necessary, but the input-voltage specifications are much less restrictive and a number of commercial ICs can be used. This configuration will be studied in Part III of this manuscript.

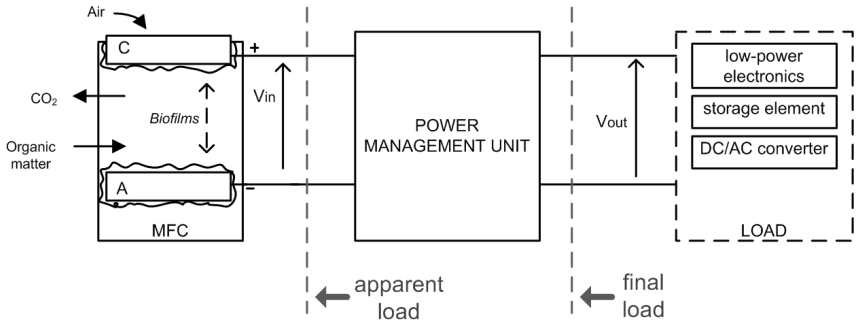

Figure 4.1: Power management unit harvesting energy from a single MFC

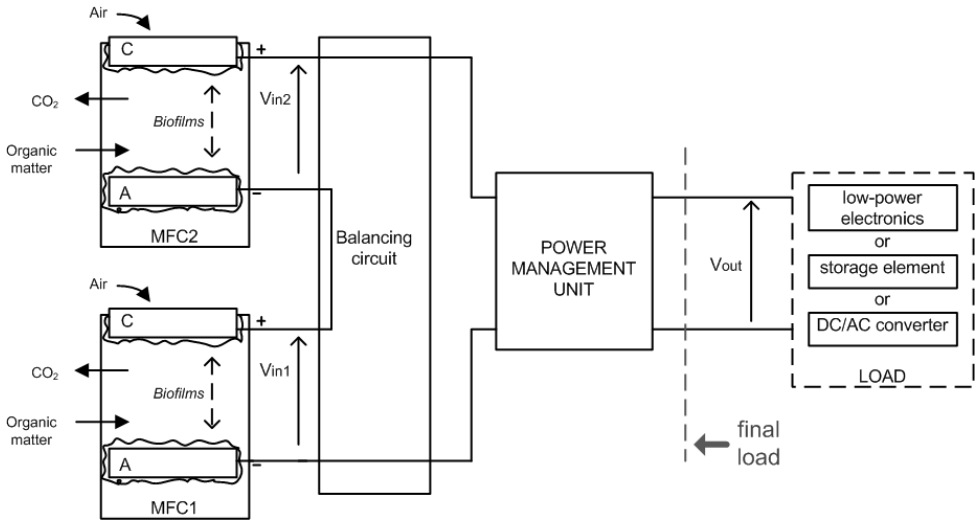

Figure 4.2: Power management unit and voltage balancing circuit harvesting energy from several MFCs connected in series

Part II

Low-voltage power management unit for microbial fuel cells

Chapter 5

Introduction and literature review

Contents

5.1 Low-voltage self-starting circuits 47
5.2 Maximum power point control 51
5.3 State-of-the-art 56
5.4 Conclusion 57

A Power Management Unit (PMU) is necessary to harvest energy from a single MFC or a group of connected MFCs for two main reasons: a) to step-up the voltage to useful levels and b) to control the operating point of the MFC(s) (i.e. MFC voltage). The PMU must perform these functions at a high efficiency. Other requirements depend on the targeted applications as outlined in the following:

1. **For large scale energy production from wastewater**, the energy conversion most probably includes a large number of associated MFCs and converters to supply electrical actuators (e.g. pumps) and/or the electrical grid. The scale is such that total output power is in the order of several kW. The front-end converter stage either operates at power levels well above 1 W, or is segmented together with the MFCs in a large-number of low-power aggregated devices. In both cases, the PMU can be connected to an external source, at least at start-up or for the control circuit supply.

2. **In low-power applications (i.e. energy harvesting and bio-batteries)**, MFCs are good candidates to substitute conventional chemical batteries which require maintenance and are environmentally harmful. In this case, the PMU operates below 1 W and relies on the MFCs alone for its own supply.

One possible PMU architecture is presented in Figure 5.1. It is composed of a DC/DC converter that is controlled on its input through a feedback loop composed of a reference, a sensor, a comparator and a controller.

The requirements on the PMU for large-scale applications are less restrictive and some commercially-available DC/DC converters dedicated to photovoltaic transducers or hydrogen fuel cells can be used [TI, 2008]. For low-power applications, the constraints on the PMU are higher not only because of the low power levels but also because of the requirement to operate autonomously without an external supply. Very few commercial converters are adapted to the requirements for low-power applications.

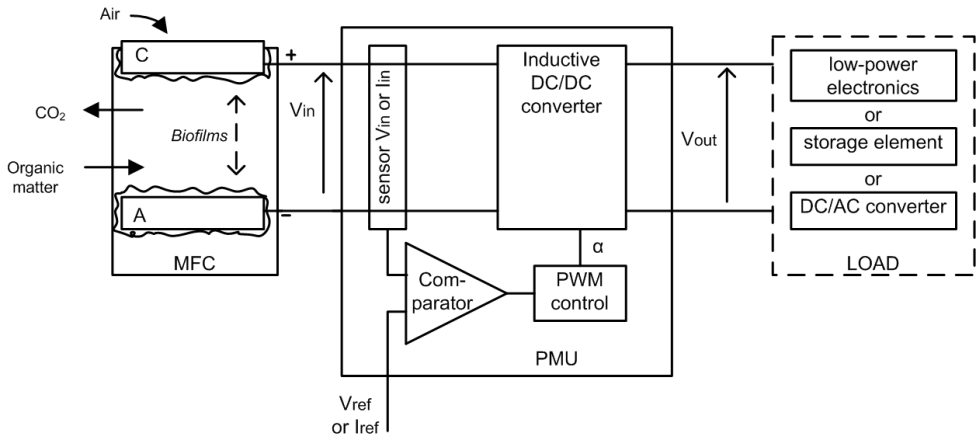

Figure 5.1: Front-end power management unit for harvesting energy from MFCs

For this reason, this thesis focuses on low-power autonomous PMUs for small-scale harvesting. Incidentally, low-power harvesting is a concept that can be extended to large-scale wastewater treatment plants with the association of a large number of low-power MFCs and front-end PMUs.

Even if only a limited amount of low-power harvesting (i.e. scavenging) integrated circuits (ICs) are currently commercially available, the market is emerging and the commercialization of low-power low-voltage PMUs by semiconductor industries is anticipated in the next future. In an effort of differentiation, we choose to demonstrate concepts adapted to MFCs specifically (i.e. based on the knowledge on MFCs in Part I) and to seek characteristics that can't apply generally to other micro-sources. As a first approach, these designs are realized on PCBs with discrete components to permit fast and low-cost prototyping.

5.1 Low-voltage self-starting circuits

5.1.1 Limitation of the threshold voltage of transistors

The start-up voltage of a circuit is the minimum voltage at which a circuit (that has no other external supply) can start operating. Standard PMUs are built using a number of passive (i.e. capacitors or inductors) and active (i.e. oscillator, PWM module, drivers and power switches) components. The active devices rely on semiconductor technologies (generally CMOS for low-power applications) that require supply voltages above a given level for their operation. When the converter operates in steady-state, it can generally self-supply through an auxiliary sub-circuit. The main challenges when operating at low-voltage concern the start-up of the circuit.

Complementary Metal Oxide Semiconductors (CMOS) is a standard technology that offers switching devices with no leakage current. This is an interesting feature for the design of low-power embedded electronics. The threshold voltage of the switches, according to the Shichman & Hodges [Shichman and Hodges, 1968] model is expressed as:

$$V_{th} = V_{t0} + \frac{t_{ox}}{\varepsilon_{ox}} \sqrt{2q\varepsilon_{si}N_a} \left\{ \sqrt{\left|2\varphi_f + V_{SB}\right|} - \sqrt{\left|2\varphi_f\right|} \right\} \tag{5.1}$$

where V_{t0} is the zero-bias threshold voltage, t_{ox} the oxide thickness, ε_{ox} the oxide permittivity, q the charge of an electron, ε_{si} the silicium permitivity, N_a the bulk doping concentration, $2\varphi_f$ the surface potential and V_{SB} the source-substrate voltage.

The threshold voltage of commercially-available discrete CMOS transistors is generally bordered between 0.5 V and some volts in CMOS technology. Very few components have their threshold voltage below 500 mV. ALD110802 (V_{TH} =0.2 V) is a noticeable exception which suffers from large on-resistance (thus making them inadequate as power switches) [Advanced Linear Devices, 2012].

When designing an integrated deep submicron IC, the technology can be chosen to decrease the threshold voltage (reducing the oxide thickness t_{ox} like in Equation 5.1). As can be seen by the Equation 5.1, V_{th} also depends on the substrate voltage. This feature is used in forward body-biased circuits like in [Chen et al., 2011] where an oscillator starts operating at 95 mV.

Table 5.1 shows the threshold voltage for standard CMOS submicron technologies. Low-threshold or sub-threshold designs therefore rely on the availability of specific low-threshold transistors in IC technologies. They operate at reduced efficiency like in [Mishra et al., 2011, Richelli et al.,] because of increased leakage currents, I_L, defined as:

$$I_L = I_{L0} \exp\left(\frac{V_{GS}}{(1 + C_d/C_{ox})\, V_T}\right) \tag{5.2}$$

where I_{L0} is a constant, V_{GS} the gate-source voltage, C_d the depletion capacitance, C_{ox} the oxide capacitance defined as $C_{ox} = \varepsilon_{ox}/t_{ox}$ and V_T the thermal voltage.

Technology	Familly	VTN (mV)	VTP (mV)
CMOS 130 nm	SVT	450	-395
	LVT	340	-300
CMOS 65 nm (GP)	HVT	432	-383
	SVT	340	-329
	LVT	324	-271

Table 5.1: Threshold voltage for various CMOS technologies of STMicroelectronics [Torki (CMP), 2012]. GP is the "general purpose" technology.

The limitation imposed by the threshold voltage of transistors is the main reason why almost no self-powered DC/DC converter starting below 300 mV is commercially available on the market. MFCs usually display an open-circuit voltage above 500 mV and the corresponding PMU needs to start-up below this voltage value. Solutions (e.g. reducing oxide thickness or changing the substrate voltage) exist to overtake the limitations relative to the threshold voltage of transistors. These can only be implemented in integrated designs and are not efficient. Other alternative solutions rely on different start-up mechanisms as described in the following sub-section.

5.1.2 Self-starting techniques

Alternative start-up mechanisms include mechanical and transformer-based methods as described in [Ramadass and Chandrakasan, 2011] and [Damaschke, 1997].

The mechanical start-up uses a "motion activated switch" like in Figure 5.2. When this switch turns-on, energy is stored in the inductor, L. When the switch turns off, this energy is released at higher

voltage in the output capacitor. This method is suitable when a mechanical vibration source is available (e.g. watches, etc.), but obviously not for MFCs.

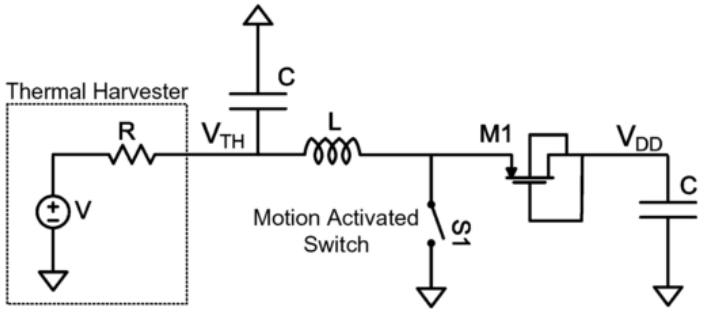

Figure 5.2: A mechanically assisted startup circuit to kick start electrical energy extraction from a TEG [Ramadass and Chandrakasan, 2011]

The transformer-based start-up is also called "Armstrong oscillator" because it was first mentioned in [Armstrong, 1914]. It is suitable for MFCs and can be implemented[1] with a rectifier as in [Grgić et al., 2009, Adami et al., 2011] or in combination to boost and flyback architectures like in [Spies et al., 2007, Damaschke, 1997].

When implemented with a rectifier, the start-up is uncontrolled. In [Grgić et al., 2009], the described rectifier has a half-wave topology like in Figure 5.3 (a). One disadvantage of the topology is that the output voltage is not referenced to the ground, which makes it harder to combine with another ground-referenced main DC/DC converter. The advantage of the circuit is that it starts-up at voltages as low as 6 mV. However, its maximum efficiency is approx. 18 %. The paper studies experimentally the association of several transformers and the use of different diodes. However, no analytical description is given to understand the logic behind the experimental results.

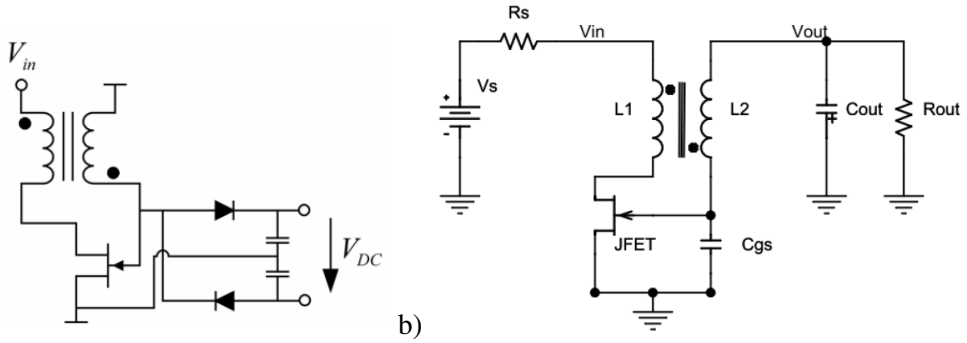

Figure 5.3: Literature transformer-based startup circuits using rectifiers in [Grgić et al., 2009] (a) and [Adami et al., 2011] (b)

The circuit described in [Adami et al., 2011] uses the internal diode of the JFET (in parallel to C_{GS}) to rectify the alternative voltage at the secondary of the transformer like in Figure 5.3 (b). The resulting output voltage is negative, which makes this circuit impractical for most applications. The

[1] The self-start-up with rectifiers, boost and flyback architectures were described and compared in [**?**].

main advantage of this circuit is its simplicity (very low number of components) and its relatively good efficiency (up to 60 %).

Implementation together with boost or flyback DC/DC converters enables a high efficiency and a Pulse-Width Modulation (PWM) control. The circuit proposed in [Damaschke, 1997] is presented in Figure 5.4. The start-up circuit supplies the control (switching circuit) of the main DC/DC converter (main circuit). The start-up circuit topology includes a transformer with three windings. The first two ensure the self-oscillation. The third is connected to the rectifier (diode D_1 and capacitor C_2). The circuit starts-up at voltages just under 300 mV and the maximum overall efficiency is 76 %. No efficiency is given for the start-up circuit alone. The same start-up circuit was simulated (Spice) in [Ben-Yaakov and Fridman, 2004] but the performances of the circuit were not discussed.

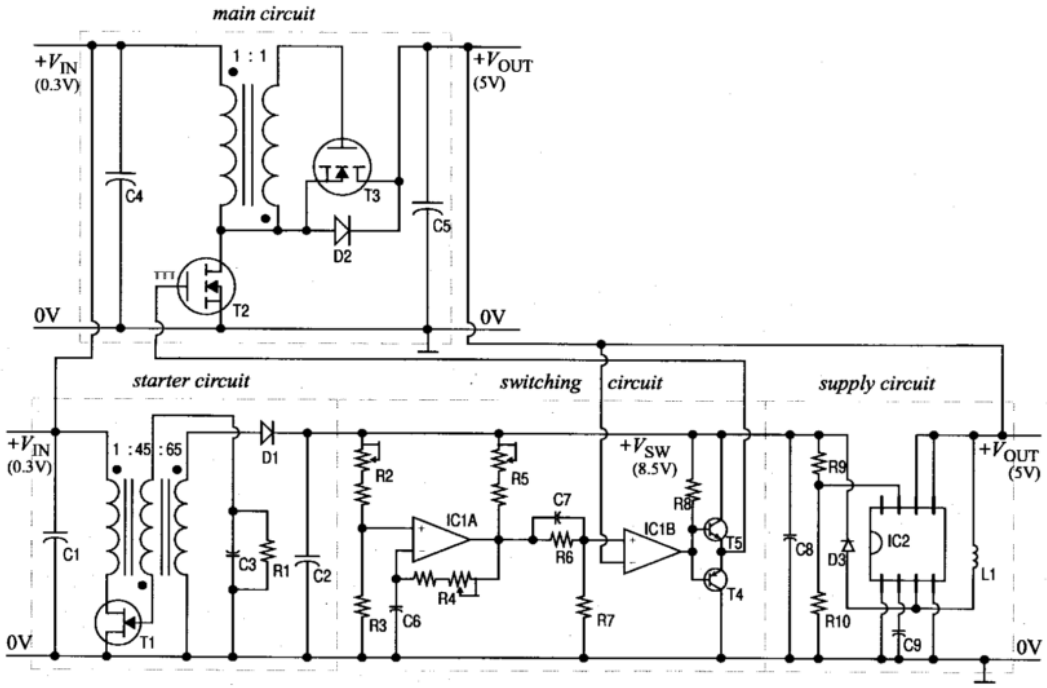

Figure 5.4: Circuit diagram of the complete circuit proposed in [Damaschke, 1997]

The main drawback of the latter circuit in Figure 5.4 is probably the high number of inductive components. The start-up circuit alone requires three coupled windings with turn ratios 1:45:65 respectively. The main circuit requires two additional coupled inductors with turn ratio 1:1. In [Mateu et al., 2007], only one pair of coupled inductors is used for the start-up and the main circuit. In this case, the start-up sub-circuit and the main circuit are "merged" like presented in Figure 5.5. The normally-on JFET T_1 in the start-up circuit is in parallel with a N-channel MOSFET T_2, which ensures the steady-state operation of the circuit at high efficiency. This circuit was recently integrated into a 5x5 mm package ASIC and proposed commercially [Fraunhofer IIS, 2010]. This chip requires an external transformer that can be sized to favor efficiency or start-up voltage. When optimized for efficiency, the circuit reaches up to 85 % maximum efficiency at 300 mV input voltage. When optimized for low-start-up, the circuit operates at voltages as low as 20 mV.

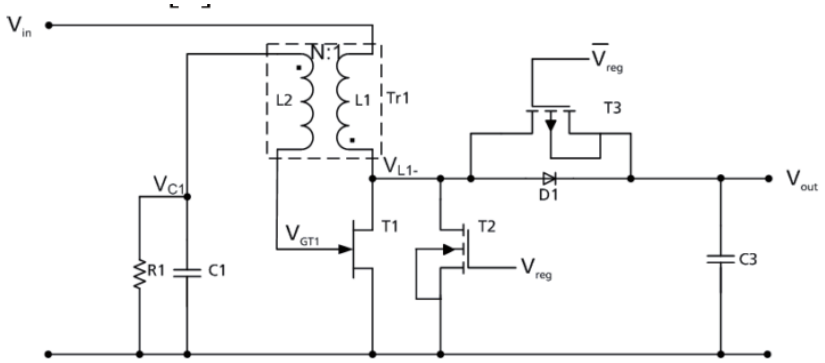

Figure 5.5: Simplified schematic of the self-start-up in [Mateu et al., 2007]

The transformer-based start-up has recently gained interest and was implemented in the LTC3108 IC [LTC, 2010]. This IC has the ability to operate at input voltages as low as 20 mV but the efficiency for input voltages above 0.2 V does not exceed 30 %. In this circuit (Figure 5.6), the start-up circuit is positioned at the input. Its voltage is rectified by a voltage doubler composed of external capacitor, C_1, and the two Schottky diodes connected to it. Other power management sub-circuits are included in the IC to permit different output voltages and battery charging. This circuit is compared to others in Section 5.3.

The transformer-based start-up method appears to be a promising method to conceive autonomous DC/DC converters for low-voltage energy harvesting applications. Several reports describe converters based on this method. No literature can be found however that describes its operation analytically. In addition, to the authors' best knowledge, no circuit demonstrated with transformer-based start-up includes maximum power point (MPP) control to improve global harvesting efficiency. The following section is a literature survey on low-power DC/DC converters implementing MPP control.

5.2 Maximum power point control

In addition to being able to start-up at low input voltage, a restrictive constraint on the PMU concerns its control. MPP control is commonly used for energy harvesting from low-power transducers.

5.2.1 Maximum power point of an energy source

Energy transducers are devices that convert one type of energy (e.g. solar, thermal, electromagnetic) into another one such as electricity. The intrinsic characteristics of the transducers are responsible for their static electrical characteristic curve defined either as V-I or P-I curves. Transducers exhibit two particular points which are open-circuit ($V = V_{OC}$ & $I = 0$) and short-circuit ($V = 0$ & $I = I_{SC}$). Between these two extremes, the power presents a maximum which defines the maximum power point (MPP). The voltage and current defining the MPP (respectively V_{MPP} and I_{MPP}) are not constant but change with input energy and operational parameters. The shape of the V-I and P-I characteristics and the influence of incident power is discussed in the following:

1. **Photovoltaic transducers** exhibit a static V-I and P-I curve like in Figure 5.7. When incident light increases, the current production increases, leading to an increase of maximum power, P_{MAX2}, at a

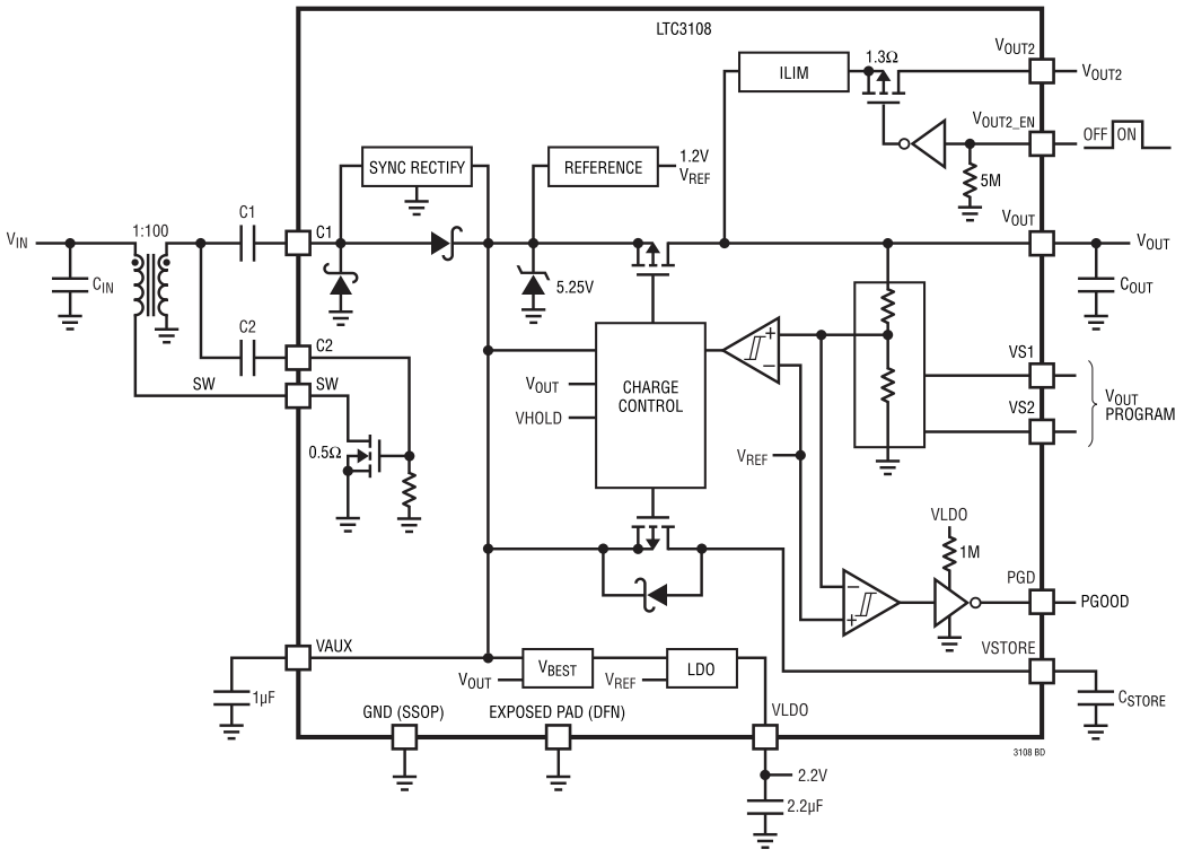

Figure 5.6: Block diagram of the LTC3108 [LTC, 2010]

higher output current, I_{MPP2} . The MPP voltage, V_{MPP}, however is almost unchanged by a change in incident lighting (e.g. because of clouds).

2. **Thermoelectric generators** (TEG) exhibit static V-I and P-I curves like in Figure 5.8. The V-I curve is linear and defined as $V_{OUT} = V_{OC} - R_{int}I$. When temperature gradient in the TEG increases, the increased heat flux causes V_{OC} to increase. The internal resistance R_{int} is unchanged and defined by the structure of the transducer. The MPP voltage and current both increase. If the transducer supplies a resistance, the optimal resistance is constant and equal to R_{int}.

3. **RF transducers** (i.e. rectennas) are composed of an antenna and a RF rectifying circuit [Marian et al., 2011]. Their static V-I and P-I curves are similar to the ones of TEG transducers.

5.2.2 Importance of maximum power point control

To harvest maximum energy from a transducer, its operating point should be set to MPP. This can be done by the PMU through proper control. If the PMU includes a switched-mode DC/DC converter, the control is realized with the duty-cycle at which the power switches are toggled (i.e. pulse width modulation). If the DC/DC converter is capacitive [Seeman, 2008], the control is less straight forward because the

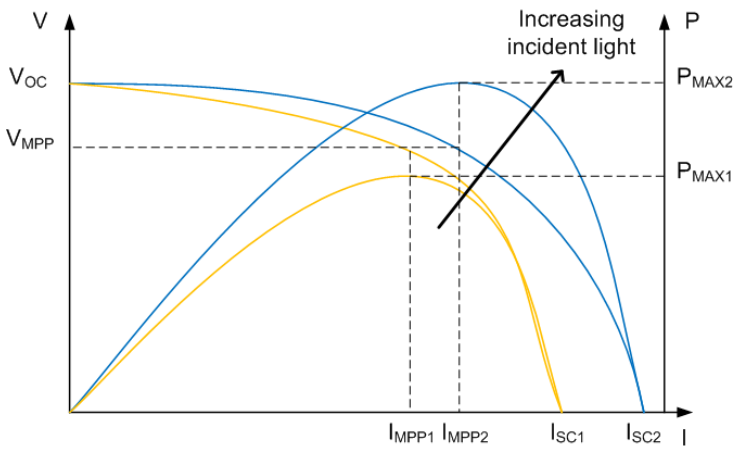

Figure 5.7: Schematic V-I and P-I characteristic curves of a photovoltaic cell for two scenarios of incident lightning.

step-up ratio is defined by the architecture of the converter. One way to change the step-up ratio is to dynamically modify the architecture like in [Le et al., 2011]. As an example, Figure 5.9 shows a topology which permits to provide four different step-up ratios. For a step-up ratio of one, the input is statically connected to the output. For a step-up ratio of 4, the three capacitors are alternatively in parallel to the input (they charge to V_{IN}) and in series with the input and connected to the output. Two intermediate scenarios are possible to provide step-up ratios of 2 and 3.

Whereas some loads can accept a variable amount of input energy (e.g. energy storage and LED) other loads consume a fixed amount of energy and require a fixed voltage at their input (e.g. microprocessor, wireless sensor). If the load does not require the total amount of electrical energy from the MFC, additional power can be stored for an eventual future need, or dispensed in an auxiliary load. In [Kim and Kim, 2011], the energy is stored in a capacitor and the DC/DC converter is turned off when the capacitor is fully charged. It turns on again when the load expresses the need.

There is a large number of MPPT methods which display various functional performance complexity levels of circuit implementation. These two criteria (i.e. performance and implementation complexity) are used in the following to analyze various MPPT techniques in the scope of a front-end PMU for MFCs .

5.2.3 Generic implementation of MPPT methods

Exhaustive reviews on generic MPPT methods (i.e. methods that work on almost any transducer) were realized in [Guo, 2010] and [Esram and Chapman, 2007].

The most common technique is the **perturbation and observation (P&O) method**. This method is defined in [Lu et al., 2010]: “After initialization, the procedure involves applying a small perturbation to the converter (e.g. varying the duty-cycle of an inductive converter). This perturbation results in a small change in the operating point of the source, and hence, in its output power. If the power increases, another perturbation in the same direction is performed. If the perturbation results in a power decrease, a perturbation in the opposite direction is performed. The process is continuously repeated until the MPP is reached. In steady state, the system oscillates around the MPP.”

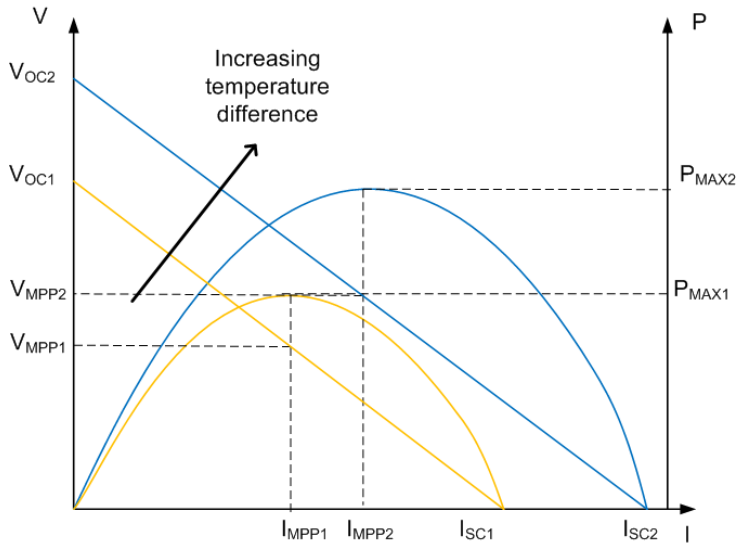

Figure 5.8: Schematic V-I and P-I characteristic curves of a TEG for two scenarios of temperature gradient.

The **gradient method** relies on the same principle, except that the gain (i.e. ratio between output power change and input perturbation) is monitored and used to size the next perturbation. If the gain is high, the MPP is far and the next perturbation is large. If the gain is low, the next perturbation is small. The gradient algorithm offers a better compromise between convergence time and oscillation around MPP than the P&O algorithm, at the cost however of a more complex algorithm.

In [Woodward et al., 2009], a novel algorithm called **multi-unit optimization method** uses two identical sources to perform a MPPT with high convergence time. It was implemented for MFCs with responses to a change of electrical load with slow dynamics. Its advantage lies in the fact that it does not need to wait stabilization of the MFC electrical characteristics. It assumes that the dynamics of the two MFCs are identical and compensate for one another. As such, the algorithm converges quickly. Its main drawback, apart from the complexity of the algorithm, is that it relies on the restrictive assumption that MFCs have strictly identical electrical characteristics. In [Woodward et al., 2010], the multi-unit method is compared to the P&O and gradient methods. "The multi-unit optimization method converged faster than the P&O method. Nevertheless, the performance of the P&O method was acceptable providing relatively low-perturbation frequency. The gradient method eventually failed to converge due to large changes in the curvature of the power curve."

The methods discussed above are suitable for most energy transducers because of their generic nature. However, MFCs are unique in the sense that their dynamics (to a change of load) are very slow and that their P-I characteristic curve presents non-linearities. Therefore, some standard MPPT methods would not necessarily comply with MFCs. The implementation of state-of-the-art MPPT algorithms most of the time requires digital electronics and power sensors, thus leading to complex and dissipative circuit implementations. It includes sensors (i.e. voltage/current/power sensors) and a controler that can either be analog or digital (e.g. microcontroller or FPGA). Digital controllers can be implemented at low power (e.g. with Microchip AN1267 or Actell IGLOO) which feature power consumption in the order of few µW in sleep mode [Tewolde, 2010]. On the contrary, the implementation of current sensors is lossy both because of the required shunt and because of the amplification stage. In addition, the convergence speed

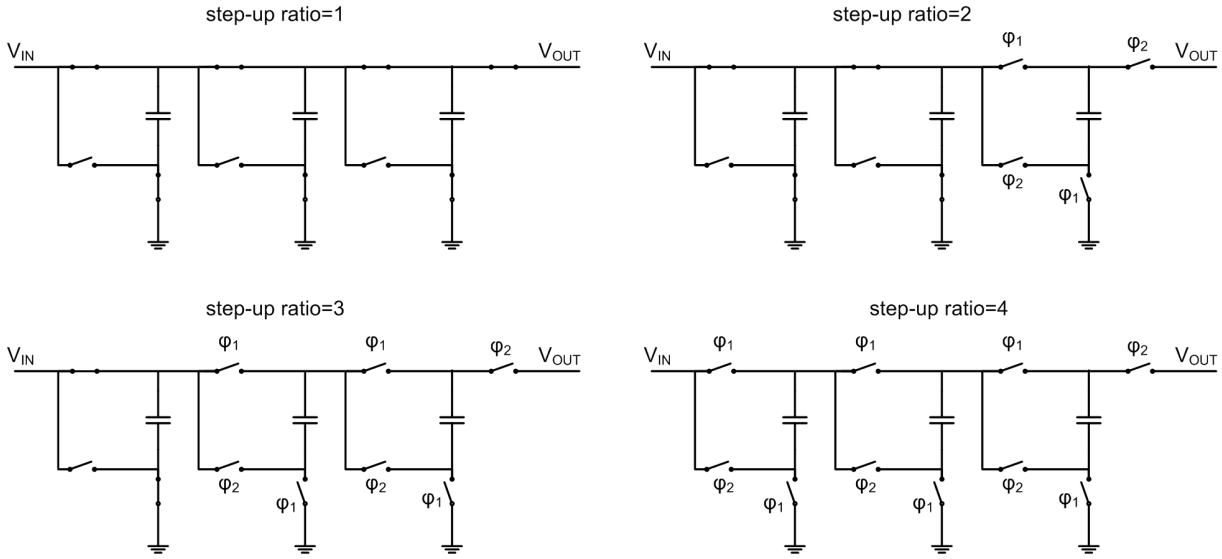

Figure 5.9: Example of series-parallel switched-capacitor topology enabling four step-up ratios [Seeman, 2008]

is not crucial in the case of MFCs of which electrical characteristics respond slowly. Other methods enable simplified MPPT and permit an easier implementation like those discussed below.

5.2.4 Low-power implementation of quasi-MPPT techniques

When the electrical characteristic curves are known a priori, this information can be used to determine the MPP based on a simpler method in terms of calculation and sensing requirements. These are not rigorously MPPT methods, but predictive methods referred here as quasi-MPPT methods, because the result is almost the same. In some cases, the overall efficiency of these methods can outperform standard MPPT methods because they are less power consuming.

Some **Model based methods** make use of elaborate dynamic models of the source. The MPP can be determined analytically by solving the optimization equation subject to operational constraints (e.g. $P_{MAX} = f(I_{OUT}, \Delta T)$ for a TEG). These methods have their own limitations as discussed in [Zhong et al., 2008]: "the optimality of such operating policies is completely dependent on the quality of the source model. Besides the model mismatch, the source operation sometimes strongly depends in a nonlinear way on many operating parameters, some of which are even unmeasurable". The implementation of such methods is not easy and requires digital implementation as well as a number of sensors to identify parameters of the model.

Simplistic models can be used to identify the MPP from a priori knowledge of the source. As an example, the MPP voltage of a solar cell is almost independent of the incident radiation. Once the MPP voltage is identified, a method assists in regulating the solar cell voltage to a constant value (V_{MPP}) thus achieving quasi-MPPT. The quality of the method relies on the validity of the assumption that V_{MPP} is constant for a given solar cell which is true only to a limited extent (e.g. operational parameters such as temperature are neglected). The advantage however is that it is implemented very easily with low-power analogue circuits.

Two low-power model-based quasi-MPPT methods are presented in [Lu et al., 2010] for solar cells: a) fractional open-circuit voltage (FOCV) and b) fractional short-circuit current (FSCC). These assume that V_{MPP} (respectively I_{MPP}) is a known fraction of V_{OC} (I_{SC}). It senses V_{OC} (I_{SC}) regularly, computes V_{MPP} (I_{MPP}) and controls the source voltage accordingly. FOCV is particularly adapted to solar transducers [Kim and Kim, 2011, Yu and Yue, 2011] and to MFCs like previously demonstrated in Section 3.3 of this manuscript. FOCV was implemented in [Park and Ren, 2012] where an hysteretic controler is used to control the MFC voltage while harvesting energy using a boost converter.

The impedance matching method implemented in [Win et al., 2011] is suitable for sources with fixed internal resistance (e.g. TEGs or rectennas) and where MPP is obtained for a same output resistance. The load resistance of the source is defined by the DC/DC converter which is sized such that its input resistance equals the internal resistance of the source. The input resistance of the converter can be modified by tuning the switching frequency and the duty-cycle. This open-loop method may suffer from the variation of the components' electrical characteristics.

5.3 State-of-the-art

A number of commercially available DC/DC converters were studied and tested in order to identify their compatibility to harvest energy from MFCs. The results are summarized in Table 5.2.

Manufacturer	TI	LTC	LTC	Seiko	Enocean	ST
Name	BQ255	LTC3105	LTC3108	S-882Z	ECT310	SPV1040
Reference	[TI, 2011b]	[LTC, 2011]	[LTC, 2010]	[Seiko, 2010]	[Enocean, 2010]	[ST, 2011]
Year of availability	2011	2011	2009	2007	2010	2011
Type	boost	boost	T_X-based	SWC	Tx-based	boost
Start-up voltage	330 mV	250 mV	20 mV	300 mV	20 mV	300 mV
Lower operating voltage	80 mV	225 mV	20 mV	300 mV	20 mV	300 mV
Regulation on the input	FOCV	FOCV	no	no	no	FOCV
Regulation on the output	yes	yes	yes	yes[d]	no[e]	no
Efficiency (10 mW, 0.3 V input)	70 %[d]	-	20 %[e]	< 20 %[e]	< 8 %[e]	-

Table 5.2: Comparative study of commercially-available low-power step-up DC/DC converters (efficiency values: [d]from datasheet, [e]experiments, - data not available)

Circuits relying on transformer-based start-up (i.e. LTC3108 and ECT310) are the only ones permitting autonomous start-up below 250 mV. We note that the boost converter from Texas Instruments (TI) permits operation down to 80 mV once started-up.

Three circuits embed MPP control features. The chip BQ255 implements FOCV but suffers from its sensing method to determine the reference voltage (V_{OC} is sensed for 256 ms every 16 s letting no time for voltage stabilization in the case of MFCs). This reference voltage can be disabled and set externally through a dedicated pin, requiring an external voltage supply. The LTC3105 also implements FOCV. The reference voltage is set by an external resistor. The MPP feature of the SPV1040 is only operational for an input voltage above 450 mV and would therefore be non-operational for harvesting energy from a single MFC.

5.4 Conclusion

In the case of MFCs, multiple parameters influence the characteristic curves and include structural as well as operational parameters (Section 2.4). What was observed in our study in Section 3.3, is that apparently similar MFCs operated under identical conditions lead to non-uniformities that can be sketched like in Figure 5.10. It appears that the OCV is similar but that the internal resistance R_{int} differs from one MFC to the other. The MPP voltage, V_{MPP}, is the same for all cells which means that regulating MFC voltage to a fraction of the OCV would be an effective way to realize a quasi-MPPT.

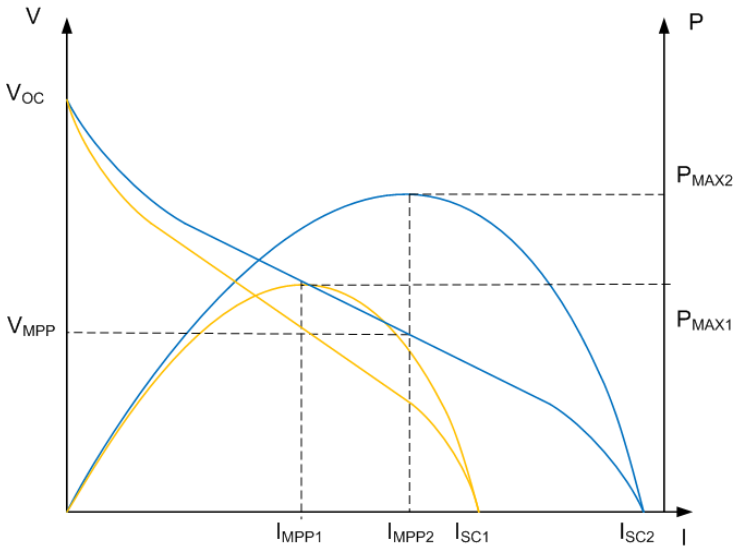

Figure 5.10: Schematic V-I and P-I characteristic curves of a MFC for two apparently similar cells.

In the following chapters, the focus is on the design of low input voltage DC/DC converters that start and operate at input voltages below 250 mV and that feature input voltage regulation for FOCV quasi-MPPT.

Chapter 6

Transformer-based low-voltage start-up circuit

Contents

6.1 Theoretical study of the oscillator 59

6.2 Theoretical study of the voltage doubler 62

6.3 Theoretical study of the full voltage-lifter 67

6.4 Experimental results 68

One of the main challenges to address when designing a PMU for MFCs concerns the autonomous operation at low-voltages. Transformer-based circuits using the Armstrong oscillator allow this feature. This oscillator was previously used in a number of circuits, but to the best of the author knowledge, no literature exists on the details of its operation. No procedure could be found to link expected performances to a circuit design. This Chapter presents an analytical study as well as an analysis based on parameter sensitivity. The oscillator is associated with a voltage-doubler to realize a low-cost start-up sub-circuit for a PMU (so-called voltage-lifter).

The voltage-lifter can be used in two types of applications as outlined below:

1. As a **start-up sub-circuit** to supply the control circuit of a main DC/DC converter. In this case, the voltage of the MFC is controlled by the main converter to approx. 0.3 V. The voltage-lifter needs to start-up at a low voltage, and to supply a small amount of current. In this application, efficiency is not crucial because the amount of energy consumed by the voltage-lifter is negligible compared to the amount of energy that the source can provide. The important criteria are the start-up voltage, the step-up ratio, and the quiescent current (input current when the output is in open-circuit).

2. As a **main DC/DC converter** to harvest energy from a very small-scale MFC. In this case, the MFC voltage is set by the voltage-lifter alone. In the absence of regulation of the voltage-lifter, it can be different from 0.3 V. In this case, harvested energy and circuit efficiency are critical.

6.1 Theoretical study of the oscillator

6.1.1 Equivalent circuit of the oscillator

The Armstrong oscillator is based on a simple association of two coupled-inductors, L_1 and L_2, one normally-on switch (JFET), J_1, and one capacitor, C_1, like presented in Figure 6.1.

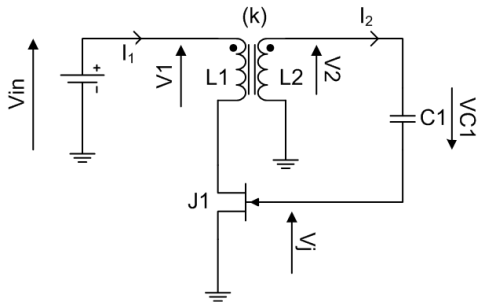

Figure 6.1: Start-up circuit

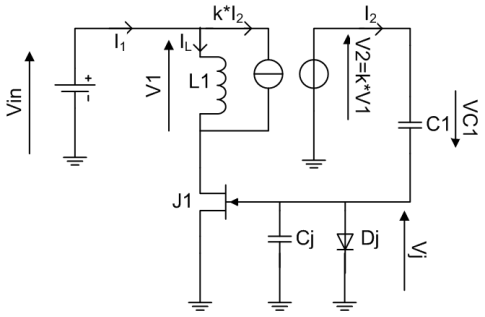

Figure 6.2: Equivalent circuit of the start-up circuit

A simple equivalent model of the oscillator is proposed in Figure 6.2. The coupled inductances are modeled as an ideal transformer with a primary inductance L_1. The JFET internal gate-source diode and parasitic gate capacitance are represented as D_J and C_J. D_J is assumed to be a perfect diode with a threshold voltage V_D. For the sake of simplicity, the gate-drain capacitance C_{GD} is neglected and only the gate-source capacitance $C_{GS} = C_J$ is considered.

The N-channel JFET is assumed to be correctly described by the Shichman and Hodges model [Shichman and Hodges, 1968]. The $I_{DS} = f(V_{GS}, V_{DS})$ equations are detailed in Table 6.1. The BF862 component is used for its threshold voltage close to 0 V. Figure 6.3 shows the characteristic curves of the model (a) and of the device (b). The parameters β, λ and V_{TH} were chosen so that theoretical (a) and experimental (b) characteristic curves are similar. The gate capacitance C_J is given in the datasheet of the component [Philips Semiconductors, 2000].

Region	Applicable range of Vgs and Vds values	Corresponding Ids equations
Off	$V_J - V_{th} \leq 0$	$I_{DS} = 0$
Linear	$0 < V_{DS} < V_J - V_{th}$	$I_{DS} = \beta V_{DS} [2(V_J - V_{th}) - V_{DS}](1 + \lambda V_{DS})$
Saturated	$0 \leq V_J - V_{th} \leq V_{DS}$	$I_{DS} = \beta (V_J - V_{th})^2 (1 + \lambda V_{DS})$

Table 6.1: Shichman and Hodges model of the JFET J_1. V_J is the gate-source voltage, V_{th} is the threshold voltage, β is the transconductance and λ is the channel-length modulation.

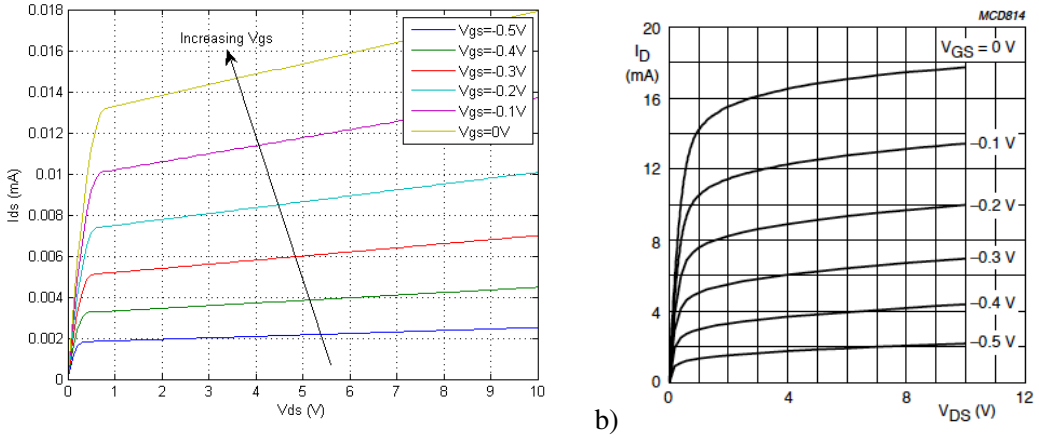

a) b)

Figure 6.3: I_{DS} versus V_{DS} for different gate-source voltages V_{GS} of JFET BF862, (a) model in Table 6.1 with V_{th} = -0.8 V, β = 20 mA.V^{-1} and λ = 0.04 V^{-1}, (b) experimental datasheet [Philips Semiconductors, 2000].

6.1.2 Analytical behavior of the oscillator

When supplied by an input voltage V_{IN}, and assuming that D_J does not conduct, the circuit is described by the three following equations:

$$I_1 = I_L + kI_2 \tag{6.1}$$

$$V_1 = L_1 \frac{dI_L}{dt} \tag{6.2}$$

$$I_2 = C_{eq} \frac{dV_2}{dt} \tag{6.3}$$

C_{eq} is the equivalent capacitance in series with the secondary winding. These equations yield:

$$\frac{dV_1}{dt} = \left(I_{ds} - \int \frac{V_1}{L_1} \right) \frac{1}{C_{eq} n^2} \tag{6.4}$$

where C_{eq} is defined differently depending on whether D_J conducts or not. When D_J does not conduct, C_{eq} equals the serial association of C_1 and C_J. Otherwise, C_{eq} equals C_1 alone. When D_J conducts ($V_2 > V_D - V_{C1}$), the current through D_J decreases the voltage V_{C1} until D_J stops conducting. This leads to the situation in steady-state where D_J never conducts theoretically. In this case, the two following equations express the voltage at the secondary winding.

$$V_J = \frac{C_{eq}}{C_1} V_2 \tag{6.5}$$

$$V_2 = V_{C1} + V_J \tag{6.6}$$

6.1.3 Simulation of the equivalent circuit

Matlab Simulink was used to simulate the analytical model like described previously. The parameters used for the simulations are given in Table 6.2.

Name	Value	Unit
V_{IN}	300	mV
L_1	25	μH
k	10	-
C_1, C_J	10	pF
V_{th}	-0.8	V
β	20	mA/V
λ	0.04	V^{-1}

Table 6.2: Parameter values for the Matlab simulation of the oscillator in Figure 6.1

The waveforms corresponding to the simulation are pictured in Figure 6.4. The waveforms permit to distinguish between two operation modes depending on the state of J_1. When J_1 is on, the current I_L in the primary winding equals I_1 and increases, the voltages V_1 and V_2 decrease with a L/R_{J1} time constant. When the voltage V_J reaches the threshold voltage of J_1, it switches off. When J_1 is off, the energy stored in L_1 initiates an oscillation with the equivalent capacitance C_{eq} at the secondary winding. The voltage describes a negative sinusoidal shape with a frequency $1/(2\pi\sqrt{L_2 C_{eq}})$.

With the circuit parameter values in Table 6.2, the circuit oscillates at 1.25 MHz. The voltage at the secondary winding oscillates with an amplitude of 8.7 V. The gate voltage of J_1 has an amplitude of 4.3 V (which is in agreement with Equation 6.5). Its maximum value is 0.3 V because of diode D_j which conducts otherwise.

The circuit parameters L_1 and n were changed and the impact on the amplitude of V_2 and on the switching frequency are plotted in Figure 6.5 and Figure 6.6 respectively.

An increase of L_1 tends to increase the amplitude of V_2 and decrease the switching frequency. The reason is that the L_1/R_J time constant is increased, leading to a longer on-time of J_1, itself leading to a decrease of the switching frequency. Since more energy is stored in L_1 during this time, the amplitude of the LC oscillation is increased and leads to an increased amplitude of V_2. Figure 6.7 shows temporal representations of V_2 which illustrate this analysis.

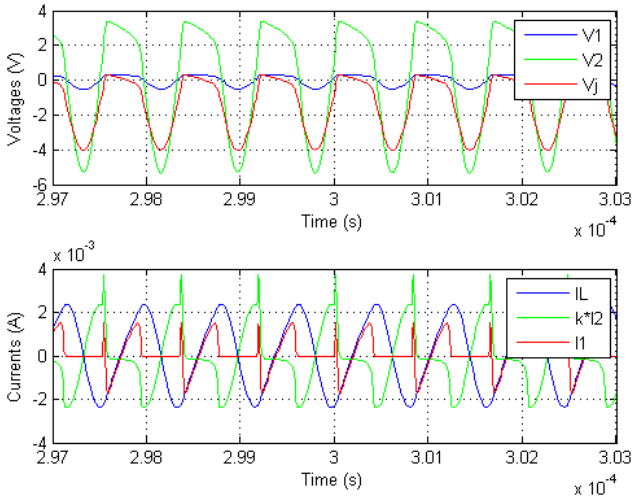

Figure 6.4: Waveforms of characteristic voltages and currents in the oscillator in Figure 6.1

When considering changes in k, Figure 6.8 highlights two phenomena which counterbalance each other. When n is high, the L_1/R_J time constant becomes negligible compared to the $2\pi\sqrt{L_2C_{eq}} = 2\pi n\sqrt{L_1C_{eq}}$ time constant. The circuit only oscillates with the latter time constant which increases linearly with n and results in a reduced switching frequency when n increases. The amplitude of V_2 is directly correlated with n because of the transformer and increases with it. For low turn-ratios, the operation changes because the time when J_1 is on now depends on the L_1/R_J time constant. When n decreases, the time during which J_1 is on is proportionally high compared to the time when J_1 is off. More energy is stored in L_1 and the amplitude during the LC oscillation increases.

The present analysis leads to the conclusion that two operating modes are possible for the oscillator. When L_1 is high and n is low, the oscillator is governed by two time constants and the switching frequency is low. High amplitudes are possible because of a disproportionally long on-time for J_1 during which energy is accumulated and released in a high amplitude oscillation in the secondary winding. When L_1 is low and n is high, the oscillator is governed by the LC oscillation alone. Amplitude of voltage V_2 can be high because of the high turn-ratio itself.

6.2 Theoretical study of the voltage doubler

This section is adapted from the study in [Ramadass, 2009] on switched-capacitor DC/DC converters. It presents an analysis of a voltage doubler composed by two switches and a capacitor. The switches are diodes D_1 and D_2 which are assumed to be sized such that they have a resistance, R_{SW}, and a threshold voltage, V_D, when they are on like in Figure 6.9. In this study, the voltage doubler is assumed to be supplied by a sinusoidal input voltage V_{IN} with a peak value, V_P, and a frequency, f_S. The load is such that the output voltage V_{OUT} is constant.

As shown in Figure 6.9, the switches D_1 and D_2 turn on during phases φ_1 and φ_2 respectively. $V_{C\varphi1}$ and $V_{C\varphi2}$ are the voltages across capacitor C at the end of φ_1 and φ_2 respectively. Phases φ_1 and φ_2 begin when V_{IN} decreases below $V_{C\varphi2} - V_D$ and above $V_{OUT} + V_D + V_{C\varphi1}$ respectively.

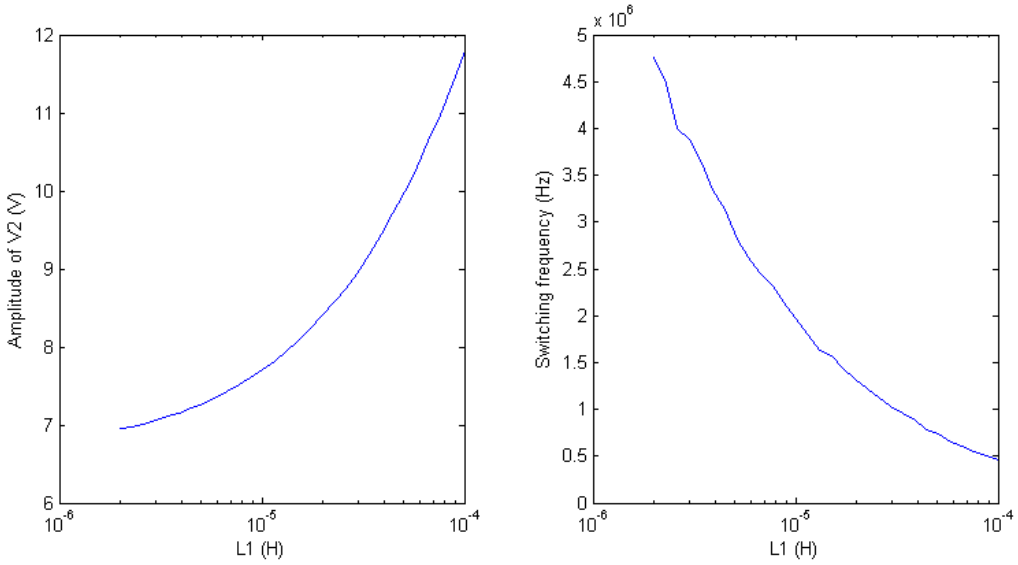

Figure 6.5: Sensitivity of V_2 and the frequency of the oscillator to L_1 at $n = 10$

6.2.1 Transient analysis

Let us first analyze the equivalent circuit during phase φ_1 (Figure 6.11 (a)). D_1 is assumed to turn on at time $t = 0$. The sinusoidal input voltage is expressed as $V_{IN} = -V_P cos(\omega t - \psi_1)$ where $\psi_1 = cos^{-1}(-(V_{C\varphi 2} - V_t)/V_P)$ and $\omega = 2\pi f_S$. The voltage across C is:

$$V_C = A_1 e^{-t/R_{SW}C} - B_1 \tag{6.7}$$

with

$$A_1 = V_{C\varphi 2} + \frac{V_P}{1+(R_{SW}C\omega)^2} cos(\psi_1) - \frac{V_P R_{SW} C\omega}{1+(R_{SW}C\omega)^2} sin(\psi_1) - V_D \tag{6.8}$$

$$B_1 = \frac{V_P}{1+(R_{SW}C\omega)^2} cos(\omega t - \psi_1) + \frac{V_P R_{SW} C\omega}{1+(R_{SW}C\omega)^2} sin(\omega t - \psi_1) - V_D \tag{6.9}$$

The diode D_1 turns off when its current cancels, what happens when t verifies:

$$-\frac{A_1}{R_{SW}} e^{-t/R_{SW}C} + C\left(\frac{V_P \omega sin(\omega t - \psi_1)}{1+(R_{SW}C\omega)^2} - \frac{V_P R_{SW} C\omega^2 cos(\omega t - \psi_1)}{1+(R_{SW}C\omega)^2}\right) = 0 \tag{6.10}$$

The voltage $V_{C\varphi 1}$ across the capacitor C at the end of phase φ_1 is the voltage across C at the beginning of phase φ_2. Let us assume now that D_2 turns on at time $t = 0$. The equivalent circuit of phase φ_2 is in Figure 6.11 (b). The input voltage is expressed as $V_{IN} = V_P cos(\omega t - \psi_2)$ where $\psi_2 = cos^{-1}((V_{C\varphi 1} + V_L + V_t)/V_P)$. The voltage across C is:

$$V_C = A_2 e^{-t/R_{SW}C} + B_2 \tag{6.11}$$

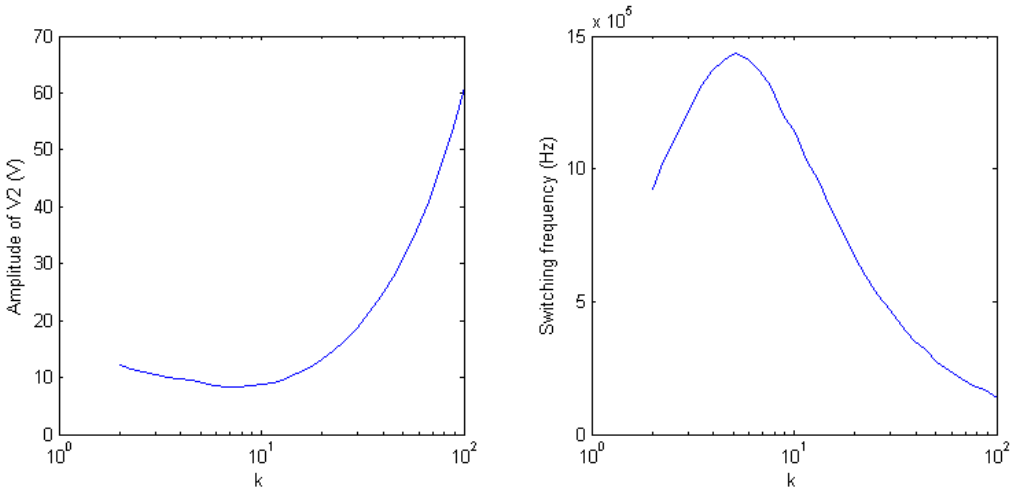

Figure 6.6: Sensitivity of V_2 and the frequency of the oscillator to k at $L_1 = 25\,\mu$H

with

$$A_2 = V_{C\varphi 1} - \frac{V_P}{1+(R_{SW}C\omega)^2}cos(\psi_2) + \frac{V_P R_{SW}C\omega}{1+(R_{SW}C\omega)^2}sin(\psi_2) + V_D + V_L \tag{6.12}$$

$$B_2 = \frac{V_P}{1+(R_{SW}C\omega)^2}cos(\omega t - \psi_2) + \frac{V_P R_{SW}C\omega}{1+(R_{SW}C\omega)^2}sin(\omega t - \psi_2) - V_D - V_L \tag{6.13}$$

The diode D_2 turns off when its current cancels which is when t verifies:

$$-\frac{A_2}{R_{SW}}e^{-t/R_{SW}C} - C\left(\frac{V\omega sin(\omega t - \psi_2)}{1+(R_{SW}C\omega)^2} - \frac{VR_{SW}C\omega^2 cos(\omega t - \psi_2)}{1+(R_{SW}C\omega)^2}\right) = 0 \tag{6.14}$$

The time dependent voltage and current across capacitor C are plotted in Figure 6.12 for different values of C.

6.2.2 Load current and equivalent resistance analysis

$V_{C\varphi 1}$ (respectively $V_{C\varphi 2}$) is the voltage at the end of phase φ_1 (φ_2) and can be calculated from Equations 6.10 and 6.7 (respectively 6.14 and 6.11). This was calculated and plotted in Figure 6.13 as a function of the switching frequency for different values of the output voltage. These are actually plotted for different values of V_{diff} defined as $V_{diff} = 2V_p - V_{OUT}$.

The voltage swing is defined as

$$V_S = V_{C\varphi 2} - V_{C\varphi 1} \tag{6.15}$$

When f_s is low, C has the time to fully charge and discharge and then $V_{C\varphi 1} = -V_P + V_D$ and $V_{C\varphi 2} = V_P - V_D - V_{OUT}$. The voltage swing, V_S, across C is maximum and equals $V_S = 2V_P - V_{OUT} - 2V_D = V_{diff} - 2V_D$.

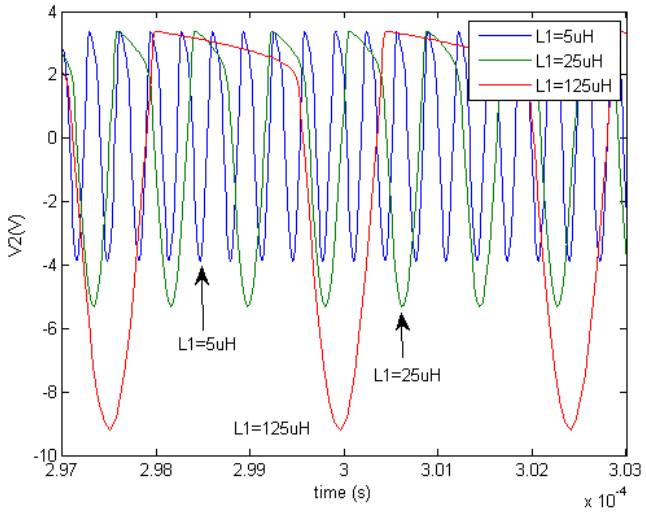

Figure 6.7: Sensitivity of V_2 and the frequency of the oscillator to L_1 at $k = 10$

When f_s is high, C has not enough time to charge and discharge and V_S cancels.

The value of C itself determines the frequency at which V_S drops. Figure 6.14 shows that the voltage swing, V_S, drops faster for large values of C (curve obtained for $V_{diff} = 2\,\text{V}$).

In a voltage doubler, the output current is expressed by:

$$I_{OUT} = f_s C V_s \tag{6.16}$$

I_{OUT} is shown in Figure 6.15 as a function of f_S for different values of C. Counter-intuitively, at high frequency, a lower value of C increases the output current because of a larger V_S.

Because the current I_{OUT} depends on the voltage swing, that itself depends on V_{diff}, the voltage doubler circuit can be seen as an ideal rectifier in series with an equivalent resistance ($R_{eq} = V_{diff}/I_{OUT}$) like in Figure 6.16. R_{eq} is plotted as a function of f_S or different values of load voltages in Figure 6.17. For low frequencies, the amount of charges transferred per switching is maximum and limited by the frequency. The equivalent resistance decreases proportionally with f_S. For high switching frequencies, the current is limited by the switches resistance R_{SW} and the equivalent resistance levels off (i.e. plateaus).

6.2.3 Efficiency analysis

Until now, only the conduction losses were considered. Additional switching losses are present due to the switching of the diodes. If we neglect the voltage drops in the switches and we assume that all the energy stored in C_D is lost, these are expressed as:

$$P_{SW} = 2 C_D V_{OUT}^2 f_s \tag{6.17}$$

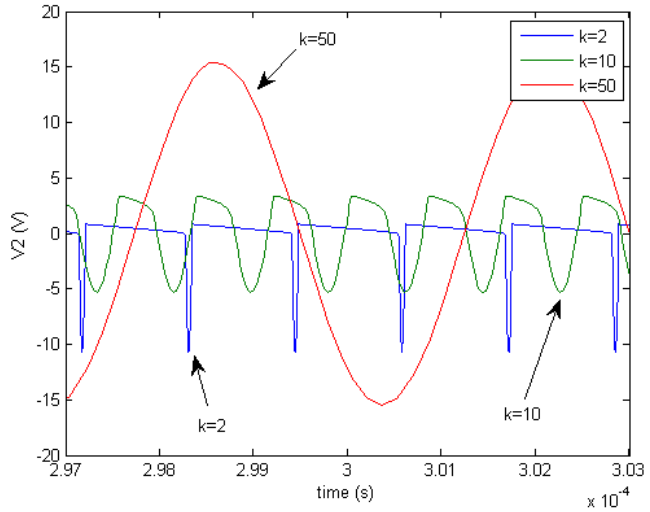

Figure 6.8: Waveforms of V_2 for different values of k at $L_1 = 25\,\mu$H

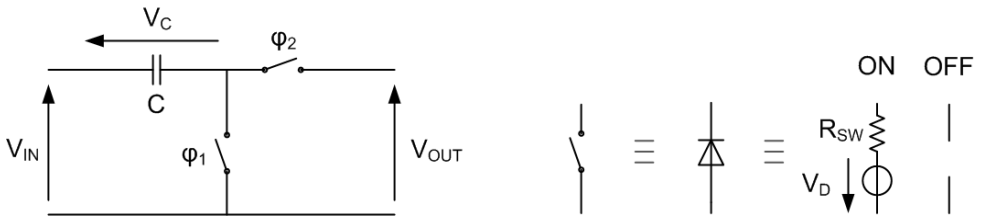

Figure 6.9: Schematic of the voltage doubler, and equivalent circuits used for the switches

where C_D is the equivalent parasitic capacitance of each of the two diodes. The efficiency of the voltage doubler is expressed as:

$$\eta = \frac{I_{OUT} V_{OUT}}{2 I_{OUT} V_P + P_{SW}} \tag{6.18}$$

For given values of V_P and V_{OUT}, I_{OUT} depends on V_D and R_{SW}. The efficiency of the voltage doubler is evaluated assuming C= 10 nF, C_D= 10 pF, R_{SW}= 5 Ω, V_D= 0.3 V and V_p= 5 V. The values of C_D, R_{SW} and V_D are typical values for Schottky diodes such as reference HSMS2860. Figure 6.18 shows the efficiency of the voltage doubler versus f_s. If conduction losses were only taken into account, the efficiency of the converter would remain constant with f_s ($\eta = V_{OUT}/(2V_P) = (2V_P - V_{diff})/(2V_P)$). The presence of switching losses, P_{SW}, makes efficiency a function of f_s. Their effect increase for low output power (i.e. as V_{diff} decreases and V_{OUT} increases).

Figure 6.19 shows the efficiency of the voltage doubler with changes in the switch resistance, R_{SW}, for V_{diff}= 2 V. The efficiency begins to drop faster for higher values of R_{SW}. R_{SW} has no influence at low frequency because C has time to fully charge and discharge whatever the value of R_{SW}, and the output current is limited by the amount of charges that can be stored in C.

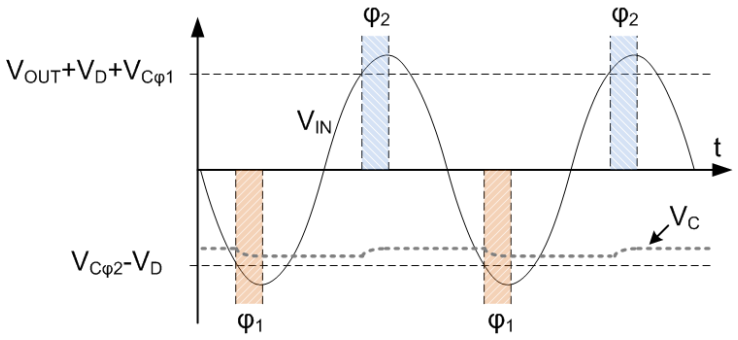

Figure 6.10: Phases φ_1 and φ_2 for a voltage doubler circuit with a sinusoidal input voltage V_{IN} and for a constant output voltage V_{OUT}

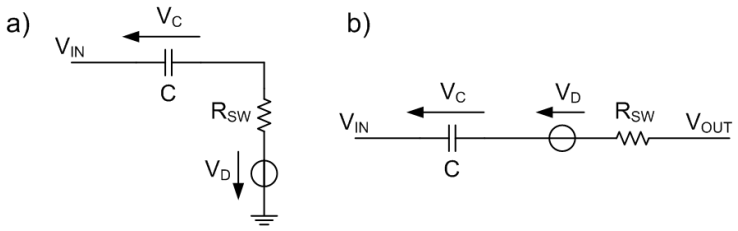

Figure 6.11: Equivalent circuit of the voltage doubler during phase φ_1 (a) and φ_2 (b)

Figure 6.20 shows the efficiency of the voltage doubler with changes in the diode threshold voltage, V_D. The efficiency drops faster for high values of V_D. At low frequency, the voltage swing is expressed as $V_S = V_{diff} - 2V_D$ and the output current is therefore influenced by V_D.

The selection of both the frequency of operation (f_s), the value of the capacitor and the size of the switches needs to be made after examining the load current and efficiency curves to determine the correct region of operation.

6.3 Theoretical study of the full voltage-lifter

The voltage-lifter circuit in Figure 6.21 is composed of an Armstrong oscillator and a voltage-doubler. The association involves a large number of components (eventually non-linear) which make it harder to give an analytic description of the voltage-lifter circuit. The circuit was simulated using Matlab Simscape software with the previous parameter values.

6.3.1 Voltage-lifter supplied by an ideal voltage source

In a first set of simulations, the voltage lifter is tested with an ideal DC voltage source at its input. In Figure 6.22, the voltage lifter is supplied by an ideal voltage source of 0.3 V and tested for different output resistance R_{OUT}. When the load resistance increases above 10 kΩ, the output voltage increases and reaches more than 5 V for R_{OUT}= 1 MΩ. The output power curve shows that P_{OUT} is maximum (i.e. 270 µW) for $R_{OUT} \approx 15$ kΩ. The efficiency curve shows that efficiency is maximum (i.e. η= 42.5 %) for R_{OUT}= 20 kΩ.

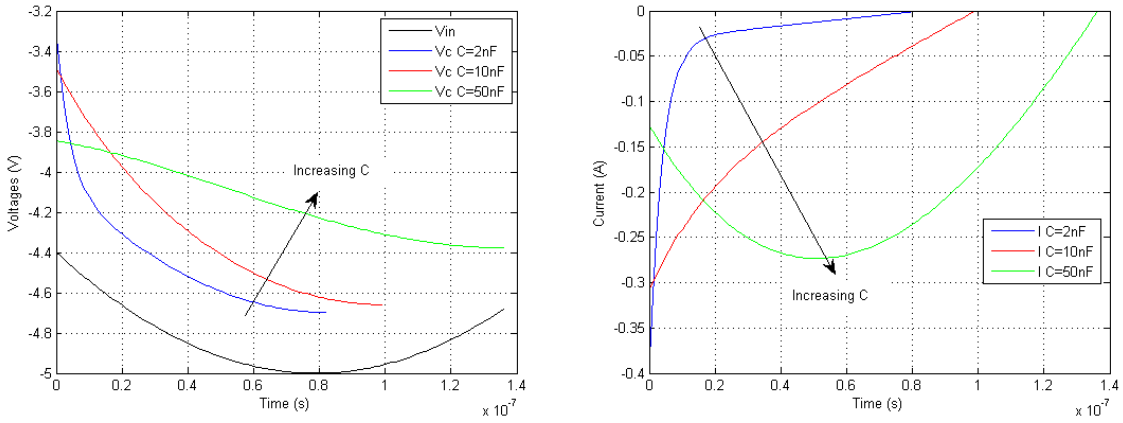

Figure 6.12: Time dependent voltage V_C and current I_C during phase φ_1 for different values of C

Figure 6.23 shows typical transient waveforms (i.e. from left to right V_2, V_{OUT}, I_1 and I_{D2}) for different output resistances R_{OUT} (i.e. from top to bottom 10 Ω, 20 KΩ and 1 MΩ respectively). The amplitude of V_2 increases with V_{OUT} and as such with R_{OUT}. The switching frequency of the oscillator increases with R_{OUT}. This increase in frequency causes extra switching losses that are partly responsible for the efficiency decrease. The current, I_1, through the JFET is the sum of the current in L_1 and the current I_2/n. For low values of R_{OUT}, the amplitude of V_2 is not large enough to completely turn the JFET off, and I_1 never cancels. The output current, I_{D2}, has a sawtooth shape and its average value is maximum for R_{OUT}= 20 KΩ.

6.3.2 Voltage-lifter supplied by the basic equivalent circuit of a low-power MFC

We now assume that the circuit is supplied by the equivalent circuit of a MFC with a maximum power of 100 µW. This assumption is realized by the use of an ideal voltage source with V_{OCeq} = 0.6 V and an internal resistance R_{int} = 900 Ω. Results are presented in Figure 6.24. The input voltage V_{IN} is below 0.3 V, indicating that the circuit draws more current than required to perform operation at MPP where the MFC delivers 100 µW (i.e. non-optimal power transfer). This low input voltage is responsible for the low output voltage. The maximum output power (i.e. 55 µW) and maximum efficiency (i.e. 75 %) are for R_{OUT} = 15 kΩ. Efficiency of the converter is maximum for low input voltages of around 140 mV compared to 300 mV like previously.

6.4 Experimental results

6.4.1 Sizing of the voltage-lifter circuit

Simulations with Simulink software use basic models for components. Orcad software was then used to simulate the circuit with PSPICE models of commercially available components (results not shown). These simulations led to the definition and sizing of active and passive components in the circuit. These are summarized in Table 6.3.

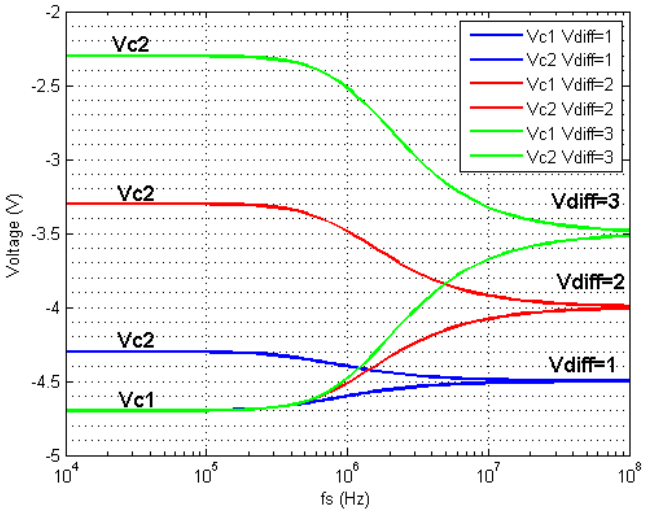

Figure 6.13: Voltage swing across C as a function of frequency for different values of differential voltage V_{diff}

Name		Manufacturer	Reference/Value
Coupled inductors	T_X	Coilcraft	LPR6235
JFET	J_1	NXP	JBF862
Diodes	D_1, D_2	Avago	HSMS286
Decoupling capacitors	C_1		16.8 pF
Resistor	R_1		1 MΩ
Charge-pump capacitor	C		2.2 pF
Input capacitor	C_{IN}		220 nF
Output capacitor	C_{OUT}		2 nF

Table 6.3: Component values for the experimental voltage-lifter

Compared to the previous analytical simulations, it was found that reducing the size of capacitors C_1 and C was necessary to optimize the output power, P_{OUT}, when the circuit is supplied by a 100 µW MFC. The circuit was realized in discrete components (Figure 6.25).

6.4.2 Testing of the experimental voltage-lifter

The ability of the circuit to start-up was verified experimentally. The experimental circuit starts-up and operates for input voltages above V_{start}= 100 mV. When the circuit is not switching, the impedance at its input, R_{input}, equals the on-resistance of the JFET plus the serial resistance of the primary winding of the coupled inductance ($\approx 40\,\Omega$). When the circuit is supplied by an ideal voltage source V_{OCeq}= 0.6 V and a resistance R_{int} in series, the circuit starts oscillating if the input voltage is above V_{start}. This condition is met when $R_{int} < R_{input}(V_{OCeq} - V_{start})/V_{start}$ (i.e. $R_{int} < 200\,\Omega$). Once started, the experimental circuit operates for R_{int} values as high as 900 Ω (i.e. $R_{int} \leq 900\,\Omega$).

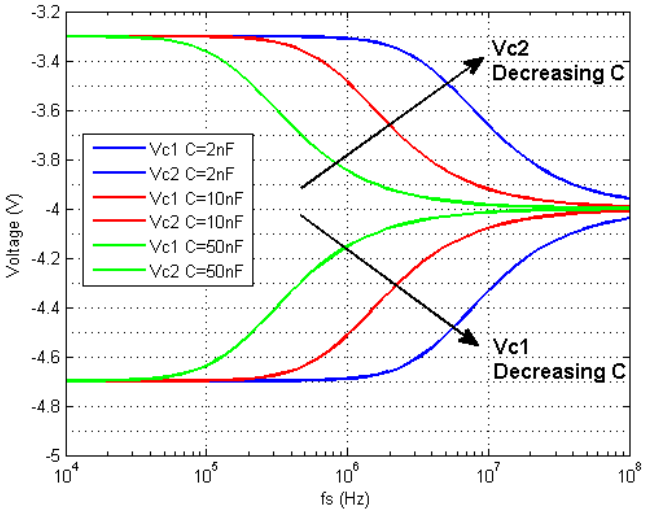

Figure 6.14: Voltage swing across C as a function of frequency and for different values of C

Figure 6.26 shows the steady-state characteristic curve of the voltage-lifter circuit supplied by an ideal source voltage of 0.3 V. The experimental curve is superimposed with the PSPICE simulation curve. Both curves are linear but with large differences on their maximum voltage and to a lesser extent on their slope. While the slope mainly depends on the voltage doubler equivalent resistance, the maximum voltage is set by the oscillator. In the experimental prototype, the parasitic capacitances at the secondary winding modified the operation of the oscillator, resulting in a decrease in the amplitude of its output voltage. The experimental curve shows that the maximum output of the voltage-lifter can reach 5 V in open-circuit, and more than 2 V for output currents up to 5 µA. The control circuit of a main boost converter will therefore need to consume less that this.

In Figure 6.27, the voltage-lifter circuit is tested with a voltage supply composed of an ideal voltage source V_{OCeq}=0.6 V and a resistance in series R_{int}= 200 Ω (i.e. maximum resistance enabling self start-up, corresponding to a minimum input power of 450 µW). Testing the converter with an equivalent circuit instead of a real MFC facilitates the control and measurement of the input electrical characteristics. The voltage curve is linear except for low current values where it plateaus. When increasing the current from open-circuit to short-circuit, the input voltage (not shown) steadily increases from 520 mV to 536 mV, indicating that less current is drawn from the source when I_{OUT} increases. The efficiency of the circuit (not shown) describes a peak of the same shape as the output power of MFC with a maximum of 16.4 % for I_{OUT}=9 µA. This low efficiency confirms that the voltage-lifter may only be used as a start-up sub-circuit to complement another main high-efficiency DC/DC converter. The conclusions of this Chapter (Chapter 6) are in the Chapter 15.

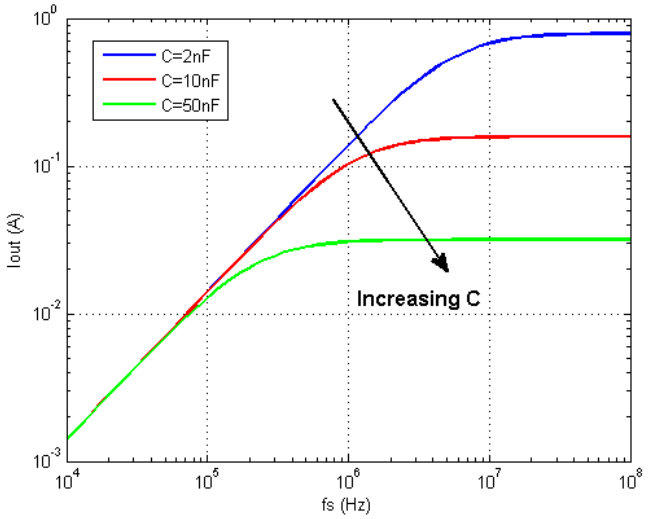

Figure 6.15: Output current as a function of frequency and for different values of capacitor C

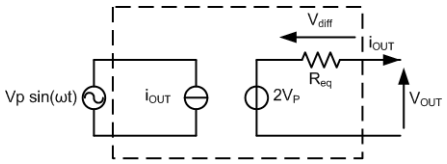

Figure 6.16: Idealized equivalent circuit of a voltage doubler

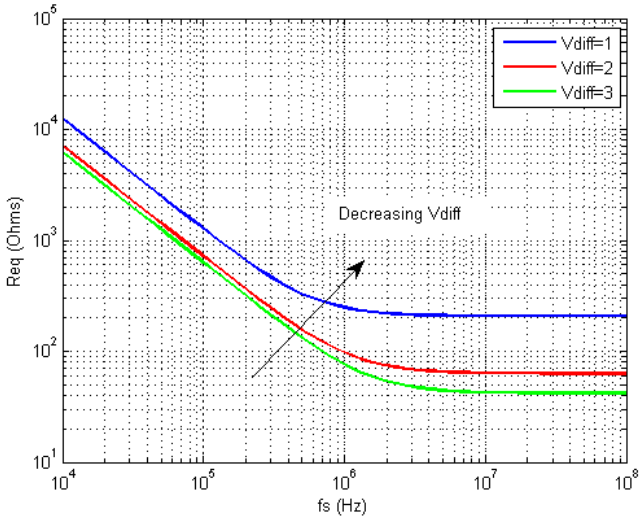

Figure 6.17: Equivalent resistance R_{eq} as a function of frequency for different values of the output voltage

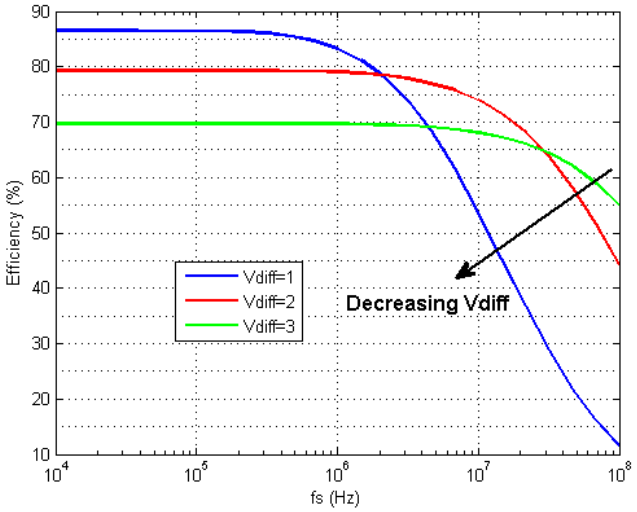

Figure 6.18: Efficiency as a function of frequency for different values of the output voltage

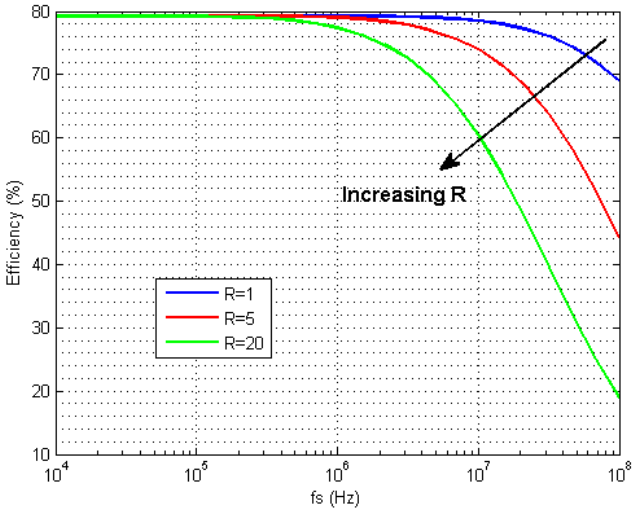

Figure 6.19: Efficiency as a function of frequency for different values of R_{SW}

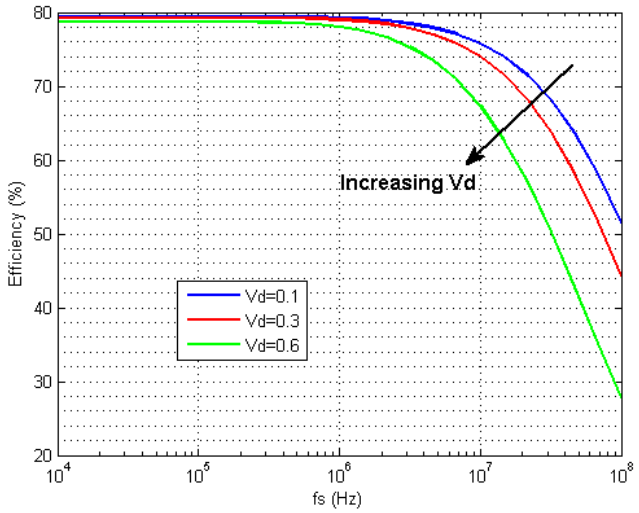

Figure 6.20: Efficiency as a function of frequency for different values of diode threshold voltage, V_D

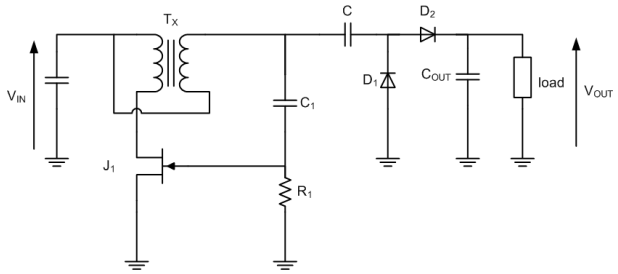

Figure 6.21: Schematic of the voltage-lifter

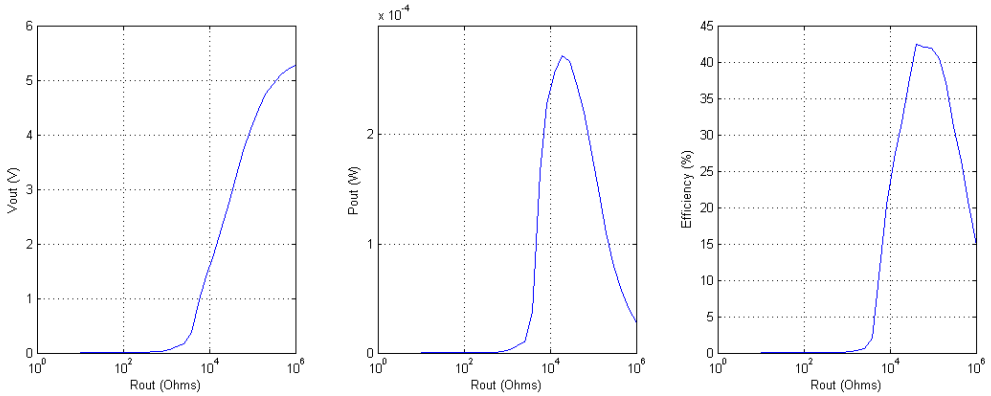

Figure 6.22: Performance curves of the full voltage-lifter supplied by an ideal voltage source

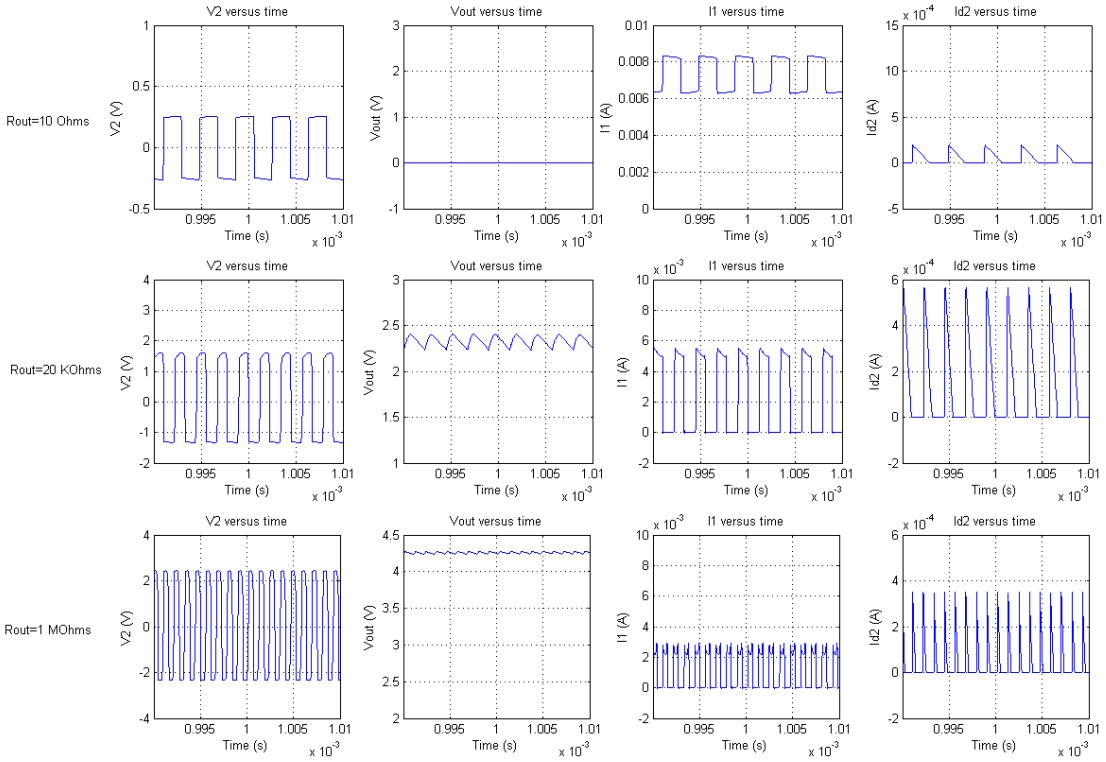

Figure 6.23: Simulation waveforms of the full voltage-lifter supplied by an ideal voltage source. From left to right: V_2, V_{OUT}, I_1 and I_{D2}. From top to bottom: $R_{OUT}=10\,\Omega$, $R_{OUT}=20\,\mathrm{k}\Omega$ and $R_{OUT}=1\,\mathrm{M}\Omega$ respectively

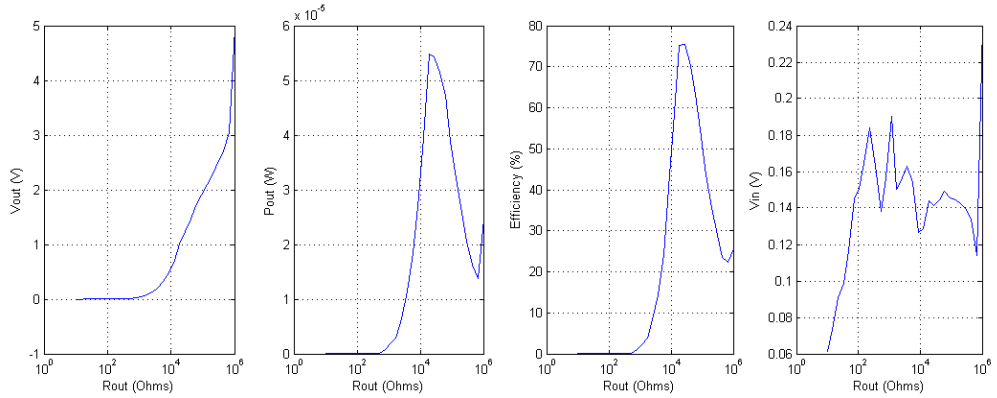

Figure 6.24: Performance curves of the full voltage-lifter supplied by an ideal voltage source V_{OCeq} in series with a resistance R_{int}

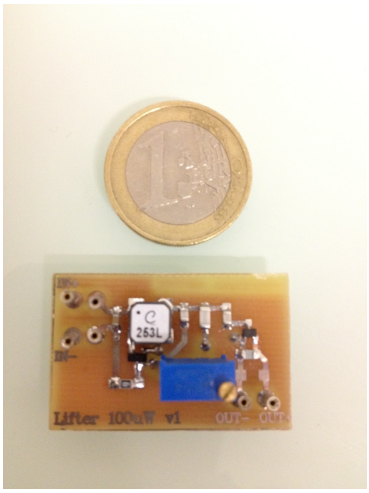

Figure 6.25: PCB of the voltage-lifter

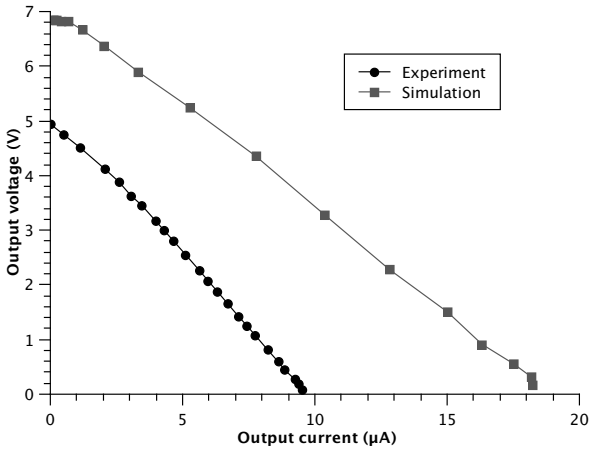

Figure 6.26: Experimental curves for a voltage lifter supplied with an ideal voltage source of 0.3 V

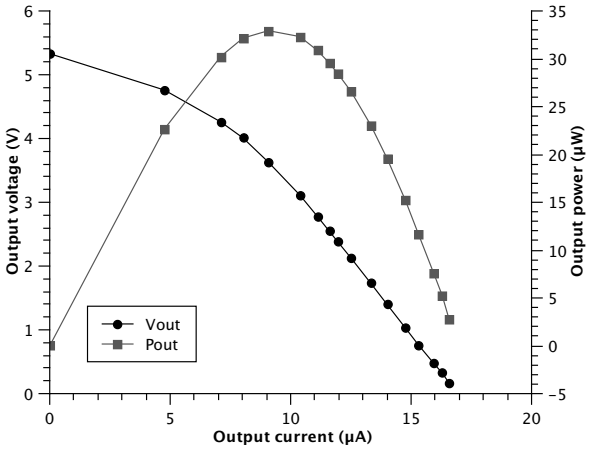

Figure 6.27: Experimental curves for a voltage lifter supplied with the equivalent circuit of a 450 µW MFC (V_{OC}= 0.6 V, R_{int}= 200 Ω)

Chapter 7

Self-starting DC/DC converters

Contents

7.1 Design and theoretical study of a self-starting flyback converter 78

7.2 Performances of the self-starting flyback converter 80

The voltage-lifter circuit is a low-efficiency circuit that can start-up at low voltages from 100 mV. It can operate at an input power down to 100 µW but its self startup functionality is operational for input power levels higher than 450 µW. Its characteristics (i.e. self start-up, low power, but also low efficiency) make it a suitable circuit to complement a main DC/DC converter and to permit low-voltage start-up.

The constraints for high step-up and high efficiency justify the use of a switched-mode PMU with an efficient regulation. This leads to the choice of a PWM inductive converter instead of a capacitive converter for the two following reasons. First, as discussed in Sub-section 5.2.2, PWM inductive converters can be controlled with more precision. Second, the transformer-based start-up circuit (i.e. voltage-lifter) described in Chapter 6 can be implemented as a merged sub-circuit to an inductive converter. The idea to merge the start-up circuit into the design of the main converter is attractive because it allows the matching of inductive components. The design of a standard main DC/DC converter is a state-of-the-art design work and is not discussed in this thesis. Two original circuits with merged start-up were investigated and conceived as part of this thesis[1]. One is derived from a standard boost topology and another one from a standard flyback topology. Since the former is extensively described in [Degrenne et al., 2011b] and [Degrenne et al., 2012a], the discussion of this manuscript mainly focuses on the latter. Because the description of the circuit is similar for the flyback and the boost circuits, the present analysis focuses on the sizing[2] of the coupled inductors. The converter was tested individually and also when several units were connected.

[1] The study of self-starting DC/DC converters for MFCs lea to the publication of two conference papers [Degrenne et al., 2011a], [Degrenne et al., 2011b] and of one Journal paper in the Journal of Low Power Electronics [Degrenne et al., 2012a].

[2] The sizing of the flyback converter was realized with the help of Marilyne Boileau who completed her bachelor internship within Laboratoire Ampère from September to December 2011.

7.1 Design and theoretical study of a self-starting flyback converter

7.1.1 Specifications

The converter's design was based specifically on the electrical characteristics of MFCs (Table 7.1). The circuit should start and operate at voltages lower than 0.3 V. The step-up ratio should be high to reach output voltages above 1 V. Because MFCs are strongly non-uniform generators, the converter should operate between 3 mW and 30 mW of input power with a nominal power level of 10 mW. Efficiency has to be as high as possible. Finally, galvanic insulation is required in order to facilitate the serial association of the outputs of the converters.

	Units	Min.	Typ.	Max.
V_{IN}	V	0.2	0.3	0.4
P_{IN}	mW	3	10	30
I_{IN}	mA	10	33	100
V_{OUT}	V	1	-	-
η	%	60	-	-
Insulation		Required		

Table 7.1: Specifications for the flyback converter

7.1.2 Circuit description

The converter presented in Figure 7.1 (a) is based on a main circuit (L_1, L_2, T_1, D_1) that is an asynchronous flyback converter operating at the boundary between the continuous and discontinuous modes (critical conduction mode). The output voltage of the converter is defined by

$$V_{OUT} = \frac{n_2}{n_1}\frac{\alpha}{1-\alpha}V_{IN} \tag{7.1}$$

where α is the duty-cycle of the converter.

When T_1 is on (phase φ_2), $V_1 = V_{IN}$, $V_2 = (-n_2/n_1)V_{IN}$ and the current ramp in L_1 is set by $V_{IN} = L_1 \cdot dI_1/dt$. Integration over phase φ_2 leads to Equation 7.2. The current I_1 increases up to its maximum value, I_{MAX} and f_S is the switching frequency.

$$L_1 = \frac{\alpha V_{IN}}{f_S I_{MAX}} \tag{7.2}$$

Figure 7.1 (b) shows ideal waveforms for the flyback main circuit with a turn-ratio $k = 1$. When T_1 is off (phase φ_1), the current through L_1 is null, and the magnetic energy stored during φ_2 is released through D_1, which has turned-on. The voltage across the secondary winding is then $V_2 = V_{OUT} + V_D$.

The inductors L_1 and L_2 are coupled to the auxiliary winding L_3. The auxiliary winding supplies the start-up sub-circuit which operates with the normally-on JFET J_1, in parallel with T_1. The auxiliary winding also supplies the control of the transistor T_1 of the main flyback circuit. This permits to regulate the input voltage to a user-defined value. Detailed description of the control can be found in [Degrenne et al., 2012a].

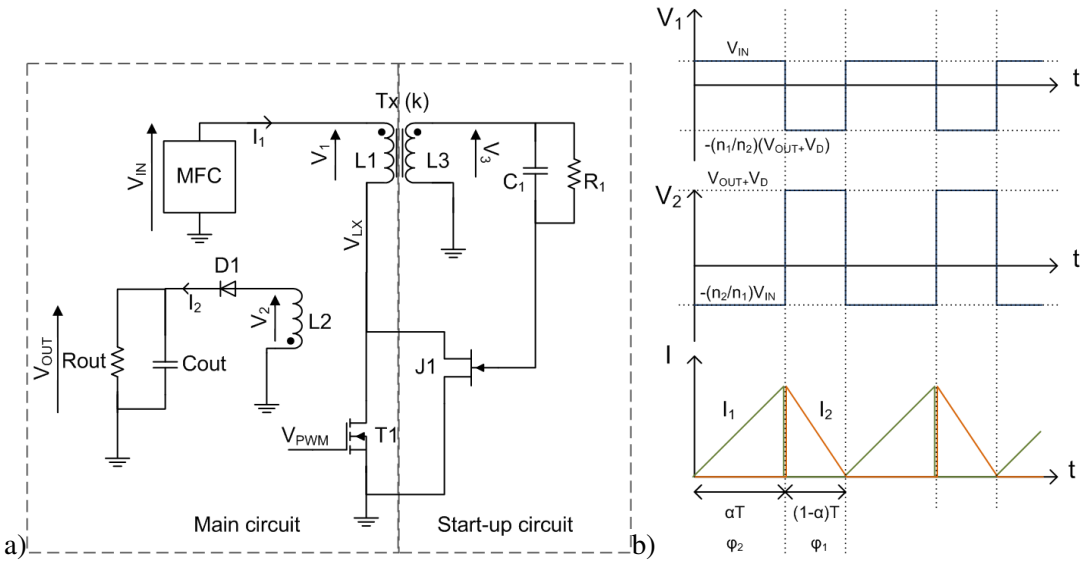

Figure 7.1: Simplified circuit of the flyback converter (a) and ideal waveforms of the main circuit ($n_2/n_1 = 1$) (b)

To achieve a high efficiency, both switching and conductive losses have to be minimized. Switching losses are addressed by a relatively low switching frequency (around 10 kHz) which is possible through the use of a transformer with a high primary inductance L_1 (thus a large magnetic material volume). T_1 is a low threshold-voltage transistor that was selected to compromise between on-resistance and parasitic gate capacitances. The serial resistance with inductances L_1 and L_2 needs to be minimized. The coupled inductances are critical in the operation of the converter and in its efficiency. Their sizing is detailed in the following.

7.1.3 Specifications for the coupled inductances

The first constraint is the value of the inductance, which must be as high as possible. Indeed, as seen in Equation 7.2, the value of the inductance has an inverse relationship to the switching frequency. The highest the inductance, the lowest the frequency and the lowest the switching losses. Assuming that the target frequency is approx. 10 kHz, the duty-cycle $\alpha = 0.5$, a maximum input current, $I_{MAX} = 66$ mA and an input voltage, $V_{IN} = 0.3$ V, the inductance of the primary winding L_1 should be at least 227 µH. The value of L_2 is $(n_2/n_1)^2$ larger.

The second constraint on the coupled inductance is the value of the equivalent series resistance of the windings L_1 and L_2. The wires used to make the inductance have their own internal resistance and are a cause of conduction losses. To keep performances at the highest, the losses allowed in the resistance of each winding are set at 1 % of the nominal power of the MFCs (i.e. 10 mW) which means 0.1 mW. Assuming that the current through L_1 is constant and equals 33 mA, the maximum resistance of the winding L_1 is 100 mΩ.

The third constraint concerns the saturation of the magnetic material (i.e. ferrite). The magnetic material is chosen to be without air-gap to maximize the value of the inductances. The result is a limited ability to store energy which is indicated by a low saturation magnetic field B_{sat}. The maximum field B_{MAX} in the magnetic material is a function of the number of turns, the maximum current in the windings

and of the permeability of the ferrite. When sizing the coupled inductors, the condition $B_{MAX} < B_{sat}$ must stand.

The fourth constraint is about the size. There are commercially available coupled inductances which have the above specifications. Other studies were made with a boost converter which was also using coupled inductances for self-starting [Degrenne et al., 2012a]. However, the footprint of this coupled inductance was about 18.5 cm^2 which represented 25 % of the printed circuit board. The intention for the flyback converter is to achieve the realization of a smaller and more efficient prototype.

7.1.4 Design of the coupled inductances

A design methodology was used to define the number of turns, the magnetic core and the winding cross section. In the absence of a corresponding commercially-available coupled inductor, the component was realized manually. It was made with a toroidal ferrite with an external diameter of 12.70 mm. The relative permeability of the material is $\mu_R = 2300$. The wire used for the two power windings, L_1 and L_2, are 0.56 mm external diameter and 0.20 mm external diameter for the control winding L_3. The number of turns is 10 for L_1, 20 for L_2 (1:2 ratio) and 60 for L_3 (1:6 ratio). The resulting characteristics of the power windings are listed in Table 7.2.

Table 7.2: Expected parameters for the designed coupled inductances

Component	Value
L_1	277 µH
L_2	1110 µH
R_1	81 mΩ
R_2	162 mΩ

7.2 Performances of the self-starting flyback converter

7.2.1 Single converter

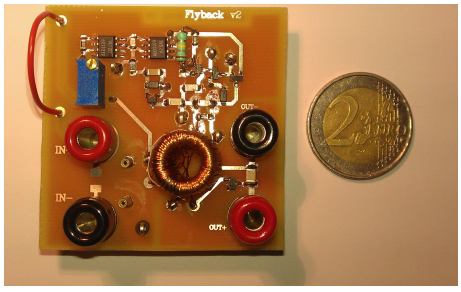

Figure 7.2: Prototype of the flyback converter

The converter was realized[1] (Figure 7.2) on a 29 cm^2 PCB. It was first tested with the equivalent circuit of typical MFCs. The MFC equivalent circuit composed of an ideal voltage source of 0.6 V

[1]

serially connected to an internal resistance R_{int}. With this equivalent circuit, the MPP voltage is known to be 0.3 V.

The graphs in Figure 7.3 show experimental waveforms (with the same horizontal and vertical scales) for different MFC equivalent internal resistances R_{int} of 3 Ω, 9 Ω and 20 Ω respectively. In this experiment, the load is a low-power LED with 1.8 V threshold voltage. The switching frequency (and as such the input current) is modified by the control sub-circuit to control the input voltage to approx. 0.3 V. For low values of R_{int} (a), the switching frequency of the circuit is approx. 3.8 kHz. The average input current of the converter (bottom curve) is around 90 mA (1 A/ V). When $R_{int} = 9\,\Omega$ (b), the switching frequency is approx. 8 kHz and the average input current is approx. 35 mA. When $R_{int} = 20\,\Omega$ (c), the switching frequency is approx. 16 kHz and the average input current is around 15 mA.

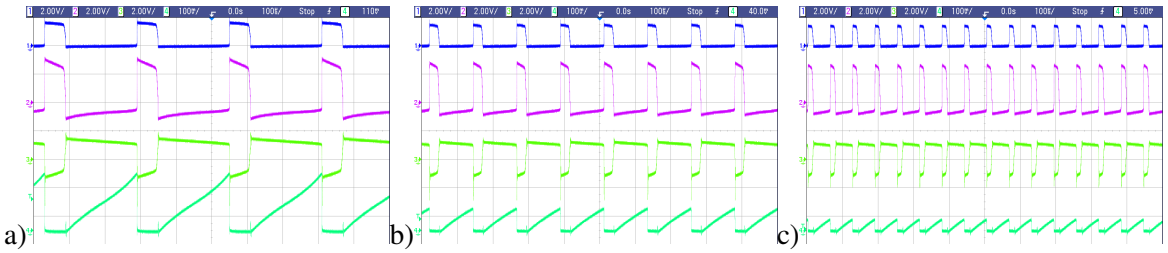

Figure 7.3: Experimental waveforms of the flyback converter circuit for different MFC internal resistance R_{int}. The input is the equivalent circuit of a MFC ($V_{IN} = 0.6$ V, $R_{int} = 3\,\Omega$ (a), $R_{int} = 9\,\Omega$ (b), $R_{int} = 20\,\Omega$ (c)), the load is a 1.8 V LED. From top to bottom: (ch1) drain voltage of T_1 (V_{LX}), (ch2) voltage across the secondary winding (V_2), (ch3) gate voltage of T_1 (V_{PWM}), (ch4) input current I_1.

Figure 7.4 shows the efficiency of the flyback converter for different resistive loads. Resistive loads were chosen because they facilitate the evaluation of the output current and power. The maximum converter efficiency ($\eta = P_{OUT}/P_{IN}$) was 62 % which is equal to the global efficiency ($\eta_G = P_{OUT}/P_{MPP}$) since the converter operates at the MPP.

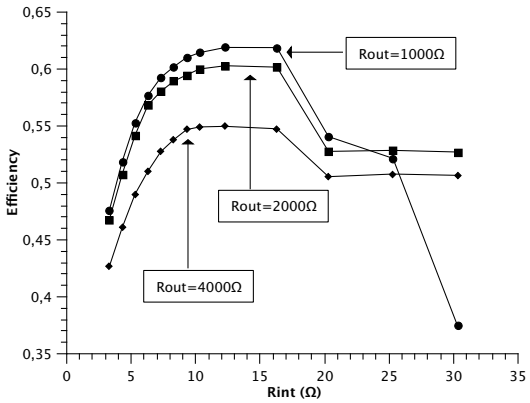

Figure 7.4: Efficiency versus internal resistance for different resistive load.

The realization of the printed circuit board circuits for the voltage-lifter and the flyback converter was done by Abderrahime Zaoui, technician at Laboratoire Ampère.

Because of the galvanic isolation, several converters can be connected in series and increase the ability to step-up voltage from a large number of MFCs.

7.2.2 Series association of converters

Two individual converters were associated in series like as shown in Figure 7.5, with each converter having its own control and individual output capacitors required as filters. This configuration theoretically permit to indirectly connect several MFCs sharing the same electrolyte.

The current I_{OUT} to the load and through the output of each converter (and its output capacitor) is therefore almost continuous in steady-state. DC/DC#1 is powered by two parallel small-scale MFCs with an equivalent MPP of 5 mW, and DC/DC#2 is powered by a single more powerful MFC with an equivalent MPP of around 30 mW. Figure 7.6 shows the addition of voltages from each converter when the load resistance, R_{OUT}, is modified. When the voltage at the output of the first converter is below 1.5 V (for small values of R_{OUT}), it stops working and its output voltage reverses. This is because the current, I_{OUT}, flows continuously through the output diode of DC/DC#1, causing a voltage drop corresponding to the threshold voltage of the diode. If the output resistance increases again, the reversed voltage at the output of DC/DC#1 prevents it from starting-up again.

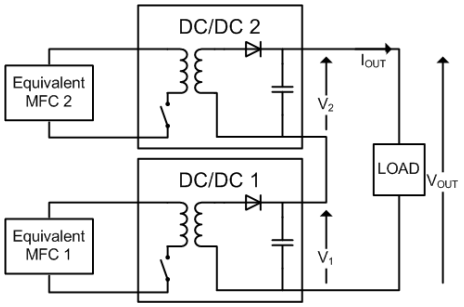

Figure 7.5: Scenario of association of two DC/DC converters in series

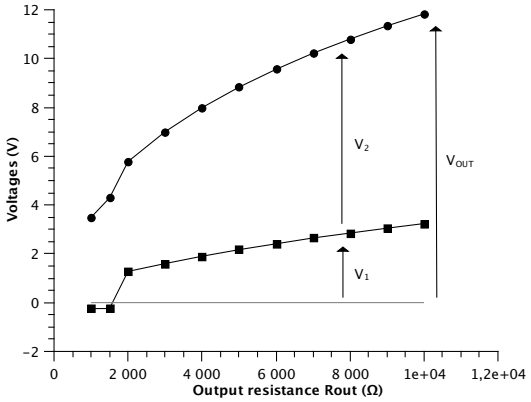

Figure 7.6: Voltages for the association of two individual flyback converters powered by different MFCs

This experiment proves the concept of indirect cell association through insulated converters. However, the converter architecture, with internal start-up feature, leads to operation problems that can be

resolved with the use of a circuit topology with an external start-up. More conclusions are given in the next Chapter.

The topic of association of MFCs and DC/DC converters is developed further in Part III.

Chapter 8

Scientific conclusions and perspectives

Contents

8.1 Conclusions **84**
8.2 Perspectives **85**

8.1 Conclusions

This part on low-voltage PMUs for MFCs first presented the analysis of a self-starting transformer-based oscillator. This oscillator was then used into a voltage-lifter and a flyback DC/DC converter to enable low-voltage autonomous step-up DC/DC conversion.

In the **voltage-lifter**, the oscillator is complemented with a voltage-doubler. This circuit starts for input voltages as low as 100 mV (or a maximum R_{int} of 200 Ω for a resistive voltage source of 0.6 V). For an input voltage of 0.3 V, the output voltage can reach 5 V in open-circuit. **This circuit can be used as an individual start-up to supply up to 5 µA at 2 V**. When used as a main DC/DC converter, it can step-up voltages of MFCs with MPPs as low as 450 µA at 0.3 V. It however operates at low efficiency (<17 %) and without MPP control which make it an impractical circuit to use as a main DC/DC converter.

The **flyback converter** includes a self-starting sub-circuit for autonomous operation at low input voltage. Its coupled inductors were sized and constructed specifically to find the best compromise between efficiency and size. This converter operates at an efficiency up to 62 % when harvesting energy from a 10 mW MFC. This circuit is PWM-controlled on its input voltage. As a consequence, it operates at MPP, permitting a good global efficiency (defined as the output power versus the maximum power deliverable from the MFC). The converter is practical to capture and store electrical energy in supercapacitors or Li-ion batteries. It can also directly power low-power LEDs. The galvanic insulation of its output offers the flexibility of connecting a number of converters in series. Experiments showed that series association of flyback converters is possible, but is causing start-up problems with the specific start-up architecture of the prototypes.

Generally, the drawback of the flyback circuit is that it requires specific high turn-ratio coupled inductors. The voltage-lifter can be realized at low-cost using small coupled inductors and a limited amount of Surface Mount Devices SMDs. The flyback converter however is more restrictive on its coupled-inductors, leading to bulky implementations, and requiring more SMDs for its control. Another issue with the flyback circuit concerns its high-side switch which is the major source of losses.

8.2 Perspectives

The design of a PMU for a single MFC or a group of MFCs connected in parallel can be foreseen in two ways:

1. In a **discrete realization**, the minimum input power to realize a PMU that includes a control block and which has a respectable efficiency is in the order of 1 mW. In this case, the threshold voltage of commercially available transistors led to the requirement of a self-starting sub-circuit. It can be implemented with a voltage-lifter circuit that supplies a highly efficient PWM-controlled inductive step-up converter.

2. In an **integrated realization**, the degree of freedom is such that a self-starting circuit is not necessary to harvest energy from MFCs. The threshold of transistors can be chosen to be sufficiently low (e.g. in the order of 0.3 V) to operate autonomously with MFCs. The integrated DC/DC converter can operate at high efficiency (e.g. synchronous operation) and be implemented either capacitively or inductively. While capacitive converters permit full monolithic integration, inductive converters permit easier MPP control. A fully integrated inductive realization (i.e. including the integration of the inductive components) like in [Bergveld et al., 2009] seems compromised because of the very specific constraints on the inductors.

When a large number of MFCs are used as a source, their plurality can be used advantageously. One way to do this is to associate insulated converters in series. This permits to avoid voltage reversal and hydraulic coupling issues. Each MFC (or association of parallel MFCs) is operated at MPP and voltage is then added at the output of the converters. In the case of a large number of MFCs, this method can become expensive because it requires a large number of PMUs. Another way to utilize the plurality of MFCs is to connect them in series. For a serial association of MFCs, the specification on the PMU is less restrictive in terms of input voltage range. However, some other features may be necessary in order to manage the group of source as investigated in Part III of this manuscript.

Part III

Efficient serial association of non-uniform microbial fuel cells

Chapter 9

Introduction

Contents

9.1 Concept of MFC-based energy grid 87
9.2 Energy management of serially connected MFCs 88
9.3 Voltage balancing circuits for MFCs 88

9.1 Concept of MFC-based energy grid

As outlined in the introduction of this manuscript, MFCs are candidates as a divided energy supply for applications which may involve a large number of elements (i.e. energy generators, energy storage and energy consumers). The examples mentioned previously in Chapter 1 are reminded below.

Because the volume of an elementary MFC is limited, the large amount of organic matter in **wastewater treatment plants** naturally leads to the association of a large number of individual MFCs [Ieropoulos et al., 2010a]. The consumption of the energy is either local (e.g. pumps) or external through the electrical grid. In **biobatteries**, the stacking permits to increase power and to step-up the voltage. The final energy consumer can be singular (e.g. a single LED) or plural (e.g. a smart phone composed of a microprocessor, a display screen, a wireless communication module...). In the latter case, each consumer may require a different supply voltage. The association of MFCs is less likely to be necessary is ultra-low power **energy scavenging** applications. However, the association with other energy transducers (e.g. thermal, solar or RF) permits to increase the total amount of energy produced and the reliability of the energy supply. The energy for these applications is likely to be previously stored in a capacitor before being used by one or several wireless sensors.

From the applications described above, the first (and to a lesser extent the second) involves a large number of constituent elements, resulting in a large degree of freedom in the way energy is collected, transported, and supplied. The energy problem can be explored in a **grid** context. This grid is an energy network which links all the elements using electrical connections and power electronic devices. The grid can either be static if it relies on fixed interconnections and energy converters, or dynamic if the interconnections and the energy converters are reconfigurable dynamically. If the grid configures itself automatically based on information about the constituent elements (generators, storages and consumers), then is can be termed a **smart grid**. A MFC-based smart grid offers the advantage of improved efficiency, reliability, economics, and sustainability of electricity services, with the advantage of being implemented

The smart-grid can be implemented at different scales. As an example, in the case of a wastewater treatment plant, these can be hundreds or even thousands of individual MFCs which supply few tens of devices.

9.2 Energy management of serially connected MFCs

This part of the manuscript takes apart the plurality of the energy storage and consumers. It concentrates on the collective of MFCs only. MFCs can be associated in parallel and make use of a low input-voltage power management unit (PMU). Alternatively, serial association takes advantage of the plurality of the MFCs to step-up voltage to levels acceptable by commercially-available DC/DC converters (i.e. few volts). In the EcoBot III, an association of 48 MFCs (4 in parallel and the 12 groups in series) is used with step-up DC/DC converters (MAX1795 and max1797) to supply a micro-controller with 3.3V and 5V respectively [Ieropoulos, 2012]. The serial association of a large number of MFCs is a challenge itself because of hydraulic couplings (when MFCs share the same substrate) and because of non-uniformities between generators which cause direct association to be inefficient like introduced in Section 2.6 and formalized mathematically in Chapter 11.

Issues relative to the **hydraulic connections** can be addressed on the MFC side by operating MFCs in batch or using intermittent hydraulic feeding [Ieropoulos et al., 2010b]. It can also be addressed using adequate power management devices such as insulated converters like mentioned in Chapter 7.

Issues relative to the **non-uniformities** of MFCs can also be addressed with insulated converters. These harvest energy from each MFC at MPP and enable connection at their output. This solution however involves a very large number of front-end PMUs each with low input-voltage specifications, leading to an expensive and poor efficient implementation.

In order to permit serial association in future applications, it is necessary to reduce the cost associated with existing solutions to deal with non-uniformities. Non-uniformities can be compensated with electronic circuits to prevent voltage reversal (in the worst case), or enable voltage equalizing (i.e. improved reliability factor). These so-called voltage balancing circuits do not replace a PMU with MPPT control, but complement it like in Figure 9.1. The specifications on the PMU required for a balanced association of MFCs are less restrictive because of the higher input voltage. The number of MFCs in the association can be chosen to enable the use of an off-the-shelf PMU.

The objective of this part of the manuscript is to demonstrate the feasibility to improve the energy harvesting from a large number of MFCs using dedicated low-cost, high-efficiency, voltage-balancing circuits. These circuits permit to efficiently harvest energy from serially connected non-uniform MFCs. They however assume that MFCs are disconnected hydraulically.

9.3 Voltage balancing circuits for MFCs

As seen in Section 3.3, the maximum power point voltage of non-uniform MFCs (V_{MPP}) is almost the same, even if their maximum power differs. This is due to large dispersions in the internal voltage drops (i.e. activation, ohmic and concentration) within the MFC whereas the internal electromotive force (i.e. the equivalent voltage source) is almost always the same. Equilibrating the individual cell voltage of a stack to V_{MPP} is therefore beneficial for power production. This particular characteristic of MFCs permitted to use the fractional open circuit voltage (FOCV) quasi-MPPT method in the flyback converter in Chapter 7.

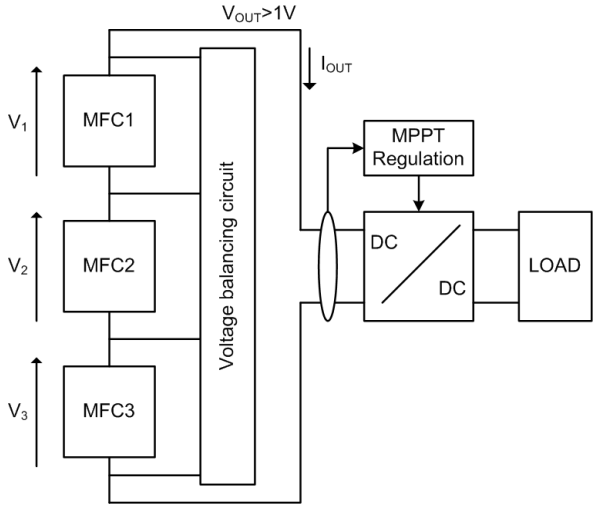

Figure 9.1: Circuit topology including a voltage balancing circuit and a PMU

Similarly, when considering n MFCs connected in series, the association produces maximum energy when the voltage of each individual cell equals its MPP voltage, V_{MPP}, which is a fraction of its OCV. When taking the hypothesis that V_{MPP} is the same for each cell of the stack, the association produces maximum energy when the voltage of each cell is equilibrated and equals V_{MPP}. The purpose of the voltage balancing circuit is to equilibrate the voltage of the cells in the configuration. The PMU can be controlled to regulate its input voltage to nV_{MPP}. In this way, the combination of the voltage balancing circuit and the PMU like in Figure 9.1 theoretically permits maximum energy production from the association.

Voltage balancing circuits are power electronic devices. They can be implemented in different topologies which are discussed in the literature review. To the author's best knowledge, no voltage balancing circuit was previously used to improve the performance of serially connected MFCs. As such, the review is inspired by circuits used to equilibrate voltages across storage elements or other energy generators which have higher voltage and power levels than MFCs. Those circuits can not be adapted as such to MFCs because of their high cost and high energy losses. A deeper study of the literature permits to identify two circuits which can be implemented at low-power and low-cost with MFCs. The **complete disconnection (CD) method** permits to avoid voltage reversal and its detrimental consequences and the **switched-capacitor (SC) method** realizes efficient voltage balancing at low cost. These two methods and a third so-called **switched-MFC (SMFC) method** (not reported in literature) are then studied in detail to evaluate the impact of key parameters on their performances. They are then compared in the Conclusions Chapter.

Chapter 10

Literature review

Contents

10.1 Methods to prevent voltage reversal of serially connected cells 91
10.2 Methods to equalize the voltage of serially connected cells 92
10.3 Conclusion of the review 95

Voltage balancing circuits can be used to equilibrate batteries, supercapacitors, photovoltaic cells, or fuel cells as outlined in the following.

- **Battery balancing circuits** permit to extend the life of batteries [Altemose,]. Li-ion cells are designed to provide a voltage in the range of approximatively 2 V to 4.3 V depending on their chemistry. During the life of the battery, the various cells in a battery may age differently. Without a voltage balancing system, the individual cell voltage will drift apart over time and the voltage of one cell may drop below its lower acceptable limit, irreversibly damaging it. Most voltage balancing circuits reported in literature concern battery balancing [Baronti and Fantechi, 2011, Kimball et al., 2007, Stuart and Zhu, 2011]. There are some commercial products available for this application [Altemose, , Delrossi, 2002]. These are adapted to the voltage and power levels of Li-ion cells and are not operational with low-voltage and low-power MFCs.

- **Supercapacitors** are promising to store electrical energy in advanced automotive applications. These have a limited voltage (e.g. 2.8 V) and are associated in series to reach a suitable voltage level. Non-uniformities are caused by manufacturing tolerances, aging behavior, and influence of temperature [Diab et al., 2006, Barrade, 2002].

- **Photovoltaic cells** are generally associated in series and in parallel into modules. These are subject to differential shades which directly impact the power output. In [Vighetti et al., 2010], a buck-boost balancing circuit permits to improve power generation by 45 % compared to a passive bypass.

Circuits from literature[1] are listed in Table 10.1. Some only prevent voltage reversal of one weak cell. The phenomenon of voltage reversal is introduced in [Oh and Logan, 2007] and described later in Chapter 11. Some other circuits actually aim to equilibrate the voltage of each cell. Both types of circuit will

[1] The literature study was assisted by Pascal Venet, Professor within Laboratoire Ampère, who works on voltage balancing circuits for supercapacitors.

be henceforth termed voltage balancing circuits. The balanced devices will be termed “cells” for the sake of a generic approach. This literature review presents and discusses those circuits in the application scope of balancing serially connected MFCs with the objective being to identify which circuit offers the best performance. The outcome of this study is that the complete disconnection (CD) and the switched capacitor (SC) circuits offer interesting features for use with MFCs.

Category	Circuit name
Voltage reversal prevention	Passive bypass
	Active bypass
	Complete disconnection (CD)
Rigorous voltage-equalizing	Digital dissipative shunting
	Analog dissipative shunting
	PWM dissipative shunting
	Switched-capacitor (SC)
	Energy converter (e.g. buck-boost)

Table 10.1: Voltage balancing circuits

10.1 Methods to prevent voltage reversal of serially connected cells

Methods that only prevent voltage reversal are the simplest methods and are commonly used with solar cells, but with limited benefits. In addition, these methods modify the number of cells in series, thus changing the MPP voltage of the stack. Three different methods are described in literature as detailed below.

10.1.1 Passive method

A straight-forward solution to prevent voltage reversal is to add protection bypass diodes in parallel to all cells like in Figure 10.1. The diode turns on when the voltage of a cell decreases below $-V_D$, V_D being the threshold voltage of the diode. This solution offers the advantage of being simple and low-cost to implement. However, even when using low-threshold Schottky diodes, it does not completely prevent cell reversal and has a limited advantage. This solution is usually implemented in photovoltaic modules [Vighetti et al., 2010, Shimizu et al., 2001] because it is clearly a low-cost solution with no quiescent energy consumption. It was also implemented in the EcoBot III to bypass several MFCs in case of voltage reversal [Ieropoulos, 2012].

10.1.2 Active methods

In the **active bypass method**, the diodes in the passive circuit are replaced by active switches (e.g. transistors) like in Figure 10.2 (a). The voltage across each cell is sensed and when it decreases below a certain voltage (e.g. 0 V), the switch turns on to short-circuit the weak cell. This method requires simple electronic (comparators, drivers and switches) that can be implemented at low cost and low-power. This method was used in a power supply using on chip hydrogen fuel cell [Frank et al., 2010]. In this System-On-Chip (SOC), each single cell is periodically checked for functionality and shorted by a bypass if found faulty.

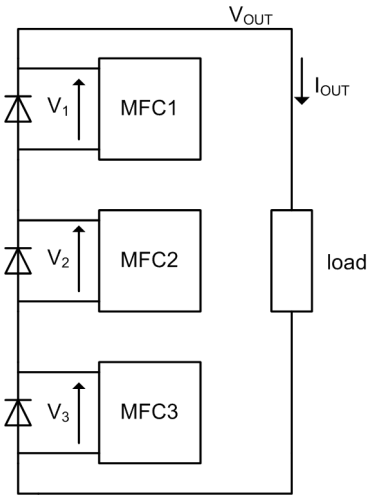

Figure 10.1: Passive bypass voltage balancing circuit

The main drawback is that when a cell is short-circuited, its voltage is set to 0 V. This operating condition might not be the best to enable the performance recovery of the concerned cell in the case of MFCs. Also, if the performance of the cell increases again, this cannot be observed by the voltage sensor. Therefore, a short-circuited cell has no chance to be re-integrated into the stack.

In **complete disconnection circuits** like in Figure 10.2 (b), a weak cell can be fully disconnected from the network until it recovers. The implementation of this method is similar to the implementation of the active bypass circuit except for a higher number of switches. The implementation is therefore low-cost and low-consumption. This method was used in [Kim and Kim, 2011] to realize a self-reconfigurable, multi-cell battery design.

The main advantage compared to the active bypass method is that the disconnected cell can recharge and be connected again. One drawback is that it requires a switch in series with each cell which creates additional losses. In the case of MFCs, the current being below 1 A, this drawback is relatively limited. This circuit will be studied in details in Chapter 12 of this manuscript.

10.2 Methods to equalize the voltage of serially connected cells

Other circuits in the literature permit to equalize the voltage of unbalanced sources connected in series. **Shunting methods** are based on deviating part of the current of a strong cell in a resistance (to decrease the current into weaker cells). In this way, only the optimal current, I_{MPP}, of the weakest cell is common to the series association. **Shuttling methods** are based on storing energy from a strong cell and then transferring this energy to a weaker cell.

10.2.1 Dissipative shunting methods

In the **dissipative shunting circuit**, the voltage across cells is sensed. If one voltage is too high, a resistor is added in parallel to the cell to deviate part of its current and artificially decrease its voltage. As such,

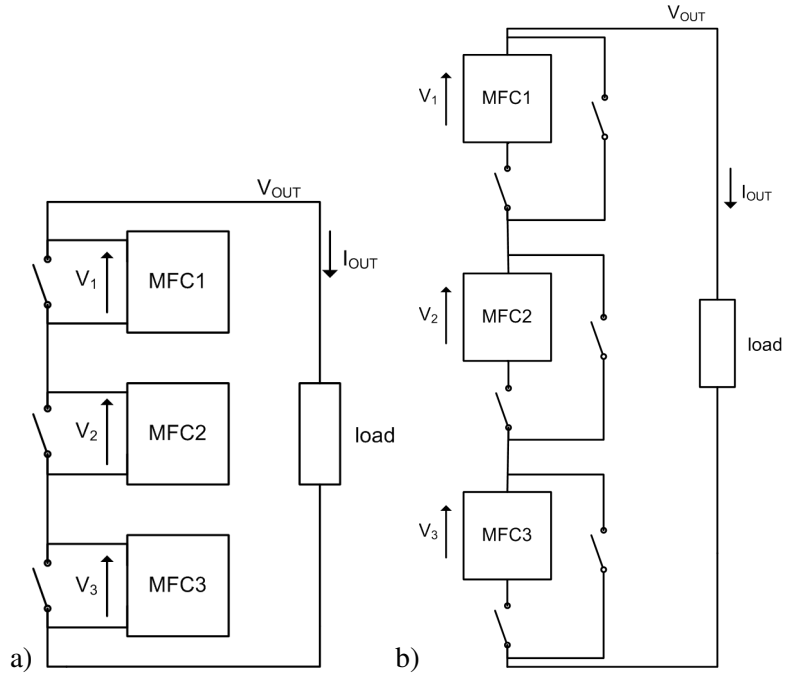

Figure 10.2: Voltage balancing circuits with active bypass (a) and complete disconnection (b)

the other weaker cells of the stack can operate ot current levels that are suitable. This solution leads to the situation that all cells operate at the power level of the weakest which leads to poor global efficiency.

The resistor is either switched (i.e. **digital dissipative method**) like in Figure 10.3 (a) or analogically controlled (i.e. **analog dissipative method**) like in Figure 10.3 (b). Both methods only require one comparator and one switch for each cell, which leads to a quite economical implementation. The digital dissipative method is used in the AIC1804 chip to balance up to 4 Li-ion batteries. This chip consumes a power in the order of tens of μW.

Another shunting strategy is the **PWM dissipative method**. It is similar to the digital dissipative method except that the resistor is switched at high frequency with a PWM control to vary the apparent shunt resistance.

Because they have poor efficiency, these circuits are not interesting in the case of low-power generators like MFCs and will not be detailed.

10.2.2 Shuttling active balancing methods

In shuttling active balancing methods, the extra-energy from strong cells is not lost but is re-injected into weaker cells. The energy transfer is realized with a storage device which can either be a capacitor (i.e. switched capacitor circuit) or an inductor (i.e. inductive shuttling circuits). Ideally, the efficiency of these circuits is 100%.

Switched capacitor circuits use capacitors to transfer charges between adjacent cells like in Figure 10.4 (a). This circuit was described by Pascual in a patent [Pascual, 1998] .

This circuit requires no control or feedback loop and can be implemented easily. In the case of MFCs, a discrete design seems feasible. It requires an oscillator to control the switches. It can be a nanopower TS3001 (Touchstone) with a tunable frequency using an external resistor. It consumes currents

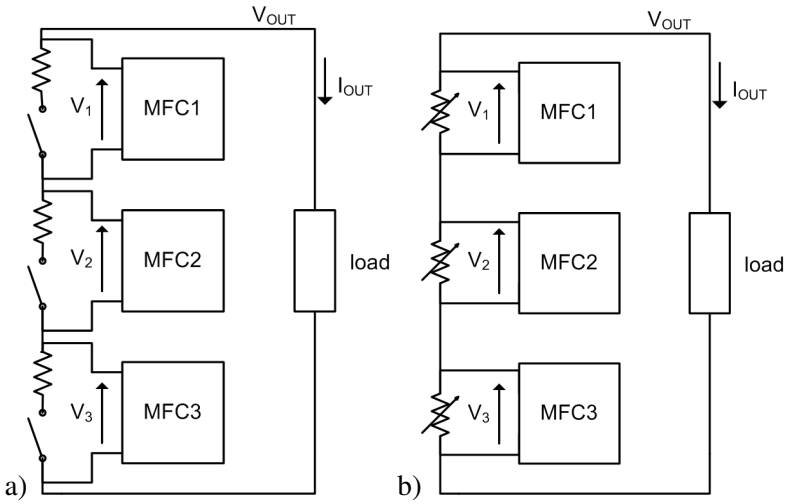

Figure 10.3: Digital (a) and analog (b) dissipative shunting methods

in the μA range and requires a supply voltage between 0.9 V and 1.8 V. The switches can be made with standard MOS components such as the DMG6968 [Diodes Incorporated, 2009] (36 mΩ at 1.8 V). The capacitor can be standard ceramic capacitors with capacitive values reaching tens of μF and which offer good performances (e.g. low equivalent series resistance) at frequencies up to 1 MHz. Because of its advantages, this circuit will be detailed analytically in Chapter 13.

This topology can also be realized using a single capacitor like in [Moore and Schneider, 2001], but at the expense of a large amount of switches. It offers the advantage of allowing charge-transfer from non-adjacent cells.

Inductive shuttling circuits are based on inductive energy converters to subtract or add energy from strong or weak cells. These methods can be classified in three groups as in [Cao et al., 2008]:

- The **cell-to-cell method** transfers energy from adjacent cells. Various topologies can be found in literature like the buck-boost converter in Figure 10.4 (b). This circuit was fully studied by Vighetti in Chapter IV of his PhD thesis [Vighetti, 2010]. Assuming that switches T_i turn off sequentially with a duty-cycle $\bar{\alpha}_i$, the voltage across each MFC is $V_i = \bar{\alpha}_i V_{OUT}$. An example of application can be found in [Vighetti et al., 2010] where 144 solar cells are balanced with different scenarios of association and shading. In some conditions, this circuit leads to a gain of 45 % compared to energy harvested using bypass diodes.

- The **single cell-to-pack method** is based on using the individual voltage of each cell as the input of one or several converters where the outputs are the pack of cells. The current of the strongest cells is transmitted to the pack through the DC/DC converter. Figure 10.5 (a) shows a cell-to-pack method that uses flyback converter topologies. The energy switched in the inductances L_i is transferred to the stack through the single secondary winding and the diode.

- The **pack-to-single-cell method** is based on using the stack voltage as the input of one or several converters where the outputs are each cell output. Part of the current of the stack is used to increase the current of the weakest cells. It can be implemented as in Figure 10.5 with flyback converters. A current from the cell stack is switched (T) into the transformer single primary winding and

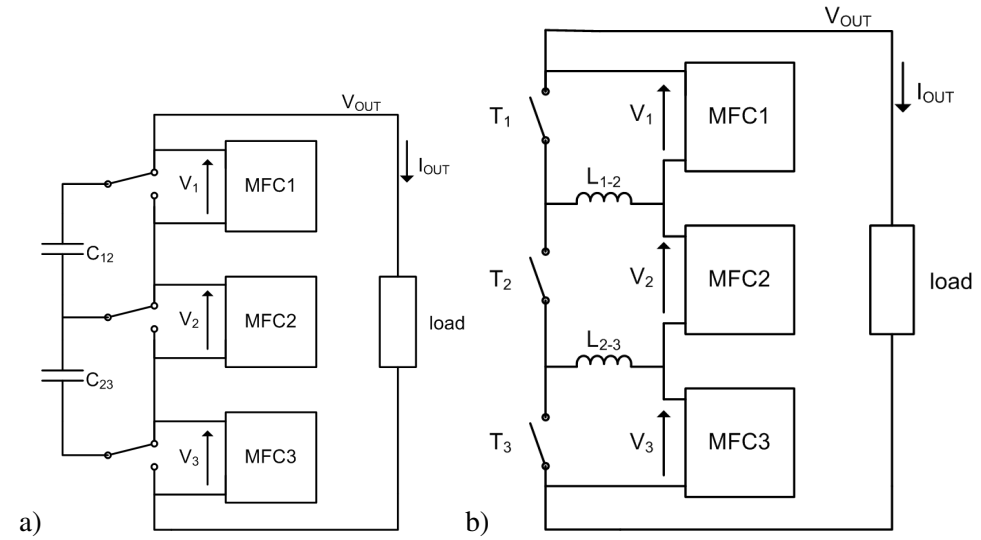

Figure 10.4: Switched-capacitor (a) and buck-boost (b) voltage-balancing circuit

induces current in each of the secondaries. The MFC with the lowest voltage V_i will have the highest current.

The control circuit for any of these inductive shuttling circuits is quite complicated because it often requires sensors as well as PWM oscillators. Another drawback is the number of inductors they require. These circuits are thus expensive and not adapted to low-power generators like MFCs. These circuits will therefore not be discussed any further.

10.3 Conclusion of the review

An extensive comparison can be found in [Daowd and Omar, 2011] which focuses on the application of battery balancing. The specifications offered by MFCs lead to focus on the criteria of component quantity and quality (informing on the cost), power consumption and balancing performances (efficiency). Table 10.3 summarizes the results from the above discussion for a n-stage voltage balancing circuit. In this table, the power consumption strongly depends on the chosen components and the efficiency on the non-uniformities between cells.

Circuits which only prevent voltage reversal are not as efficient as circuits which equilibrate the voltages. Compared to the passive and active bypass circuits, the **complete shunting circuit** permits for a weak cell to be disconnected until it recovers and it is eventually reconnected to the stack. This can be useful in some applications where one MFC only is defective and impeding the stack. One drawback is that when one cell is disconnected, the MPP voltage of the stack (theoretically equal to nV_{MPP}) is changed. If the PMU is set to control the stack voltage to nV_{MPP}, the efficiency will be slightly decreased.

The most efficient circuits are the ones which perfectly equalize the voltage across each MFC of the stack. The switched capacitor and inductive shuttling methods permit this and have therefore a theoretically high efficiency. As an example of inductive shuttling method, the buck-boost circuit requires $n-1$ inductive components. These are particularly expensive and are not used efficiently in the case of

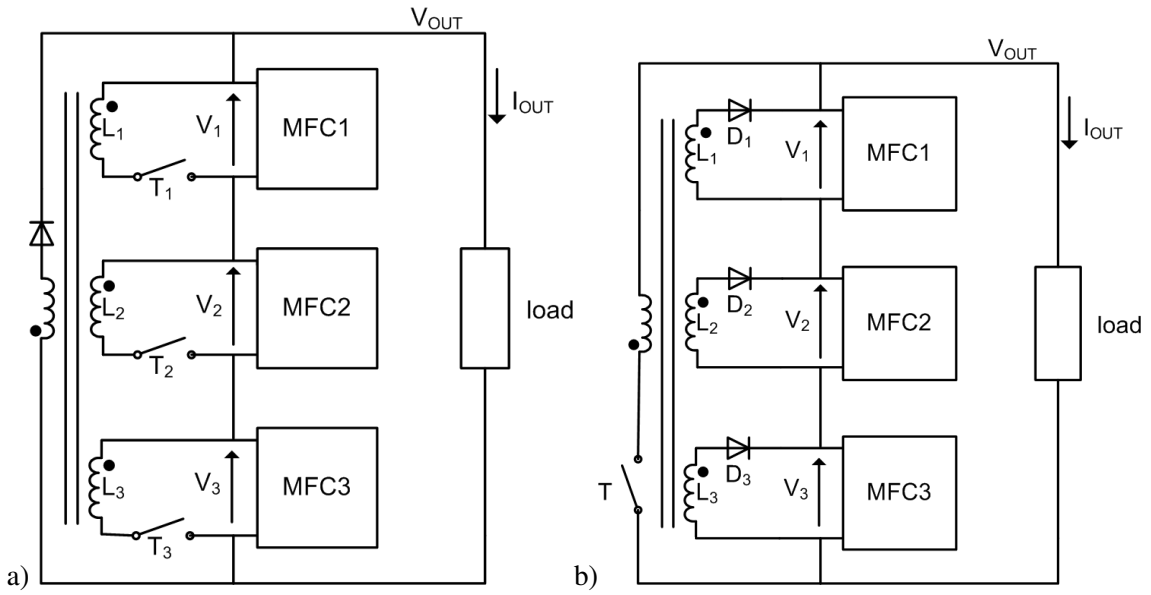

Figure 10.5: Flyback-type shared-transformer cell-to-pack (a) and pack-to-cell (b) voltage-balancing methods

low-power generators like MFCs. For this reason, this circuit is not adapted to MFCs. Generally, any inductive shuttling methods suffer from this drawback. The switched capacitor circuit however only requires switches, capacitors and a single oscillator. These require smaller footprints and lower cost. The **switched capacitor circuit** therefore offers good perspectives.

The following Chapters of Part III studies the MFC serial association (SA) without voltage balancing (reference) and with complete disconnection (CD) shunting and switched capacitor (SC) shuttling circuits. These two circuits are studied in detail in order to evaluate the impact of some design parameters on the performances. Then, a novel voltage-balancing switched-MFC (SMFC) circuit is introduced, analyzed and compared to the CD and SC circuits.

Circuit	Component count						P	Efficiency
	Sw	R	C	L	Cp	Osc		
None	0	0	0	0	0	0	**0**	**very poor**
Passive bypass	n	0	0	0	0	0	**0**	**very poor**
Active bypass	n	0	0	0	n	0	**low**	**poor**
CD	2n	0	0	0	n	0	**low**	**poor**
Digital shunting	n	n	0	0	n	n	**high**	**poor**
Analog shunting	n	n	0	0	n	0	**low**	**poor**
PWM shunting	n	n	0	0	n	1	**high**	**poor**
SC	n(*2)	0	n-1	0	0	1	**low**	**good**
Buck-boost	n	0	0	n-1	n	n	**high**	**good**

Table 10.2: Estimation of component quantity and quality, power consumption and efficiency for n-stage circuits. The components are from left to right: number of switches, resistors, capacitors, inductors, comparators and oscillators.

Chapter 11

MFC association in series without voltage balancing circuit

Contents

11.1 Operation of a two-stage MFC association 98

11.2 Operation of an n-stage MFC association 101

This section will study the operation and the performance corresponding to the serial association of MFCs without any voltage balancing circuit[1]. This scenario corresponds to the reference to which voltage balancing circuits will be compared. The objective of this section is to formalize theoretically the phenomena that occur when non-uniform MFCs are connected in series. This section first studies the most simple case of two MFCs and then the case of n MFCs. The energy that can be harvested from a non-uniform stack is evaluated with different scenarios of non-uniformities.

11.1 Operation of a two-stage MFC association

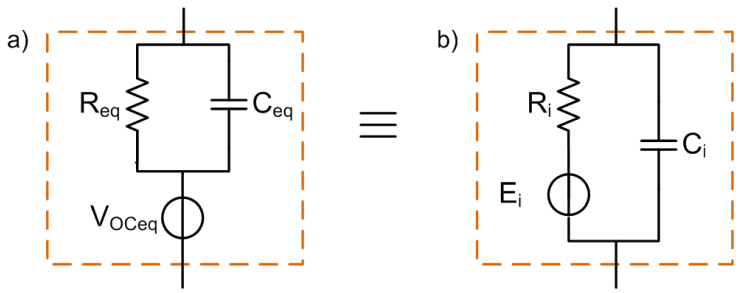

Figure 11.1: Basic equivalent circuit of a MFC

Let us consider the serial association of two MFCs and suppose that these MFCs behave like the simplistic equivalent circuit (b) derived from (a) in Figure 11.1 (i.e. voltage source in series with a

[1] A similar analysis was done on RF transducers (i.e. rectennas) with Vlad Marian, doctoral student at Laboratoire Ampère. The results led to a joint paper in the Antennas and Wireless Propagation Letters [Degrenne et al., 2012d].

resistor, both of them in parallel with a capacitor). This circuit is satisfactory for the static study of the serial association. MFC1 is defined by the triple (E_1, R_1, C_1) and MFC2 by (E_2, R_2, C_2) like in Figure 11.2. When connected to a load (V_{OUT}) (Figure 11.2), the current flowing through the circuit in steady-state is expressed as

$$I_{OUT} = \frac{E_1 + E_2 - V_{OUT}}{R_1 + R_2} \tag{11.1}$$

The voltage across MFC1 and MFC2 is expressed as

$$V_1 = E_1 - R_1 \frac{E_1 + E_2 - V_{OUT}}{R_1 + R_2} \tag{11.2}$$

$$V_2 = E_2 - R_2 \frac{E_1 + E_2 - V_{OUT}}{R_1 + R_2} \tag{11.3}$$

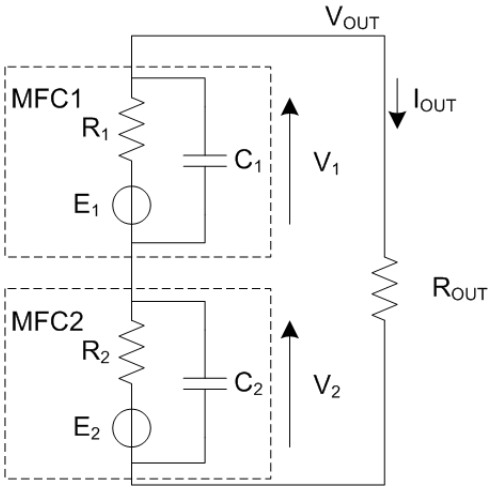

Figure 11.2: Serial association of two MFCs

Let us consider now that the open-circuit voltage of both MFCs is similar ($E_1 = E_2 = 0.6V$), whereas the internal resistances differ ($R_1 = 18\Omega$, $R_2 = 6\Omega$). This assumption results from the MFC characterization in Section 3.3 of this manuscript. As such, the maximum power available from MFC1 and MFC2 is 5 mW and 15 mW respectively. The V-I and P-I polarization curves for individual and associated MFCs are given in Figure 11.3.

We assume that a PMU controls the output voltage of the stack to match the theoretical stack MPP voltage of 0.6 V. The current, I_{OUT}, is the intersection of the V-I curve for the associated MFCs with the horizontal curve corresponding to $V_{OUT} = 0.6$ V. In Figure 11.3 (a), $I_{OUT} = 26$mA. The operating point of each MFC is defined as the intersection of their polarization curve and the vertical line corresponding to $I = I_{OUT}$. For this operating point, the voltages of each MFC is different, leading to a non-optimal operating point. In Figure 11.3 (b), the MPP of the stack is 15 mW instead of 20 mW. For high values of current, the voltages V_1 and V_2 drift apart, eventually leading to a negative value of V_1. This phenomenon

is usually discussed as “voltage reversal”. The weakest MFC (MFC1) absorbs power instead of contributing to power generation. This analysis assumes that the equivalent model of the MFCs is still valid for negative MFC voltage values (which was not verified experimentally in Part I).

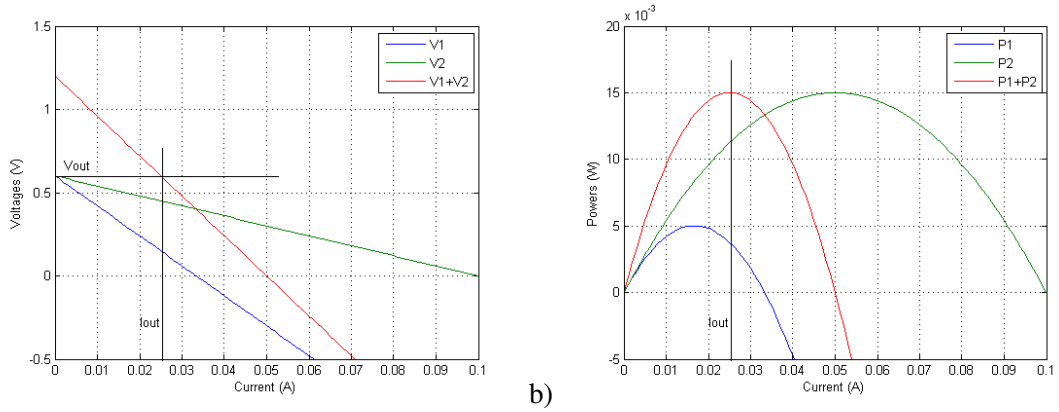

a) b)

Figure 11.3: V_1 and V_2 (a) and P_1 and P_2 (b) as a function of load current

Let us assume that two MFCs are in series and are operated at their theoretical maximum power point voltage, $V_{OUT} = (E_1 + E_2)/2 = 0.6V$. When the MFCs are non-uniform ($P_{1MPP} \neq P_{2MPP}$), voltages V_1 and V_2 are not balanced. V_1 is given in Figure 11.4 (left axis, straight line) for different values of P_{1MPP}, with the condition $P_{1MPP} + P_{2MPP} = 20$ mW. When P_{1MPP} is maximum (and P_{2MPP} is minimum), V_1 is close to 0.6 V and V_2 close to 0 V. The power of the association ($P_{OUT} = P_1 + P_2$) is plotted in Figure 11.4 (right axis, parabolic curve). The power delivered by the association of the two MFCs is less than 20 mW when the absolute difference between P_{1MPP} and P_{2MPP} increases because MFCs are not operated at their maximum power point.

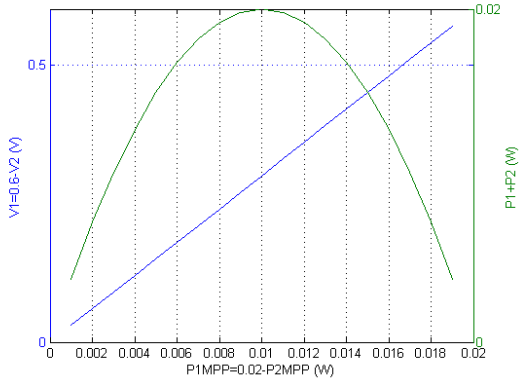

Figure 11.4: V_1 and P_{OUT} as a function of P_{1MPP} (at constant total MPP power $[P_{1MPP} + P_{2MPP}]$)

11.2 Operation of an n-stage MFC association

The previous discussion on the serial association of two MFCs can be extended to n MFCs. MFCi is defined by the triple (E_i, R_i, C_i). When connected to a load (V_{OUT}), the current flowing through the circuit is expressed as

$$I_{OUT} = \frac{\sum E_i - V_{OUT}}{\sum R_i + R_{OUT}} \tag{11.4}$$

The voltage across each MFCi of the stack is expressed as

$$V_i = E_i - R_i \frac{\sum E_i - V_{OUT}}{\sum R_i + R_{OUT}} \tag{11.5}$$

The power of the association is expressed as

$$P_{OUT} = I_{OUT} \cdot V_{OUT} = I_{OUT} \cdot \sum V_i \tag{11.6}$$

Efficiency is defined as the ratio between the output power and the maximum power that can be harvested from the association with an ideal voltage-balancing. The latter is expressed as

$$P_{IN-MAX} = \sum P_{iMPP} = \sum \frac{E_i^2}{4R_i} \tag{11.7}$$

The efficiency can be derived from Equations 11.6 and 11.7. It is expressed as

$$\eta = \frac{n}{\sum \frac{R_i}{n} \sum \frac{1}{R_i}} \tag{11.8}$$

Let us consider a set of 10 MFCs which share the same open-circuit voltage, $E_i = 0.6$ V, have non-uniform internal resistance but the mean value of their maximum power, P_{iMPP}, is 10 mW. Table 11.1 shows the simulated efficiency of the association, $P_{OUT}/\sum P_{iMPP}$, for different scenarios of dispersion. The standard deviation (Std) is given as an indication of non-uniformity. When all P_{iMPP} equal 10 mW (uniform scenario), the output power equals the sum of the individual MPP powers and the efficiency is 100 %. When only one MFC is very weak ($P_{2MPP} = 1$ mW) and all others MFCs have uniform strength ($P_{iMPP}(i \neq 2) = 11$ mW), the weak MFC absorbs energy and strongly handicaps the efficiency of the association which drops to 55 %. When the MFCs are consistently non-uniform, the efficiency decreases with non-uniformities. For a slightly non-uniform association ($P_{iMPP}(i = odd) = 8$ mW and $P_{iMPP}(i = even) = 12$ mW), the efficiency is very slightly affected (96 %). For a moderately non-uniform association ($P_{iMPP}(i = odd) = 5$ mW and $P_{iMPP}(i = even) = 15$ mW), the efficiency decreases to 75 %. Finally, for a moderately non-uniform association ($P_{iMPP}(i = odd) = 2$ mW and $P_{iMPP}(i = even) = 18$ mW), the efficiency is very low (36 %).

Table 11.1: Efficiency for different scenarios of cell dispersion for a series of 10 MFCs with average maximum power of 10 mW. In the uniform scenario, all P_{iMPP} equal 10 mW ($R_i = 9\,\Omega$), leading to a standard deviation (Std) of 0 mW. In the uniform scenario with one faulty cell, all P_{iMPP} equal 11 mW ($R_i = 8.2\,\Omega$), except for P_{2MPP} that equals 1 mW ($R_2 = 90\,\Omega$). In the scenario with low non-uniformities, P_{iMPP} either equal 8 mW or 12 mW. In the scenario with medium non-uniformities, P_{iMPP} either equal 5 mW or 15 mW. In the scenario with high non-uniformities, P_{iMPP} either equal 2 mW or 18 mW.

Dispersion scenario	Std (mW)	Maximum power series (mW)	**Efficiency (%)**
Uniform	0	(10, 10, 10, 10, 10, 10, 10, 10, 10, 10)	**100**
Uniform - one faulty cell	3.2	(11, 01, 11, 11, 11, 11, 11, 11, 11, 11)	**55**
Low non-uniformity	2.1	(8, 12, 8, 12, 8, 12, 8, 12, 8, 12)	**96**
Medium non-uniformity	5.3	(5, 15, 5, 15, 5, 15, 5, 15, 5, 15)	**75**
High non-uniformity	8.4	(2, 18, 2, 18, 2, 18, 2, 18, 2, 18)	**36**

Chapter 12

MFC association with a complete disconnection circuit

Contents

12.1 Theoretical study of a two-stage MFC association 103

12.2 Operation of an n-stage MFC association 105

The Complete Disconnection (CD) method was identified in the literature review as a promising circuit to be implemented in stacks of MFCs. In the CD method, a weak MFC is disconnected from the association when its voltage decreases below a certain threshold voltage V_{TH-LOW}.

One option is to reconnect the cell when its voltage reaches $V_{TH-HIGH}$. This method can lead to different results based on the chosen threshold voltages. If V_{TH-LOW} is only slightly inferior to $V_{TH-HIGH}$, the voltage of a weak MFC fluctuates and is included between both voltages. When connected to the stack, its voltage is initially $V_{TH-HIGH}$. It decreases with its own time-constant until it reaches V_{TH-LOW}. It is then disconnected until its voltage increases back up to $V_{TH-HIGH}$.

A second option is to keep this cell disconnected from the stack but connected to an external load that is optimized for MFC recovery. Indeed, Section 2.5 of this manuscript suggests that particular operating points (favoring high current densities) permit to increase performances in the long term. After a given time, the MFC will be able to be connected again to the stack. The following analysis will consider this option. As such, the simulations consider that once a MFC is disconnected, it is not reconnected. The down threshold voltage is chosen to be 0 V to simply avoid voltage reversal.

One issue identified in the literature review is that the CD voltage balancing is not adapted to a static FOCV quasi-MPP. For this circuit, the PMU will be assumed to include an ideal MPPT such as a P&O algorithm.

12.1 Theoretical study of a two-stage MFC association

For the analysis of the CD circuit, a simple MFC equivalent model like the one used in the serial association is sufficient. The switches used in the circuit are supposed to have an on-resistance, R_{SW}, like in Figure 12.1. The output voltage V_{OUT} is the sum of MFC voltages V_1 and V_2 from which the voltage drops across the on-resistance of the switches are subtracted.

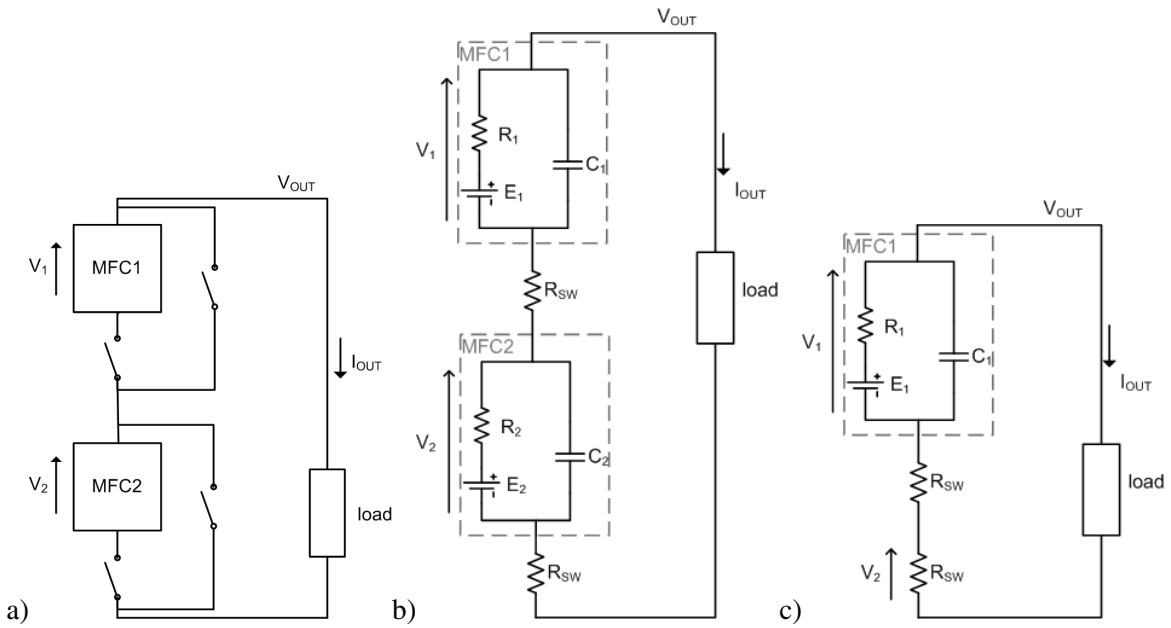

Figure 12.1: Schematic (a) and equivalent model of the complete disconnection circuit when no MFC is disconnected (b) and when MFC2 is disconnected (c)

If R_1 and R_2 differ significantly, the voltage across the weakest MFC reverses and it is switched off. This creates a discontinuity on the V-I characteristic curve of the stack like in Figure 12.2(a). When the difference between R_1 and R_2 is small, the MPP is reached before the weakest MFC is disconnected (blue and red curves in Figure 12.2(b)). When the difference between R_1 and R_2 is high, the maximum power point of the stack is reached when the weakest MFC is disconnected (green curves in Figure 12.2 (b)). The P-I static characteristic curve eventually displays two local maxima, which may impede the operation of a MPP algorithm.

Figure 12.3 (a and b) shows the voltage V_1 (V_2 can be obtained by symmetry) and the output power $P_{OUT} = P_1 + P_2$ with changes in maximum power of MFC1 such that $P_{1MPP} + P_{2MPP} = 20\,mW$. The load is chosen so that P_{OUT} is maximized (equivalent to an ideal MPPT). These were plotted for different values of R_{SW}. These values were chosen to be very high (0.2 Ω, 1 Ω, and 5 Ω) to artificially amplify conduction losses for the sake of discussion. More realistic values are in the order of few mΩ only like the component DMG6968 [Diodes Incorporated, 2009].

The voltage V_1 exhibits three states as P_{1MPP} increases from 0 to 20 mW. For low values of P_{1MPP}, MFC1 is disconnected and voltage V_1 corresponds to the voltage drop across R_{SW} like mentioned in Figure 12.1. When P_{1MPP} increases, V_1 is connected to the stack. As P_{1MPP} further increases, V_1 increases and V_2 decreases until MFC2 is disconnected. MFC1 is then connected alone to the load and the maximum power point is obtained for $V_1 \approx 0.3$ V.

When $P_{1MPP} = P_{2MPP} = 10$ mW, $V_1 = V_2 = 0.3$ V for R_{SW}= 0.2 Ω, which is close to an ideal circuit. For higher switch on-resistance, the voltage V_1 is higher because the MPP voltage of 0.3 V includes the voltage drop across R_{SW}.

The power of the stack ($P_1 + P_2$) correspondingly displays three states. The "normal" state is when no MFC is disconnected (P_1 in the order of 10 mW). The power curve approaches the curve for the serial association in Figure 11.4 at the difference of the voltage drops across both R_{SW}. Despite the

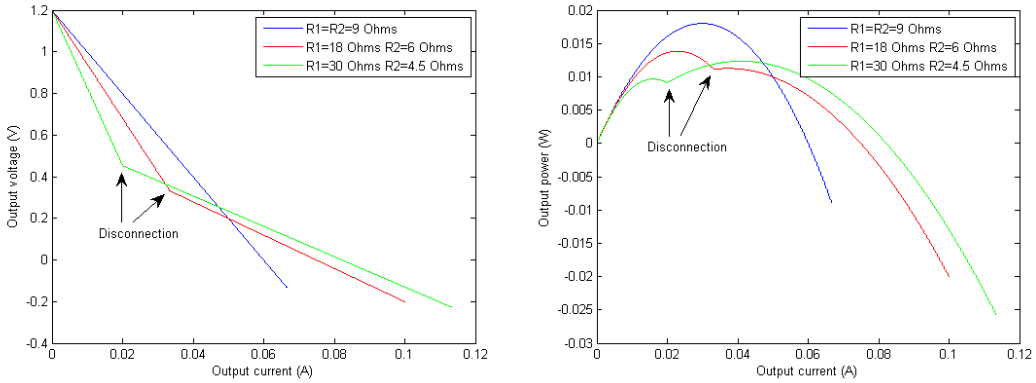

Figure 12.2: Simulated V-I and P-I static electrical characteristic curves for two equivalent MFCs connected in series with a complete disconnection circuit for different internal equivalent resistances

continuous decrease when P_1 increases or decreases, the output power rises again when one MFC is disconnected. The complete disconnection method is therefore particularly useful when MFCs are strongly non-uniform (i.e. P_1 is very low or very high). When the on-resistance of the switches increases, the output power decreases because of the additional resistive losses.

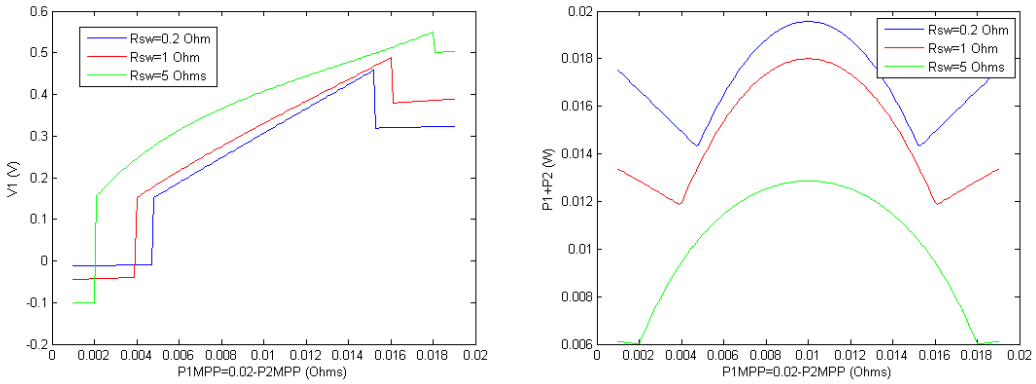

Figure 12.3: Voltages V_1 and V_2 for two MFCs connected in series with a complete disconnection circuit for different internal resistances

12.2 Operation of an n-stage MFC association

Let us consider the association of ten MFCs with a complete-shunting voltage balancing circuit. Such a circuit was simulated using Matlab and the results for various scenarios of non-uniformity are presented in Table 12.1. The losses in the switches are taken into account, but not the losses in their control. The on-resistance of the switches were deliberately overestimated ($R_{SW} = 1\,\Omega$) to amplify the loss phenomena.

When all cells are uniform, the stack efficiency is 90 %. The losses are in the switch resistances (R_{SW}) in series with the MFCs. When the ten MFCs are uniform except for one defective cell, the circuit disconnects the defective cell from the stack and permits the association to reach an efficiency of

Table 12.1: Efficiency for different dispersion for a series of 10 MFCs

Dispersion scenario	Std (mW)	Maximum power series (mW)	**Efficiency (%)**
Uniform	0	(10, 10, 10, 10, 10, 10, 10, 10, 10, 10)	**90**
Uniform - one faulty cell	3.2	(11, 01, 11, 11, 11, 11, 11, 11, 11, 11)	**86.1**
Low non-uniformity	2.1	(8, 12, 8, 12, 8, 12, 8, 12, 8, 12)	**86.7**
Medium non-uniformity	5.3	(5, 15, 5, 15, 5, 15, 5, 15, 5, 15)	**69.2**
High non-uniformity	8.4	(2, 18, 2, 18, 2, 18, 2, 18, 2, 18)	**34.6**

86.1 %, which is almost similar as for a fully uniform stack. When the ten MFCs are non-uniform, no cell is suffering from voltage reversing, even when the non-uniformity is important. As such, no cell is disconnected. The result is a poor global efficiency because the MFCs operate at unbalanced voltage.

Chapter 13

MFC association with a switched-capacitor circuit

Contents

13.1 Theoretical study of a two-stage MFC association 107

13.2 Loss analysis and performance study of a two-stage circuit 109

13.3 Performance study for an n-stage MFC association 111

The switched capacitor method is attractive because it permits to fully equilibrate the voltage of each MFCs and as such operates them at MPP.

In a two MFC circuit, a capacitor C_{12} (so-called "pump capacitor") is alternately connected in parallel with MFC1 and MFC2 at frequency f_S like in Figure 13.1. When the MFCs are unbalanced (e.g. $P_2 > P_1$), the capacitor charges when it is connected to the strongest MFC (MFC2), and discharges when it is connected to the weakest MFC (MFC1). The transfer of charges is limited by the resistances in series with the voltage source within MFCs and the capacitor C_{12}. These resistances include the on-resistances R_{SW} of the switches and the ohmic resistance R_{Ohm} of the MFCs. The equivalent series resistance of the capacitors are negligible compared to R_{SW}. The ohmic resistance of a 10 mW MFC can reach a few ohms, and is therefore high compared to R_{SW}. It will strongly handicap the performances of the SC circuit. Practically, a capacitor is added in parallel with the MFCs to "hide" the ohmic resistor at high frequencies. In this configuration, the basic electrical model used until now in Figure 11.1 is still valid and it is used in this section as well.

In this Chapter, the SC circuit is described analytically in its two-stage version. A loss analysis permits to evaluate the performance of the circuit for two-stage and n-stage topologies.

13.1 Theoretical study of a two-stage MFC association

Figure 13.2 shows the equivalent electrical circuit of the switched capacitor voltage balancing circuit. Capacitor C_{12} is connected via switches with an on-resistance R_{SW}.

The pump capacitor is assumed to be significantly lower than the internal capacitance of the MFCs ($C_{12} \ll C_1$ and $C_{12} \ll C_2$). As such, the voltage across a MFC is considered constant during a switching period.

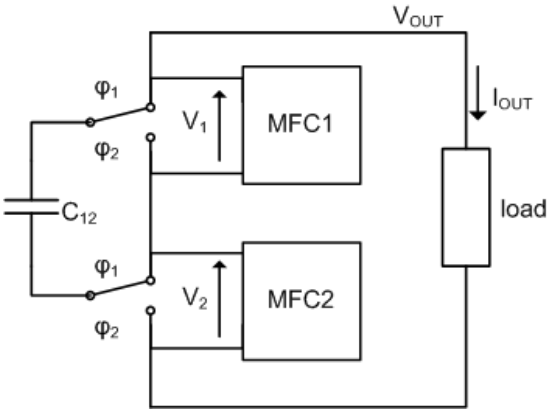

Figure 13.1: Schematic of the switched-capacitor circuit

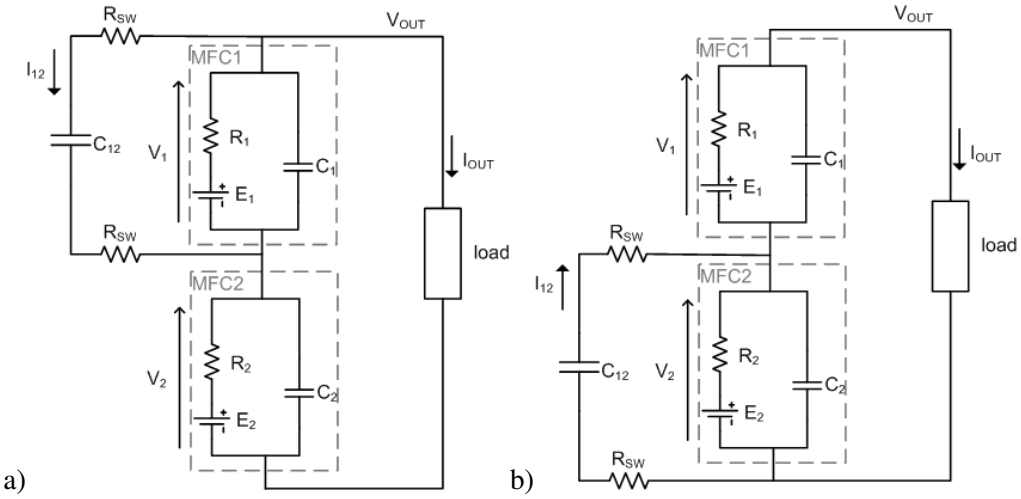

Figure 13.2: Equivalent switched-capacitor circuit during phase φ_1 (a) and φ_2 (b)

In steady state, $V_{C12\varphi1}$ and $V_{C12\varphi2}$ are the voltages across the capacitor C_{12} at the end of phase φ_1 and φ_2 respectively.

$$V_{C12\varphi1} = V_1 + (V_{C12\varphi2} - V_1)\exp(-t/\tau) \tag{13.1}$$

$$V_{C12\varphi2} = V_2 + (V_{C12\varphi1} - V_2)\exp(-t/\tau) \tag{13.2}$$

where $\tau = 2R_{SW}C_{12}$, and t is the time for which the switches are on in one phase. Assuming that the time for which the switches are on in both phases is the same, $t = 1/(2f_S)$, the voltage swing across C_{12} every half-cycle is given by:

$$V_S = V_{C12\varphi1} - V_{C12\varphi2} = (V_1 - V_2)\frac{1-\exp(-t/(2R_{SW}C_{12}))}{1+\exp(-t/(2R_{SW}C_{12}))} \tag{13.3}$$

Let us define the constant K as:

$$K = \frac{1-\exp(-t/(2R_{SW}C_{12}))}{1+\exp(-t/(2R_{SW}C_{12}))} = \frac{1-\exp(-1/(4fR_{SW}C_{12}))}{1+\exp(-1/(4fR_{SW}C_{12}))} \tag{13.4}$$

and

$$V_{DIFF} = V_1 - V_2 \tag{13.5}$$

The average current supplied to the capacitor C_{12} during phase φ_1 is given by

$$\langle I_{12} \rangle = f_S C_{12} V_S = f_S C_{12} K V_{DIFF} = f_S C_{12} K (V_1 - V_2) \tag{13.6}$$

For the two-stage switched-capacitor circuit, we therefore have the following equations:

$$\begin{cases} \langle I_{12} \rangle = f_S C_{12} k (V_1 - V_2) \\ V_1 = E_1 - R_1 (I_{OUT} + I_{12}) \\ V_2 = E_2 - R_2 (I_{OUT} - I_{12}) \\ V_1 + V_2 = V_{OUT} \end{cases} \tag{13.7}$$

The solution of this system of four equations and four unknowns gives the expression for $\langle I_{12} \rangle$, V_1, V_2 and I_{OUT}.

13.2 Loss analysis and performance study of a two-stage circuit

There are three types of losses in a SC circuit: a) the conduction losses in the on-resistances R_{SW} of the switches, b) the losses in the internal resistances R_1 and R_2, and c) the switching losses in the switches. The losses in the capacitors (resistive and leakage losses) are negligible.

Both conduction losses and losses in the internal resistances of MFCs are already accounted for in the expressions of I_{OUT}, as discussed in the previous section.

During phases φ_1 and φ_2, current flows through the closed switches resulting in **conduction losses** in the on-resistance R_{SW} of the switches. The instantaneous losses in the switch resistors are $2R_{SW}i_{12}^2$, i_{12} being the time-dependent value of the current supplied to the capacitor C_{12}.

Losses in the internal resistances R_1 and R_2 are caused by an improper impedance matching. MFCs operate at a voltage slightly different to their MPP voltage, resulting in a suboptimal power transfer.

Switching losses can be approximated by the following expression

$$P_{SW} = n f_S C_{eq} V_G^2 \tag{13.8}$$

where C_{eq} is the equivalent parasitic capacitance of one switch and V_G is the amplitude of the gate voltage. In the following, C_{eq} and V_G are estimated to be 200 pF and 1 V respectively based on the component DMG6968 [Diodes Incorporated, 2009]. This transistor has a threshold voltage of 0.7 V and can therefore be controlled by a signal with an amplitude of 1 V.

The circuit efficiency can therefore be expressed as

$$\eta = \frac{I_{OUT}V_{OUT} - nf_S C_{eq} V_G^2}{E_1^2/4R_1 + E_2^2/4R_2} \tag{13.9}$$

This expression, associated to the resolution of the four-equation system (13.7) enables to plot the efficiency versus frequency for various values of R_{SW} and C_{12} in Figure 13.3 (b) and Figure 13.4 (b) respectively.

The voltages V_1 and V_2 of an unbalanced serial association of two MFCs are given in Figure 13.3 (a). At low switching frequency, the circuit is not useful and voltages are not balanced. The difference between V_1 and V_2 decreases as switching frequency increases (voltage balancing). For high switching frequencies, the voltage difference is positively correlated to the switch on-resistance R_{SW}. This difference can be as low as 30 mV for $R_{SW} = 0.2\,\Omega$.

The efficiency of the association with changes in switching frequency is plotted in Figure 13.3 (b) for different switch on-resistances. Efficiency for $f_S = 1$ Hz is approx. 75 %. Efficiency increases with switching frequency (because of efficient voltage balancing) and reaches up to 98 % for $R_{SW} = 0.2\,\Omega$.

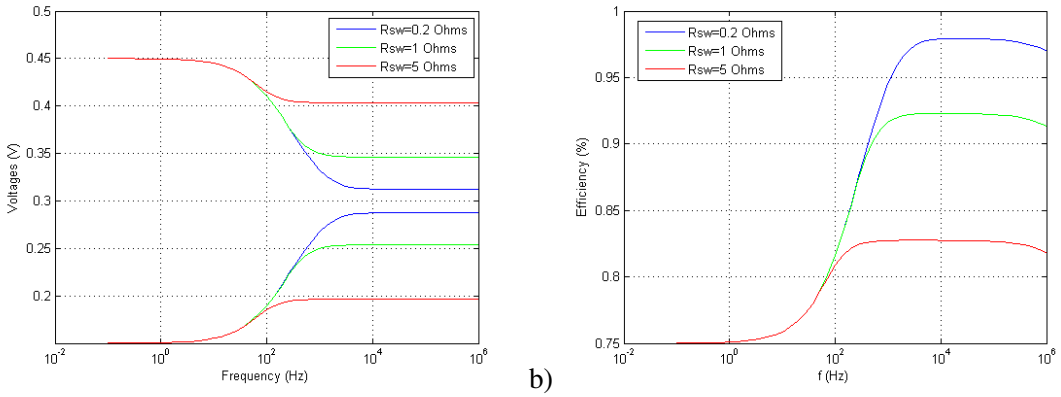

Figure 13.3: Voltages V_1 and V_2 (a) and efficiency (b) with changes in switching frequency for different switch on-resistance R_{SW} values ($R_1 = 18\,\Omega$, $R_2 = 6\,\Omega$ and $C_{12} = 200\,\mu$F)

The influence of the capacitor value, C_{12}, is investigated in Figure 13.4. A high value allows to achieve similar performances but at lower frequency (i.e. below 1 kHz with a 1 mF capacitor). The use of a low-cost SMD ceramic capacitors with values below 50 µF therefore requires switching frequencies above 10 kHz.

The curves in Figures 13.3 and 13.4 are obtained with a moderately non-uniform association of two MFCs. The impact of the dispersion between both MFCs is illustrated in Figure 13.5. These curves are plotted for the same mean maximum power of 10 mW per MFC. Figure (a) shows that the current I_{12} varies linearly with the maximum power difference between MFC1 and MFC2. Figure (b) shows how the dispersion of MFCs impacts the efficiency. Whatever the non-uniformity, the efficiency is always above 91.5 %.

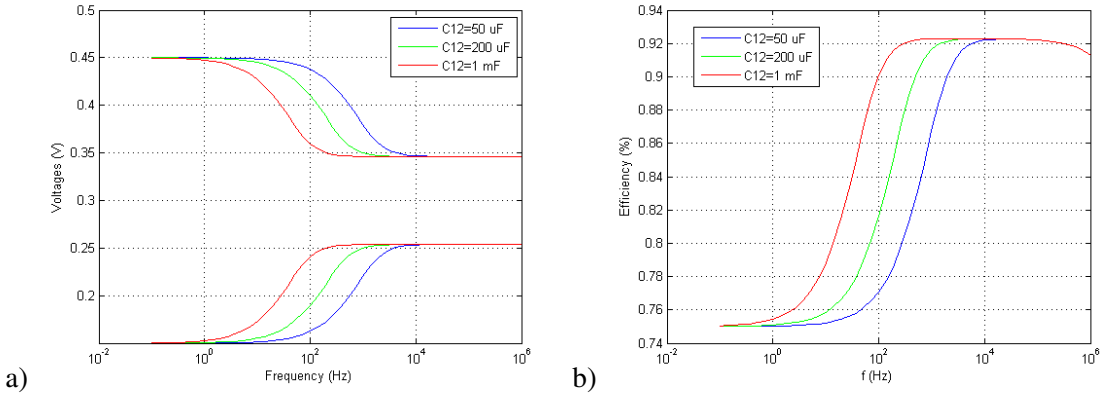

a) b)

Figure 13.4: Voltages V_1 and V_2 (a) and efficiency (b) with changes in switching frequency for different capacitor C_{12} values ($R_1 = 18\,\Omega$, $R_2 = 6\,\Omega$ and $R_{SW} = 1\,\Omega$).

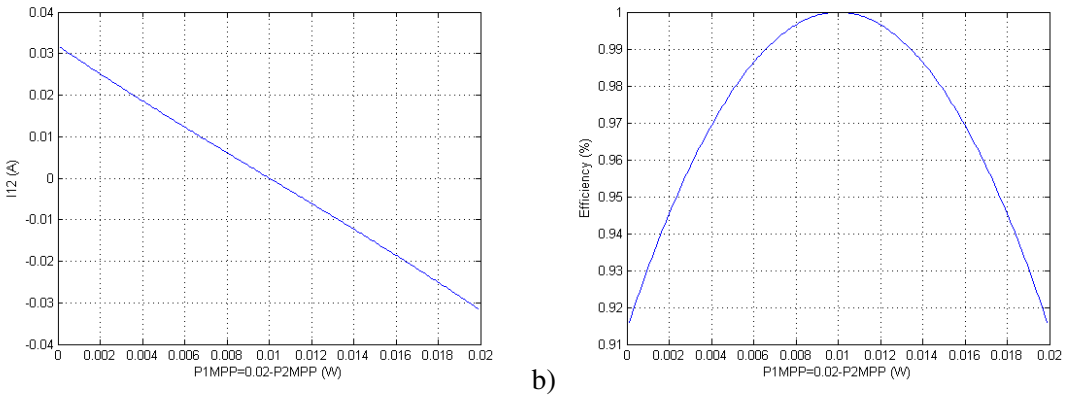

a) b)

Figure 13.5: Average current $\langle I_{12} \rangle$ (a) and global efficiency (b) as a function of individual MFC dispersion.

13.3 Performance study for an n-stage MFC association

A 10-stage SC circuit was simulated with different dispersion scenarios. The simulations use parameter values C_{12}= 200 µF, f_S= 10 kHz, and R_{SW}= 1 Ω. When the ten MFCs have the same maximum power, the cells are naturally balanced. Efficiency is 99.9 % because of very small switching losses. When only one cell is faulty, the efficiency is still high (94.9 %). The SC circuit harvests energy from all the cells and redistribute it to the faulty cell. As a consequence, the voltage of all the MFCs are well equalized. When the MFCs are consistently non-uniform, the SC circuit achieves good overall performances. For slightly, moderately and strongly non-uniform scenarios, the efficiency is 99.1 %, 94.5 % and 85.9 % respectively.

Table 13.1: Efficiency for different dispersion for a series of 10 MFCs

Dispersion scenario	Std (mW)	Maximum power series (mW)	**Efficiency (%)**
Uniform	0	(10, 10, 10, 10, ...)	**99.9**
Uniform - one faulty cell	3.2	(11, 01, 11, 11, ...)	**94.9**
Low non-uniformity	2.1	(8, 12, 8, 12, ...)	**99.1**
Medium non-uniformity	5.3	(5, 15, 5, 15, ...)	**94.5**
High non-uniformity	8.4	(2, 18, 2, 18, ...)	**85.9**

Chapter 14

Switched-MFC circuit

Contents

14.1 Theoretical analysis of a two-stage switched-MFC circuit 114

14.2 Loss analysis and performance study of a two-stage circuit 115

14.3 Generalization to an n-stage switched-MFC circuit 117

The switched-MFC (SMFC) circuit has not been previously mentioned in the literature. It is inspired by switched-capacitor DC/DC converters like in [Seeman, 2008]. The assessment is that apart from the ohmic losses, the MFCs behave like capacitors and can therefore be associated like in switched-capacitor DC/DC converters. Similarly to the SC circuit, the ohmic resistor is negatively affecting the efficiency of the SMFC circuit. In practice, a capacitor is connected in parallel with each MFC. This is equivalent to using a basic electrical equivalent circuit for MFCs like in Figure 11.1.

A two-stage switched-MFC circuit is shown in Figure 14.1. It is composed of two MFCs and of a load which are connected by a network of four switches.

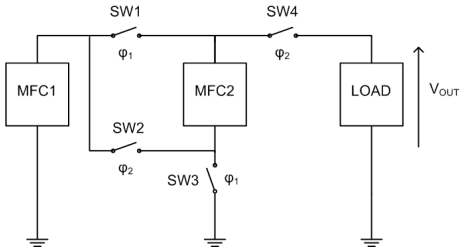

Figure 14.1: Ideal vision of a two-stage switched MFC

During phase φ_1, switches SW1 and SW3 are closed and both MFCs are in parallel and disconnected from the load. In phase φ_2, switches SW2 and SW4 are closed and both MFCs are in series and connected to the load.

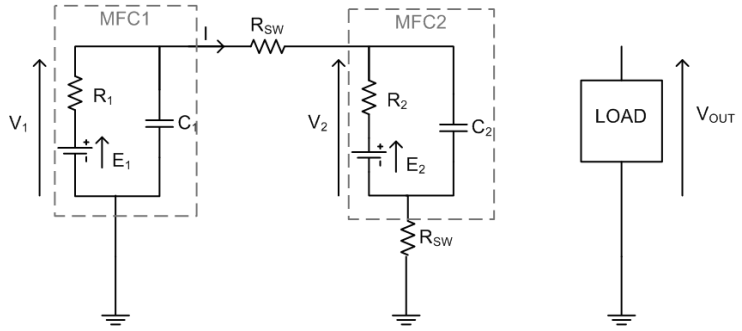

Figure 14.2: Schematic of the switched-MFC circuit during phase φ_1

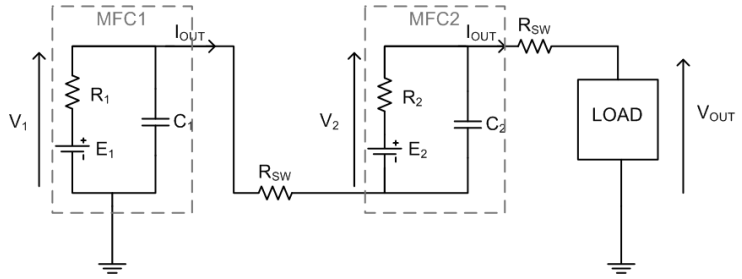

Figure 14.3: Schematic of the switched-MFC circuit during phase φ_2

14.1 Theoretical analysis of a two-stage switched-MFC circuit

The equivalent circuit during phase φ_1 is given in Figure 14.2. This circuit is governed by the two linear differential equations; shown below:

$$\frac{dV_1}{dt} = -(\frac{1}{2R_{SW}C_1} + \frac{1}{R_1C_1})V_1 + \frac{1}{2R_{SW}C_1}V_2 + \frac{1}{2R_1C_1}E_1 \tag{14.1}$$

$$\frac{dV_2}{dt} = (\frac{1}{2R_{SW}C_2})V_1 - (\frac{1}{2R_{SW}C_2} + \frac{1}{R_2C_2})V_2 + \frac{1}{2R_2C_2}E_2 \tag{14.2}$$

This system can be solved analytically and V_1 and V_2 can be plotted as a function of time in Figure 14.4 (a) ($E_1 = 0.6V, R_1 = 18\Omega, C_1 = 1mF, E_2 = 0.6V, R_2 = 6\Omega, C_2 = 1mF, R_{SW} = 1\Omega, V_1(t=0) = 0.12, V_2(t=0) = 0.44V$).We can see the superposition of two phenomena: the voltage balancing of the capacitors which occurs with a short time constant $R_{SW}C_1$ and $R_{SW}C_2$ and the charging of the capacitors which occurs with time constants R_1C_1 and R_2C_2. The voltage curves tend to reach a value close to $E_1 = E_2 = 0.6V$.

The current I in Figure 14.4 (b) is negative because MFC1 is weaker than MFC2 ($R_1 > R_2$) and therefore the balancing current flows from MFC2 to MFC1. The current curve is also very representative of the two phenomena. It is high at time $t = 0$, decreases at a fast rate and then continues to decrease at a slower time-constant.

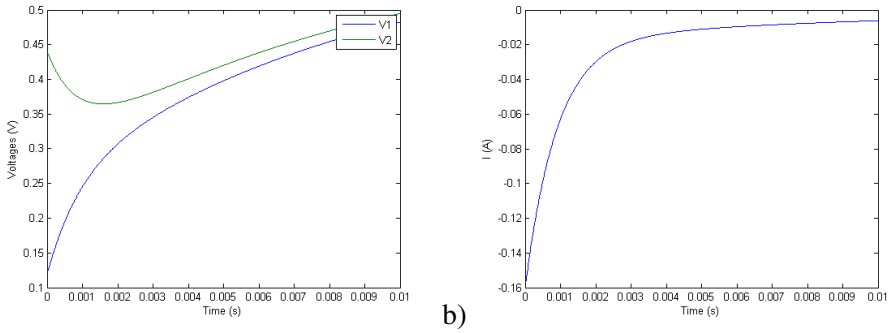

a) b)

Figure 14.4: Voltages V_1 and V_2 (a) and current I between MFCs (b) versus time during φ_1.

The equivalent circuit during phase φ_2 is given in Figure 14.3. This circuit is governed by the two linear differential equations below:

$$\frac{dV_1}{dt} = -(\frac{1}{2RC_1} + \frac{1}{R_1C_1})V_1 - \frac{1}{2RC_1}V_2 + \frac{1}{R_1C_1}E_1 + \frac{1}{2RC_1}V_{OUT} \tag{14.3}$$

$$\frac{dV_2}{dt} = -\frac{1}{2RC_2}V_1 - (\frac{1}{2RC_2} + \frac{1}{R_2C_2})V_2 + \frac{1}{R_2C_2}E_2 + \frac{1}{2RC_2}V_{OUT} \tag{14.4}$$

V_1 and V_2 are plotted as a function of time in Figure 14.5. The initial values are $V_1(t=0) = V_2(t=0) = 0.45V$. We can see the superposition of two phenomena: the discharge of the capacitors C_1 and C_2, which occurs with a time constant $R_{SW}C_1$ and $R_{SW}C_2$ and the generation of electrical current in the $R_1 - E_1$ and $R_2 - E_2$ branches, which is a constant phenomenon. The voltage V_1 and V_2 converge towards the following values:

$$V_1(t \to \infty) = E_1 - R_1 \cdot \frac{E_1 + E_2 - V_{OUT}}{R_1 + R_2 + 2R} (= 0.115V) \tag{14.5}$$

$$V_2(t \to \infty) = E_2 - R_2 \cdot \frac{E_1 + E_2 - V_{OUT}}{R_1 + R_2 + 2R} (= 0.438V) \tag{14.6}$$

The load current I_{OUT} is very high at the very beginning of phase φ_2 because the energy stored during phase φ_1 in the capacitors is discharged at a fast rate. The current then converges towards the value $(E_1 + E_2 - V_{OUT})/(R_1 + R_2 + 2R)$ with a slower time-constant.

14.2 Loss analysis and performance study of a two-stage circuit

During phases φ_1 and φ_2, current flows through the open switches resulting in conductive losses in the on-resistance R_{SW} of the switches. The losses in the switches on-resistances are $2R_{SW}I^2$ during φ_1 and $2R_{SW}I_{OUT}^2$ during φ_2. They can also be expressed as

$$P_{COND-\varphi 1} = \frac{(V_1(t) - V_2(t))^2}{2R_{SW}} \tag{14.7}$$

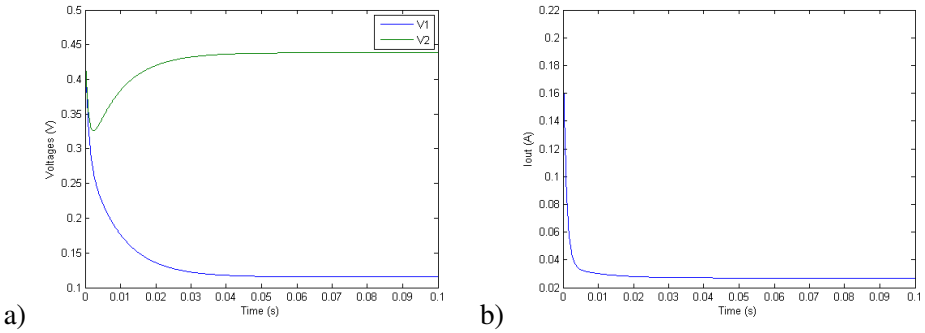

a) b)

Figure 14.5: Voltages V_1 and V_2 (a) and current I_{OUT} (b) versus time during phase φ_2

$$P_{COND-\varphi 2} = \frac{(V_1(t) + V_2(t) - V_{OUT})^2}{2R_{SW}} \tag{14.8}$$

The switching losses are in the form of :

$$P_{SW} = nf_S C_{eq} V_G^2 \tag{14.9}$$

The circuit efficiency can therefore be expressed as:

$$\eta = \frac{I_{OUT}V_{OUT} - nf_S C_{eq} V_G^2}{E_1^2/4R_1 + E_2^2/4R_2} \tag{14.10}$$

This expression allows the calculation of the efficiency versus frequency for various values of R_{SW}, C_{eq}, R_1 and R_2.

Figure 14.6 shows efficiency when the internal resistance of the two MFCs differs (while still producing the same amount of power $E_1^2/(4R_1) + E_2^2/(4R_2)$). At a low frequency, the voltages V_1 and V_2 across each MFC have time to equilibrate and increase to $0.6V$ during phase φ_1 and to decrease and unbalance during phase φ_2. This situation results in MFCs with voltages that are far from the optimal $E_1/2$ and $E_2/2$ for MFC1 and MFC2 and high extra losses in MFCs themselves. At a high frequency, the losses during the equalization predominate. When MFCs are connected in parallel and their voltages are initially different, there is production of a high circulating current between MFCs. These currents cause extra conduction losses in the switches. The effect of the on-resistance of the switches is shown in Figure 14.7.

We can see from the loss analysis that the operating frequency of the switched-MFC circuit can be low, in the order of 10^3 or 10^4 Hz. Figure 14.8 shows that at these frequencies, the switching losses have very low impact on global efficiency. Figure 14.7 shows that the switch on-resistances will have to be as low as possible. The presence of high currents for low on-resistance values have to be taken into account in the selection of switches.

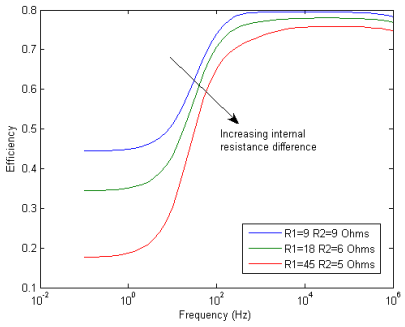

Figure 14.6: Efficiency versus frequency for changes in MFC internal resistances, R_1 and R_2

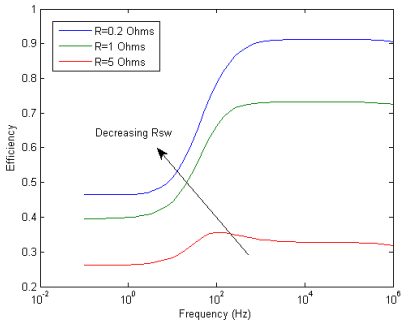

Figure 14.7: Efficiency versus frequency for changes in switch on-resistances, R_{SW}

14.3 Generalization to an n-stage switched-MFC circuit

The switched-MFC method requires $[3(n-1)+1]$ switches to balance n microbial fuel cells. The reasoning for a two-stage SMFC circuit can be extended to a n-stage SMFC circuit. In a first instance, the operation of a four-stage SMFC circuit is discussed. Then, the performance is evaluated for ten MFCs with different dispersion scenarios.

For a four-stage SMFC circuit with non-uniform MFCs ($P_{1MPP} = 2$ mW, $P_{2MPP} = 10$ mW, $P_{3MPP} = 18$ mW, $P_{4MPP} = 10$ mW), the voltage of each cell with changes in frequency is given in Figure 14.9 (a).

For low frequencies, the voltage during phase φ_1 increases to 0.6 V for all MFCs. During phase φ_2, the MFCs become unbalanced. The voltages of MFC2 and MFC4 are approx. 0.425 V, the voltage of MFC3 is approx. 0.5 V and the voltage of MFC1 is -0.275 V. These dispersed voltage values lead to a poor global efficiency at low frequencies, close to 25 % like shown in Figure 14.9 (b).

At high frequencies, the voltages during phase φ_1 and phase φ_2 converge to 0.247 V, 0.299 V, 0.363 V and 0.330 V for MFC1 to MFC4 respectively. The balancing is therefore not perfect but permits to improve the efficiency to 74.3 % at 10 kHz. We note that the convergence voltages MFC04 is higher than 0.3 V because it receives energy from the strong adjacent cell MFC3.

A 10-stage SMFC circuit was then simulated with different scenarios of MFC dispersion. The switching frequency, f_S, was set to 10 kHz, and the switch on-resistance, R_{SW}, to 1 Ω. The performance of the circuit when the ten MFCs are uniform is 79.5 %. This is a relatively low value because of the number of switches in series with the MFCs. The current through these switches during phase φ_2 is not constant (i.e.

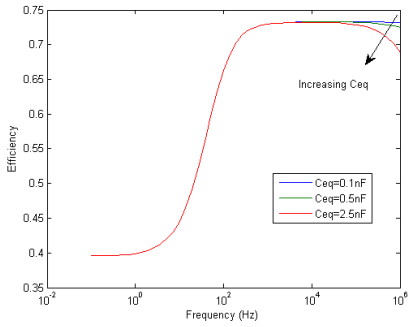

Figure 14.8: Efficiency versus frequency for changes in switch equivalent gate capacitance, C_{eq}

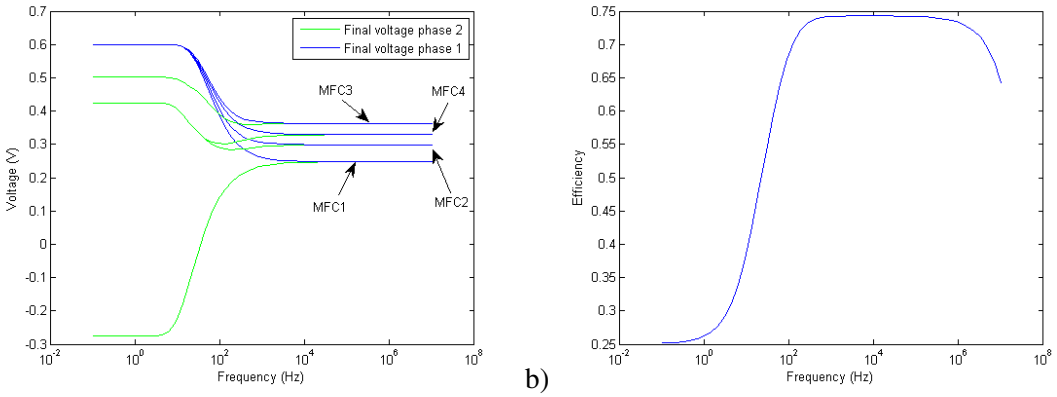

a) b)

Figure 14.9: MFC voltages (a) and efficiency (b) plotted with changes in frequency for 4 switched MFCs

high peak of current), leading to high conduction losses. The non-uniformities do not lead to significant decrease in the efficiency. A strongly non-uniform scenario leads to an efficiency of 70.1 %.

Table 14.1: Efficiency for different dispersion scenarios in a series of 10 MFCs

Dispersion scenario	Standard deviation (mW)	Maximum power series (mW)	**Efficiency (%)**
Uniform	0	(10, 10, 10, 10, 10, 10, 10, 10, 10, 10)	**79.5**
Uniform - one faulty cell	3.2	(11, 01, 11, 11, 11, 11, 11, 11, 11, 11)	**77.0**
Low non-uniformity	2.1	(8, 12, 8, 12, 8, 12, 8, 12, 8, 12)	**79.0**
Medium non-uniformity	5.3	(5, 15, 5, 15, 5, 15, 5, 15, 5, 15)	**75.9**
High non-uniformity	8.4	(2, 18, 2, 18, 2, 18, 2, 18, 2, 18)	**70.1**

These results can be moderated by the high switch resistance of 1 Ω, which affects this circuit more than the others. Such a resistor value was introduced to amplify conduction losses for the sake of clarity. Practically, these switches can be realized in MOSFET technology for a low-cost, highly efficient implementation. The on-resistance of the switches can easily be decreased to few tens of mΩ. The efficiency results for $R_{SW} = 50\,\text{m}\Omega$ are in Chapter 15.

Chapter 15

Scientific conclusions and discussions

Contents

15.1 Comparison of the voltage balancing circuits 119

15.2 Perspectives 120

The analysis of the association of MFCs without balancing circuit (SA), and with CD, SC or SMFC voltage balancing circuits provides good understanding of their operation and allows the evaluation of their performances when associated with MFCs. In the following, the circuits are compared and some perspectives are proposed.

15.1 Comparison of the voltage balancing circuits

The **complete-disconnection circuit** was studied statically, in the sense that a weak MFC is removed from the stack when its voltage reverses and not reconnected later. In this configuration, the circuit offers good performances when a small fraction of MFCs are defective. In this case, they are efficiently disconnected from the stack so that they do not hamper the global performance. When too many MFCs are faulty, they may not reverse and will not be disconnected from the stack. However, they will still unbalance the stack, leading to a poor global efficiency. In any MFC dispersion scenario, the circuit causes conduction losses that decrease the efficiency. This can be partly solved by choosing switches with low on-resistance.

In the complete disconnection circuit, the MPP voltage of the stack is decreased when one MFC is disconnected. This implies that the PMU that controls the voltage of the stack should implement an adapted MPPT algorithm. This will not be a FOCV quasi-MPPT.

The **switched-capacitor circuit** is the most efficient voltage-balancing circuit. It benefits from the fact that there is no switch in series with the MFCs. The switches are only crossed by the balancing current. One drawback is that it requires a minimum of $n-1$ capacitors with quite high values (several µF). In practice, extra filtering capacitors with higher values will be added in series with the MFCs to "hide" the ohmic resistor at high frequencies. In this case, this circuit requires $2n-1$ capacitors. The number of capacitors and their high values (e.g. pump capacitor of several µF and filtering capacitors of hundreds µF at $f_S = 100\,\text{kHz}$ for 10 mW MFCs) prohibits a fully-integrated design of this circuit. However, a discrete compact implementation using off-the-shelf components is possible.

The **switched-MFC circuit** suffers from its switches which are in series with the MFCs. These are crossed by high currents that cause subsequent losses. It is necessary to decrease the on-resistance of the switches and to increase the switching frequency to combat these conduction losses (at the expense of the switching losses). The main advantage of this circuit compared to the switched-capacitor circuit is that it theoretically requires no storage elements. In practice however, a capacitor is added in parallel with each MFC.

The simulated global efficiencies of all circuits are summarized in Figure 15.1. These circuits are compared using a realistic switch on-resistance value, R_{SW} of 50 mΩ.

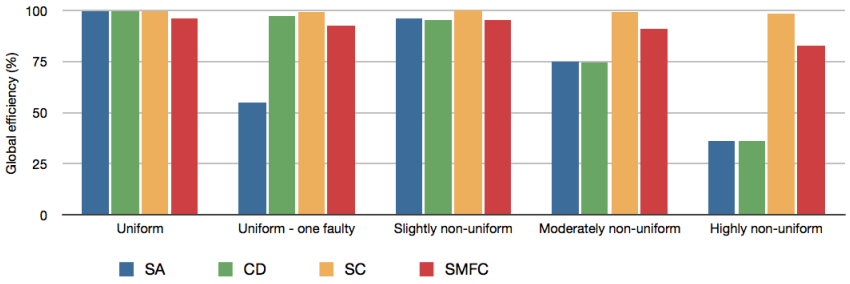

Figure 15.1: Comparison of the global efficiency for the four types of circuit connection, discussed thus far, with different dispersion scenarios ($R_{SW} = 50\,\text{m}\Omega$)

15.2 Perspectives

This part of the manuscript gives a simulation-based comparison of circuits to balance the voltage of non-uniform MFCs electrically connected in series (and not connected hydraulically). Since the switched-capacitor method promises very good implementation and low-cost, low-power discrete implementation, a natural perspective of this work is the realization of a prototype and the testing with MFCs.

The switched-MFC circuit is apparently less efficient that the SC circuit. However, this circuit may offer other interesting features. First, the MFCs can be connected in series and in parallel according to a large panel of scenario which enable to step-up the voltage with different ratios. In Figure 15.2, the phase φ_2 of a four-stage SMFC circuit connects MFCs in such a way to achieve twice, three times and four times the individual cell voltage at the output of the circuit. The topology of the stack can therefore be dynamically re-arranged to generate different output voltages. Second, the architecture of the SMFC circuit permits to realize the same functionalities as the complete disconnection method. It can reconfigure the MFC association if faulty cells must be put apart from the stack.

Finally, the analysis of the voltage balancing circuits was done based on equivalent circuits representing the electrical characteristics of MFCs. Further studies on MFCs need to confirm that the SC and the SMFC circuits do not hinder their operation (i.e. their biological behavior). Indeed, both the SC and the SMFC circuits cause flow of electrons from strong MFCs to weak MFCs. It was already demonstrated in [Bonanni et al., 2012, Deeke et al., 2012] that MFCs have the ability to store charges when a current flows into them. However, these phenomena were not quantified and the long-term effect on their performances has never been investigated.

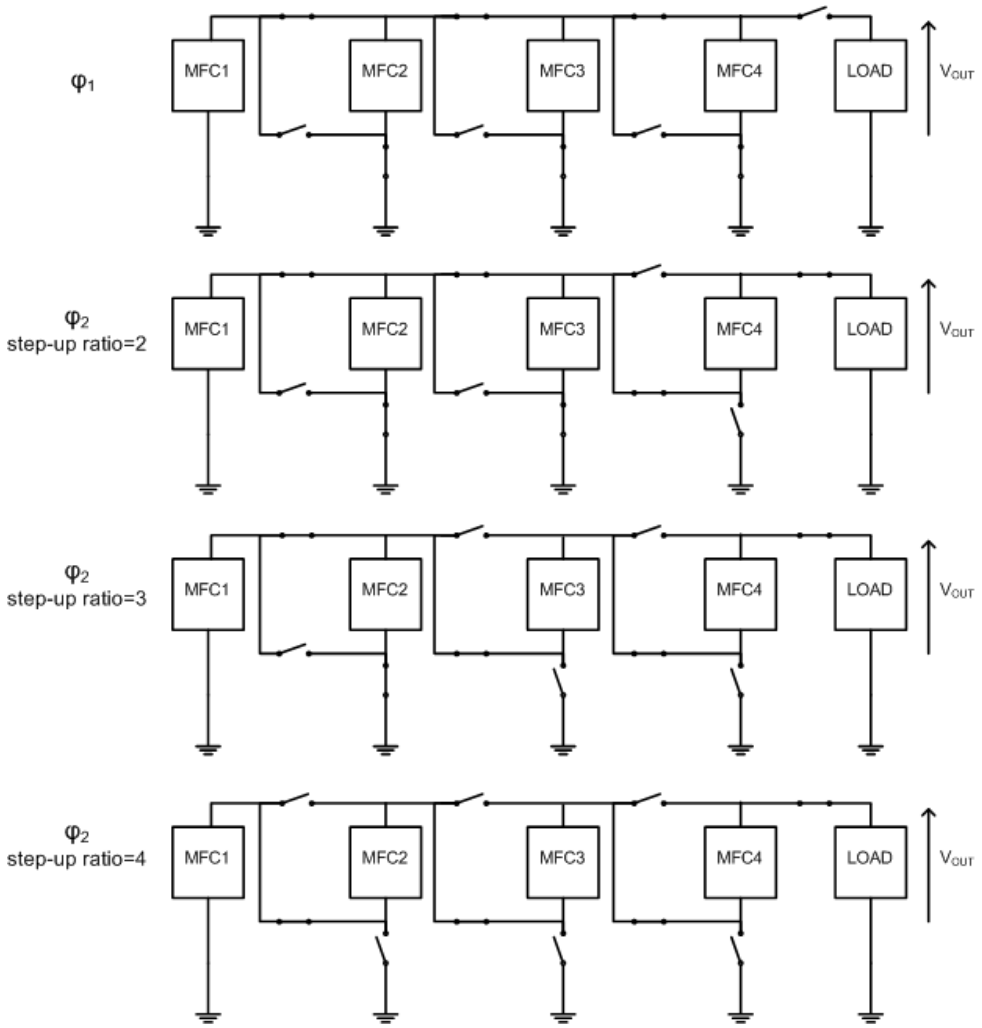

Figure 15.2: Different step-up capacity using switched-MFC circuit

Chapter 16

General conclusions

Contents

16.1 Scientific contribution of the thesis 122

16.2 Answers to questions from the introduction 123

16.3 Scientific perspectives 124

16.4 Personal view 125

16.1 Scientific contribution of the thesis

This thesis focussed on the energy generators (i.e. the microbial fuel cells), the power management unit (i.e. DC/DC converters) and other power electronics that permit to manage the association of a large number of MFCs (i.e. voltage balancing circuits).

Details of the MFCs are studied in Part I. This manuscript presented a realistic analysis of MFCs because it made a correlation of the way energy can be harvested by the PMU. It highlighted the recent advances on MFCs and focused on their electrical characteristics. In addition, MFCs were evaluated at their MPP using a dedicated measurement tool, engineered for the experiment. Energy conversion efficiencies and other performance indicators were studied at this operating point. Two MPPT algorithms were compared. The "fractional open-circuit voltage" algorithm proved to perform almost as well as the state-of-the-art "perturbation and observation" algorithm. The former allows easier implementation in a PMU.

Following from this, choices were made to focus on an autonomous, ultra-low input-voltage, self-oscillating circuit. Typical applications include stand-alone energy harvesting from MFCs. This specific circuit is based on the association of a transformer and of a normally-on transistor. The first approach was theoretical in order to shed light on the operation. The oscillator was then implemented as a sub-circuit of two DC/DC step-up converters so as to harvest energy from only one MFC. The voltage-lifter can operate at powers of few hundreds of μW and is particularly adapted to ultra-low power applications. The flyback converter includes FOCV quasi-MPPT. It has strict constraints on its main inductive component, leading to high footprint and high cost. For both circuits, prototypes were realized in discrete components. They allow start-up at very low-voltages, and moreover, the MPPT controller improves the global efficiency of energy harvesting from MFCs.

Voltage balancing circuits theoretically enable efficient serial association of non-uniform MFCs. Several voltage balancing circuits were detailed in Part III. The analytical equations corresponding to their operation were derived and permitted to give a good understanding of the loss phenomena. The switched-capacitor circuit achieves very high performances for different scenarios of MFC dispersion. In comparison, the switched-MFC circuit doesn't perform as well, but it offers the potential of obtaining multiple step-up ratios. These two voltage-balancing circuits offer a low-cost effective solution to increase the energy generation of MFCs in wastewater treatment plants or in bio-batteries. These can perhaps foster better integration between MFCs and electronics and increase the reliability in case of a faulty MFC.

16.2 Answers to questions from the introduction

A number of unanswered questions were outlined in the introduction. These are addressed again in light of the research work carried out, as follows:

What does limit the maximum power density of MFCs?

The maximum power density depends on voltage drops (i.e. activation, ohmic and concentration) and current drops within a MFC. Modeling and identification of the model parameters with the V-I characteristic curve of MFCs allows to identify which drop causes the majority of the losses in a given MFC. In the MFCs studied herewith, activation is the main cause of losses which decreases the power density of MFCs. Further studies with reference electrodes would facilitate the attribution of activation activation to the anode or cathode electrode.

How should energy be harvested to improve the power delivered by MFCs?

The P-I static characteristic curve exhibits an interesting point which is called maximum power point (MPP). Energy can be constantly harvested at MPP with the use of a PMU with a specific control. This control can use a number of methods. This manuscript studied and compared the P&O and the FOCV methods.

What are the electrical characteristics of MFCs as they are operated at the maximum power point?

The electrical characteristics strongly depend on the type of MFCs and its operating conditions. In our experiments, MFCs sustained a power density of 1 $mW.L^{-1}$. The ratio between the output electrical energy and the energy content of the input organic matter was in the order of 7.3 % on average (Coulombic efficiency of 38.4 % and equivalent potential efficiency of about 18.1 %).

How to step-up the voltage of a single MFC?

Step-up DC/DC converters increase the voltage of a single MFC. These can either be inductive or capacitive. The former facilitates regulation which is an advantage to include a MPPT control loop. Various topologies of inductive converters exist, but the most simple (i.e. boost and flyback) use a minimum number of components and can potentially be implemented at low-cost and high efficiency. They either require an external supply with a voltage above 1 V, or a specific start-up sub-circuit. Designing a discrete converter operating at 10 mW or below is challenging and requires special care in the design.

How does a low-voltage start-up circuit operate?

There are different ways to realize a circuit which autonomously steps-up an input voltage below 0.3 V. One of the most practical ways is to use a self-oscillating circuit based on the association of a high turn-ratio transformer and a normally-on switch. This association ensures self-operation to input voltages as low as 20 mV.

How can a start-up strategy be implemented into a low-power DC/DC step-up converter?

One solution is to associate the start-up oscillator to a rectifier. This manuscript studied a voltage doubler rectifier. A second solution is to associate the start-up oscillator with a standard switched-mode step-up DC/DC converter. This manuscript gave the example of a flyback converter.

How can a low-cost MPPT control be implemented in a low-power DC/DC step-up converter?

The fractional open-circuit method can be implemented at low-cost in a boost or flyback DC/DC converter. Ultra-low threshold voltage transistors are used to realize a simple voltage comparator.

How do non-uniform electrical characteristics quantitatively affect the performances of a serial association of MFCs ?

Making few assumptions on the electrical characteristics of MFCs, the equations for n MFCs associated in series were derived in Part III. It appeared that when only one out of the MFCs is faulty (i.e. its internal resistance is much higher than the other ones), the stack efficiency can be reduced by almost a factor of two. Other dispersion scenarios were investigated.

How do voltage-balancing methods operate?

Voltage balancing relies on different mechanisms. Some of them bypass weak cells, some shunt strong cells and other shuttle energy between cells. The energy shuttling method was proven to be the most efficient.

Which voltage-balancing circuits offers the best performances?

Complete disconnection, switched-capacitor and switched-MFC methods were analyzed and compared. The results showed that the switched-capacitor method permits to achieve a very good equalization of the MFC voltages and can be implemented at low cost.

16.3 Scientific perspectives

There are still a lot of challenges to address before MFCs can be considered as economical electrical energy generators. Most of the current work focuses on the issues relative to their high cost and to their low power densities. Works in materials, micro-biology, chemistry and electrochemistry are investigated. The electrical issues are generally overlooked because they are considered to have no influence on the cost and performances of MFCs. This thesis showed that electrical engineering permits to define the rate at which energy is harvested, and as such influences the internal mechanisms and the performances of the MFC. Generally, the influence of the operating point (i.e. the voltage-current couple) on the performances is not well understood. In some applications, maximizing the power may not be the priority. One can think instead of maximizing energy conversion efficiency, substrate consumption or bacterial growth. Further research can help reveal some of the mechanisms that influence of electrical load on performances.

In term of power-electronics, the perspective is clearly the integration of the circuits. The manuscript proves the feasibility of some concepts (i.e. self-starting and MPPT) using discrete prototypes, but integration would permit a wider degree of freedom. First, it would allow to better optimize losses, in particular through the use of synchronous architectures. Second, the control would include much more functionalities to realize a more elaborated feedback strategy. The control can be much more elaborate and consume less power. The issue with integration concerns passive elements, in particular the inductive components. In the absence of acceptable solutions to integrate the inductive circuits presented in this manuscript, other capacitor-based converters can be used.

Part III introduced the concept of the MFC-grid from the perspective of multi-cell voltage-balancing. It would be interesting to realize experiments to validate the theoretical studies in this manuscript. Particularly the switched-capacitor voltage-balancing circuit. Most of the time, this manuscript only studied

the power electronics from the MFC side (so-called front-end power electronics). In some applications, this first electronic stage will not be sufficient, and other stages of conversion may be required between the MFCs and the final load. It would be interesting to study what is the optimum number and size of MFCs, where the converters can favorably be positioned in a MFC-grid, and what are their specifications.

16.4 Personal view

I was often asked, during the three years of this work, on wether the technology of MFC will, one day, become mature and be implemented as a power source in industrial applications. It is an extremely difficult question for which I am not able to give a straight-forward answer. This thesis showed that the power-electronics is challenging, but that it does not constitute a bottleneck. The acceptation rather depends on the progress of research to develop low-cost and high-performance MFCs. It also depends on the cost, performance and environmental footprint of competing technologies, that are different from an application to another.

MFCs, as electrical generators, have only little chance to compete with other large-scale fossil or renewable energy sources. For instance, in wastewater treatment plants, the electrical energy alone is not competitive, and MFCs can only become interesting when also considering the added value of the waste treatment.

When MFCs are considered as portable power sources, the added value can be better because the cost and the environmental footprint of competitive technologies (e.g. Li-ion batteries) is high. However, another criteria for this application is the portability and the power density, in which MFCs are not competitive.

Finally, when MFCs are considered as ambient energy scavengers, the added value can be good compared to other solar, thermoelectric, or piezoelectric harvesters. It is particularly true in very specific environments such as oceans, lakes, sewage systems, and food processing industries. In my opinion, the first applications for which MFCs will be used as power supplies is energy scavenging. For these applications, MFCs can also be used as self-supplied sensors (toxicity, BOD...).

Even though the outcome of the technology is still unsure, it's potential applications are wide and necessary for the society (energy, waste treatment, water availability...). I believe that it is the role of researchers to investigate the potentials of MFC technology further.

Bibliography

[Adami et al., 2011] Adami, S.-E., Degrenne, N., Vollaire, C., Allard, B., Buret, F., and Costa, F. (2011). Autonomous ultra-low power DC/DC converter for Microbial Fuel Cells. In *Proceedings of ICECS*, pages 398–401. IEEE.

[Advanced Linear Devices, 2012] Advanced Linear Devices (2012). "Quad/dual N-channel enhancement mode EPAD precision matched pair mosfet array," ALD110802/ALD110902 datasheet.

[Aelterman, 2009] Aelterman, P. (2009). *Microbial fuel cells for the treatment of waste streams with energy recovery*. PhD thesis, Ghent University.

[Aelterman et al., 2006] Aelterman, P., Rabaey, K., Pham, H. T., Boon, N., and Verstraete, W. (2006). Continuous Electricity Generation at High Voltages and Currents Using Stacked Microbial Fuel Cells. *Environmental Science & Technology*, 40(10):3388–3394.

[Aelterman et al., 2008] Aelterman, P., Versichele, M., Marzorati, M., Boon, N., and Verstraete, W. (2008). Loading rate and external resistance control the electricity generation of microbial fuel cells with different three-dimensional anodes. *Bioresource technology*, 99(18):8895–902.

[Ahn and Logan, 2010] Ahn, Y. and Logan, B. (2010). Effectiveness of domestic wastewater treatment using microbial fuel cells at ambient and mesophilic temperatures. *Bioresource technology*, 101(2):469–75.

[Allen and Bennetto, 1993] Allen, R. M. and Bennetto, H. P. (1993). Microbial fuel-cells. *Applied Biochemistry and Biotechnology*, 39-40(1):27–40.

[Altemose,] Altemose, B. Y. G. Batteries and Fuel Cells Achieving cell balancing for lithium-ion batteries. *Electronic Products*, pages 21–22.

[Armstrong, 1914] Armstrong, E. H. (1914). "Wireless receiving system", US Patent 1,113,149.

[Bard and Faulkner, 1981] Bard, A. J. and Faulkner, L. R. (1981). *Electrochemical methods - Fundamentals and applications*, volume 125.

[Baronti and Fantechi, 2011] Baronti, F. and Fantechi, G. (2011). Hierarchical platform for monitoring, managing and charge balancing of LiPo batteries. In *IEEE Vehicle Power and Propulsion Conference*, pages 1–6.

[Barrade, 2002] Barrade, P. (2002). Series connection of supercapacitors: Comparative study of solutions for the active equalization of the voltages. *networks*, pages 1–6.

[Behera et al., 2010] Behera, M., Jana, P. S., and Ghangrekar, M. M. (2010). Performance evaluation of low cost microbial fuel cell fabricated using earthen pot with biotic and abiotic cathode. *Bioresource technology*, 101(4):1183–9.

[Ben-Yaakov and Fridman, 2004] Ben-Yaakov, S. and Fridman, I. (2004). SPICE compatible model of self-oscillating converter. In *Proceedings of Convention of Electrical and Electronics Engineers in Israel*, pages 342–345. IEEE.

[Bennetto et al., 1983] Bennetto, H. P., Stirling, J. L., Tanaka, K., and Vega, C. A. (1983). Anodic reactions in microbial fuel cells. *Biotechnology and bioengineering*, 25(2):559–68.

[Bergveld et al., 2009] Bergveld, H., Karadi, R., Nowak, K., Iochem, S., Ferreira, J., Ledain, S., Pieraerts, E., and Pommier, M. (2009). A 65-nm-CMOS 100-MHz 87%-efficient DC-DC down converter based on dual-die system-in-package integration. In *Proceedings of ECCE*, pages 3698–3705. IEEE.

[Bonanni et al., 2012] Bonanni, P. S., Schrott, G. D., Robuschi, L., and Busalmen, J. P. (2012). Charge accumulation and electron transfer kinetics in Geobacter sulfurreducens biofilms. *Energy & Environmental Science*, 5(3):6188.

[Bullen et al., 2006] Bullen, R., Arnot, T., Lakeman, J., and Walsh, F. (2006). Biofuel cells and their development. *Biosensors and Bioelectronics*, 21(11):2015–2045.

[Canfield et al., 1963] Canfield, J., Goldner, B., and Lutwack, R. (1963). NASA Technical Report. Technical report, Magna Corporation, Anaheim, CA.

[Cao et al., 2008] Cao, J., Schofield, N., and Emadi, A. (2008). Battery balancing methods: A comprehensive review. In *Vehicle Power and Propulsion ...*, pages 3–8.

[Cao et al., 2009] Cao, X., Huang, X., Liang, P., Xiao, K., Zhou, Y., Zhang, X., and Logan, B. E. (2009). A new method for water desalination using microbial desalination cells. *Environmental science & technology*, 43(18):7148–52.

[Chang et al., 2004] Chang, I. S., Jang, J. K., Gil, G. C., Kim, M., Kim, H. J., Cho, B. W., and Kim, B. H. (2004). Continuous determination of biochemical oxygen demand using microbial fuel cell type biosensor. *Biosensors and Bioelectronics*, 19(6):607–613.

[Chen et al., 2011] Chen, P., Ishida, K., Ikeuchi, K., Zhang, X., Honda, K., Okuma, Y., Ryu, Y., Takamiya, M., and Sakurai, T. (2011). A 95mV-startup step-up converter with Vth-tuned oscillator by fixed-charge programming and capacitor pass-on scheme. In *Proceedings of ISSCC*, number June 2009, pages 216–218. IEEE.

[Cheng and Logan, 2007] Cheng, S. and Logan, B. E. (2007). Ammonia treatment of carbon cloth anodes to enhance power generation of microbial fuel cells. *Electrochemistry Communications*, 9(3):492–496.

[Cheng and Logan, 2011] Cheng, S. and Logan, B. E. (2011). Increasing power generation for scaling up single-chamber air cathode microbial fuel cells. *Bioresource technology*, 102(6):4468–73.

[Choi and Chae, 2011] Choi, S. and Chae, J. (2011). A series array of microliter-sized microbial fuel cell. In *Proceedings of MEMS*, pages 1289–1292. IEEE.

[Cinquin et al., 2010] Cinquin, P., Gondran, C., Giroud, F., Mazabrard, S., Pellissier, A., Boucher, F., Alcaraz, J.-P., Gorgy, K., Lenouvel, F., Mathé, S., Porcu, P., and Cosnier, S. (2010). A glucose biofuel cell implanted in rats. *PloS one*, 5(5):e10476.

[Clauwaert et al., 2008] Clauwaert, P., Aelterman, P., Pham, T. H., De Schamphelaire, L., Carballa, M., Rabaey, K., and Verstraete, W. (2008). Minimizing losses in bio-electrochemical systems: the road to applications. *Applied microbiology and biotechnology*, 79(6):901–13.

[Cohen, 1931] Cohen, B. (1931). The bacterial Culture as an Electrical Half-Cell. *Journal of bacteriology*, 21:18–19.

[Damaschke, 1997] Damaschke, J. (1997). Design of a low-input-voltage converter for thermoelectric generator. *IEEE Transactions on Industry Applications*, 33(5):1203–1207.

[Daowd and Omar, 2011] Daowd, M. and Omar, N. (2011). Passive and active battery balancing comparison based on MATLAB simulation. In IEEE, editor, *Vehicle Power and ...*.

[Deeke et al., 2012] Deeke, A., Sleutels, T. H. J. A., Hamelers, H. V. M., and Buisman, C. J. N. (2012). Capacitive bioanodes enable renewable energy storage in microbial fuel cells. *Environmental science & technology*, 46(6):3554–60.

[Degrenne et al., 2012a] Degrenne, N., Allard, B., Buret, F., Adami, S.-E., Labrousse, D., Vollaire, C., and Morel, F. (2012a). A 140 mV Self-Starting 10 mW DC / DC Converter for Powering Low-Power Electronic Devices from Low-Voltage Microbial Fuel Cells. *Journal of low-power electronics*, 8(4):485–497.

[Degrenne et al., 2011a] Degrenne, N., Allard, B., Buret, F., Morel, F., Adami, S.-E., and Labrousse, D. (2011a). Comparison of 3 self-starting step-up DC:DC converter topologies for harvesting energy from low-voltage and low-power microbial fuel cells. In IEEE, editor, *Proceedings of EPE*, pages 1–10.

[Degrenne et al., 2011b] Degrenne, N., Allard, B., Buret, F., Morel, F., Adami, S.-E., and Labrousse, D. (2011b). Self-starting DCDC boost converter for low-power and low-voltage microbial electric generators. In IEEE, editor, *Proceedings of ECCE*, pages 889–896.

[Degrenne et al., 2012b] Degrenne, N., Buret, F., Allard, B., and Bevilacqua, P. (2012b). Electrical energy generation from a large number of microbial fuel cells operating at maximum power point electrical load. *Journal of Power Sources*, 205:188–193.

[Degrenne et al., 2012c] Degrenne, N., Ledezma, P., Bevilacqua, P., Buret, F., Allard, B., Greenman, J., and Ieropoulos, I. A. (2012c). Bi-directional Electrical Characterisation of Microbial Fuel Cell. *Bioresource Technology*, In Press.

[Degrenne et al., 2012d] Degrenne, N., Marian, V., Vollaire, C., Buret, F., Verdier, J., and Allard, B. (2012d). Voltage Reversal in Unbalanced Rectenna Association. *IEEE Antennas and Wireless Propagation Letters*, 11:941–944.

[Dekker et al., 2009] Dekker, A., Ter Heijne, A., Saakes, M., Hamelers, H., and Buisman, C. J. N. (2009). Analysis and improvement of a scaled-up and stacked microbial fuel cell. *Environmental science & technology*, 43(23):9038–42.

[Delrossi, 2002] Delrossi, R. (2002). Cell Balancing Design Guidelines. *Technology*, pages 1–4.

[Dewan et al., 2008] Dewan, A., Beyenal, H., and Lewandowski, Z. (2008). Scaling up Microbial Fuel Cells. *Environmental Science & Technology*, 42(20):7643–7648.

[Di Lorenzo et al., 2009] Di Lorenzo, M., Curtis, T. P., Head, I. M., and Scott, K. (2009). A single-chamber microbial fuel cell as a biosensor for wastewaters. *Water research*, 43(13):3145–54.

[Diab et al., 2006] Diab, Y., Venet, P., and Rojat, G. (2006). Comparison of the Different Circuits Used for Balancing the Voltage of Supercapacitors: Studying Performance and Lifetime of Supercapacitors. *Power Quality*.

[Diodes Incorporated, 2009] Diodes Incorporated (2009). "N-channel enhancement mode MOSFET" DMG6968U datasheet.

[Donovan et al., 2010] Donovan, C., Dewan, A., Peng, H., Heo, D., and Beyenal, H. (2010). Power Management System for a 2.5W Remote Sensor Powered By a Sediment Microbial Fuel Cell. *Journal of Power Sources*, 196(3):1171–1177.

[Du et al., 2007] Du, Z., Li, H., and Gu, T. (2007). A state of the art review on microbial fuel cells: A promising technology for wastewater treatment and bioenergy. *Biotechnology advances*, 25(5):464–82.

[Emefcy, 2012] Emefcy (2012). "Spiral Aerobic Biofim-Reactor", http://www.emefcy.com/, (accessed the 28/08/2012).

[Enocean, 2010] Enocean (2010). "ECT 310 Perpetuum - EnOcean powered by Thermal Energy," ECT 310 datasheet.

[Esram and Chapman, 2007] Esram, T. and Chapman, P. L. (2007). Comparison of Photovoltaic Array Maximum Power Point Tracking Techniques. *IEEE Transactions on Energy Conversion*, 22(2):439–449.

[Fan et al., 2007] Fan, Y., Liu, H., and Hu, H. (2007). Enhanced Coulombic efficiency and power density of air-cathode microbial fuel cells with an improved cell configuration. *Journal of Power Sources*, 171(2):348–354.

[Frank et al., 2010] Frank, M., Kuhl, M., Erdler, G., and Freund, I. (2010). An Integrated Power Supply System for Low Power 3.3 V Electronics Using On-Chip Polymer Electrolyte Membrane (PEM) Fuel Cells. *Solid-State Circuits,*, 45(1):205–213.

[Fraunhofer IIS, 2010] Fraunhofer IIS (2010). "Micro Energy Power Management ASIC 2," ME-PMA2 datasheet.

[Ghoreyshi et al., 2011] Ghoreyshi, A., Jafary, T., Najafpour, G., and Haghparast, F. (2011). Effect of Type and Concentration of Substrate on Power Generation in a Dual Chambered Microbial Fuel Cell. pages 1174–1181.

[Gil, 2003] Gil, G. C. (2003). Operational parameters affecting the performance of a mediator-less microbial fuel cell. *Biosensors and Bioelectronics*, 18:327–334.

[Grgić et al., 2009] Grgić, D., Ungan, T., Kostić, M., and Reindl, L. M. (2009). Ultra-low input voltage DC-DC converter for micro energy harvesting. In *Proceedings of PowerMeMs*, pages 265–268.

[Guo, 2010] Guo, H.-J. (2010). Review and critical analysis of the research papers published till date on maximum power point tracking in wind energy conversion system. *Energy Conversion*, 1:4075–4082.

[Habermann and Pommer, 1991] Habermann, W. and Pommer, E. (1991). Biological fuel cells with sulphide storage capacity. *Applied Microbiology and Biotechnology*, 35(1).

[Hasvold et al., 1997] Hasvold, O. i., Henriksen, H., MelvËęr, E., Citi, G., Johansen, B. O., Kjø nigsen, T., and Galetti, R. (1997). Sea-water battery for subsea control systems. *Journal of Power Sources*, 65(1-2):253–261.

[He and Angenent, 2009] He, Z. and Angenent, L. T. (2009). Application of Bacterial Biocathodes in Microbial Fuel Cells. *Electroanalysis*, pages 2009–2015.

[IEA, 2011] IEA (2011). World Energy Outlook 2011. Technical report, International Energy Agency.

[Ieropoulos et al., 2010a] Ieropoulos, I., Greenman, J., and Melhuish, C. (2010a). Improved energy output levels from small-scale Microbial Fuel Cells. *Bioelectrochemistry (Amsterdam, Netherlands)*, 78(1):44–50.

[Ieropoulos et al., 2012] Ieropoulos, I., Greenman, J., and Melhuish, C. (2012). Urine utilisation by microbial fuel cells; energy fuel for the future. *Phys. Chem.*, 14(1):94–98.

[Ieropoulos et al., 2010b] Ieropoulos, I., Greenman, J., Melhuish, C., and Horsfield, I. (2010b). EcoBot-III: a robot with guts. In *Artificial Life XII*, pages 733–740. MIT Press.

[Ieropoulos et al., 2010c] Ieropoulos, I., Winfield, J., and Greenman, J. (2010c). Small Scale Microbial Fuel Cells and Different Ways of Reporting Output. *Image (Rochester, N.Y.)*, 28(9):1–9.

[Ieropoulos, 2012] Ieropoulos, I. A. (2012). "Ecobot Circuitry" E-mail communication - the 14th of Nov. 2012.

[Ieropoulos et al., 2008] Ieropoulos, I. A., Greenman, J., and Melhuish, C. (2008). Microbial fuel cells based on carbon veil electrodes: Stack configuration and scalability. *International Journal of Energy Research*, 32(13):1228–1240.

[Ivey, 2009] Ivey, B. (2009). nanoWatt and nanoWatt XLP Technologies: An Introduction to Microchip Low-Power Devices.

[Karube et al., 1977] Karube, I., Matsunaga, T., Tsuru, S., and Suzuki, S. (1977). Biochemical fuel cell utilizing immobilized cells of clostridium butyricum. *Biotechnology and Bioengineering*, 19(11):1727–1733.

[Katuri et al., 2011] Katuri, K. P., Scott, K., Head, I. M., Picioreanu, C., and Curtis, T. P. (2011). Microbial fuel cells meet with external resistance. *Bioresource technology*, 102(3):2758–66.

[Kerzenmacher et al., 2008] Kerzenmacher, S., Ducrée, J., Zengerle, R., and von Stetten, F. (2008). Energy harvesting by implantable abiotically catalyzed glucose fuel cells. *Journal of Power Sources*, 182(1):1–17.

[Kerzenmacher et al., 2009] Kerzenmacher, S., Mutschler, K., Kräling, U., Baumer, H., Ducrée, J., Zengerle, R., and Stetten, F. (2009). A complete testing environment for the automated parallel performance characterization of biofuel cells: design, validation, and application. *Journal of Applied Electrochemistry*, 39(9):1477–1485.

[Kim et al., 2008] Kim, I., Chae, K., Choi, M., and Verstraete, W. (2008). Microbial fuel cells: recent advances, bacterial communities and application beyond electricity generation. *Environmental Engineering Research*, 13(2):10–15.

[Kim and Kim, 2011] Kim, J. and Kim, C. (2011). A Regulated Charge Pump With a Low-Power Integrated Optimum Power Point Tracking Algorithm for Indoor Solar Energy Harvesting. *Circuits and Systems II: Express Briefs, IEEE Transactions on*, 58(99):1–5.

[Kimball et al., 2007] Kimball, J. W., Kuhn, B. T., and Krein, P. T. (2007). Increased Performance of Battery Packs by Active Equalization. In *2007 IEEE Vehicle Power and Propulsion Conference*, pages 323–327. IEEE.

[Larminie and Dicks, 2003] Larminie, J. and Dicks, A. (2003). *Fuel cell systems explained*. John Wiley & Sons, 2nd edition.

[Larrosa-Guerrero et al., 2010] Larrosa-Guerrero, a., Scott, K., Head, I., Mateo, F., Ginesta, A., and Godinez, C. (2010). Effect of temperature on the performance of microbial fuel cells. *Fuel*, 89(June):3985–3994.

[Le et al., 2011] Le, H., Sanders, S., and Alon, E. (2011). Design Techniques for Fully Integrated Switched-Capacitor DC-DC Converters. *Solid-State Circuits, IEEE Journal of*, 46(9):2120–2131.

[Ledezma et al., 2010] Ledezma, P., Ieropoulos, I., and Greenman, J. (2010). Comparative analysis of different polymer materials for the construction of microbial fuel cell stacks. *Journal of Biotechnology*, 150:142–143.

[Lejeune, 2003] Lejeune, P. (2003). Contamination of abiotic surfaces: what a colonizing bacterium sees and how to blur it. *Trends in Microbiology*, 11(4):179–184.

[Liu et al., 2008] Liu, H., Cheng, S., Huang, L., and Logan, B. (2008). Scale-up of membrane-free single-chamber microbial fuel cells. *Journal of Power Sources*, 179:274–279.

[Liu et al., 2005a] Liu, H., Cheng, S., and Logan, B. (2005a). Production of electricity from acetate or butyrate using a single-chamber microbial fuel cell. *Environmental science & technology*, 39(2):658–662.

[Liu et al., 2005b] Liu, H., Cheng, S., and Logan, B. E. (2005b). Power generation in fed-batch microbial fuel cells as a function of ionic strength, temperature, and reactor configuration. *Environmental science & technology*, 39(14):5488–93.

[Liu and Ramnarayanan, 2004] Liu, H. and Ramnarayanan, R. (2004). Production of Electricity during Wastewater Treatment Using a Single Chamber Microbial Fuel Cell. *Environmental Science & Technology*, 38(7):2281–2285.

[Logan, 2010] Logan, B. (2010). Scaling up microbial fuel cells and other bioelectrochemical systems. *Applied microbiology and biotechnology*, 85(6):1665–71.

[Logan et al., 2007] Logan, B., Cheng, S., Watson, V., and Estadt, G. (2007). Graphite Fiber Brush Anodes for Increased Power Production in Air-Cathode Microbial Fuel Cells. *Environmental Science & Technology*, 41(9):3341–3346.

[Logan et al., 2006] Logan, B., Hamelers, B., Rozendal, R., Schröder, U., Keller, J., Freguia, S., Aelterman, P., Verstraete, W., and Rabaey, K. (2006). Microbial fuel cells: methodology and technology. *Environ. Sci. Technol.*, 40:5181–5192.

[Logan, 2009] Logan, B. E. (2009). Exoelectrogenic bacteria that power microbial fuel cells. *Nature reviews. Microbiology*, 7(5):375–81.

[Lovley and Nevin, 2011] Lovley, D. R. and Nevin, K. P. (2011). A shift in the current: New applications and concepts for microbe-electrode electron exchange. *Current opinion in biotechnology*, 22(3):441–448.

[LTC, 2010] LTC (2010). "Ultralow voltage step-up converter and power manager," LTC3108 datasheet.

[LTC, 2011] LTC (2011). "400mA Step-Up DC/DC Converter with Maximum Power Point Control and 250mV Start-Up," LTC3105 datasheet.

[Lu et al., 2010] Lu, C., Raghunathan, V., and Roy, K. (2010). Maximum power point considerations in micro-scale solar energy harvesting systems. In *Circuits and Systems (ISCAS), Proceedings of 2010 IEEE International Symposium on*, number 1, pages 273–276. IEEE.

[Lyon et al., 2010] Lyon, D. Y., Buret, F., Vogel, T. M., and Monier, J.-M. (2010). Is resistance futile? Changing external resistance does not improve microbial fuel cell performance. *Bioelectrochemistry (Amsterdam, Netherlands)*, 78(1):2–7.

[Marian et al., 2011] Marian, V., Vollaire, C., Verdier, J., and Allard, B. (2011). An Alternative Energy Source for Low Power Autonomous Sensors. In *European Conference on Antennas and Propagation*, pages 405–409.

[Mateu et al., 2007] Mateu, L., Pollak, M., and Spies, P. (2007). Step-up converters for human body energy harvesting thermogenerators. *Technical Digest PowerMEMS*, pages 213–216.

[McKendry, 2002] McKendry, P. (2002). Energy production from biomass (Part 2): Conversion technologies. *Bioresource technology*, 83(1):47–54.

[Middaugh et al., 2006] Middaugh, J., Cheng, S., Liu, W., and Wagner, R. (2006). How to Make Cathodes with a Diffusion Layer for Single-Chamber Microbial Fuel Cells.

[Mishra et al., 2011] Mishra, B., Botteron, C., and Farine, P. a. (2011). A 120mV startup circuit based on charge pump for energy harvesting circuits. *IEICE Electronics Express*, 8(11):830–834.

[Monier et al., 2008] Monier, J.-M., Niard, L., Haddour, N., Allard, B., and Buret, F. (2008). Microbial Fuel Cells: From biomass (waste) to electricity. In *Proceedings of MELECON*, pages 663–668. IEEE.

[Moore and Schneider, 2001] Moore, S. and Schneider, P. (2001). A review of cell equalization methods for lithium ion and lithium polymer battery systems.

[Oh and Logan, 2007] Oh, S. and Logan, B. (2007). Voltage reversal during microbial fuel cell stack operation. *Journal of Power Sources*, 167(1):11–17.

[Oh et al., 2010] Oh, S. T., Kim, J. R., Premier, G. C., Lee, T. H., Kim, C., and Sloan, W. T. (2010). Sustainable wastewater treatment: how might microbial fuel cells contribute. *Biotechnology advances*, 28(6):871–81.

[Osman et al., 2011] Osman, M. H., Shah, a. a., and Walsh, F. C. (2011). Recent progress and continuing challenges in bio-fuel cells. Part I: Enzymatic cells. *Biosensors and Bioelectronics*, 26(7):3087–102.

[Pant et al., 2010] Pant, D., Van Bogaert, G., Diels, L., and Vanbroekhoven, K. (2010). A review of the substrates used in microbial fuel cells (MFCs) for sustainable energy production. *Bioresource technology*, 101(6):1533–43.

[Park and Ren, 2012] Park, J.-D. and Ren, Z. (2012). Hysteresis controller based maximum power point tracking energy harvesting system for microbial fuel cells. *Journal of Power Sources*, 205:151–156.

[Pascual, 1998] Pascual, C. (1998). "Switched capacitor system for automatic battery equalization," US Patent 5,710,504.

[Patil et al., 2010] Patil, S. a., Harnisch, F., Kapadnis, B., and Schröder, U. (2010). Electroactive mixed culture biofilms in microbial bioelectrochemical systems: The role of temperature for biofilm formation and performance. *Biosensors and Bioelectronics*.

[Philips Semiconductors, 2000] Philips Semiconductors (2000). "N-channel junction FET," BF862 datasheet.

[Pinto et al., 2011] Pinto, R. P., Srinivasan, B., Guiot, S. R., and Tartakovsky, B. (2011). The effect of real-time external resistance optimization on microbial fuel cell performance. *Water research*, 45(4):1571–8.

[Potter, 1911] Potter, M. C. (1911). Electrical Effects Accompanying the Decomposition of Organic Compounds. *Proceedings of the Royal Society of London. Series B, Containing Papers of a Biological Character*, 84(571):260–276.

[Qian et al., 2009] Qian, F., Baum, M., Gu, Q., and Morse, D. E. (2009). A 1.5 microL microbial fuel cell for on-chip bioelectricity generation. *Lab on a chip*, 9(21):3076–81.

[Rabaey et al., 2005] Rabaey, K., Clauwaert, P., Aelterman, P., and Verstraete, W. (2005). Tubular microbial fuel cells for efficient electricity generation. *Environmental science & technology*, 39(20):8077–82.

[Ramadass, 2009] Ramadass, Y. (2009). *Energy processing circuits for low-power applications*. PhD thesis, Massachusetts Institute of Technology.

[Ramadass and Chandrakasan, 2011] Ramadass, Y. K. and Chandrakasan, A. P. (2011). A Battery-Less Thermoelectric Energy Harvesting Interface Circuit With 35 mV Startup Voltage. *IEEE Journal of Solid-State Circuits*, 46(1):333–341.

[Ren et al., 2012] Ren, H., Lee, H.-S., and Chae, J. (2012). Miniaturizing microbial fuel cells for potential portable power sources: promises and challenges. *Microfluidics and Nanofluidics*, 13(3):353–381.

[Richelli et al.,] Richelli, A., Colalongo, L., Tonoli, S., and Kovács-vajna, Z. M. A 0.2V-1.2V converter for power harvesting applications. *IEEE Transactions on Power Electronics*, 24(6):1541–1546.

[Rismani-Yazdi et al., 2011] Rismani-Yazdi, H., Christy, A. D., Carver, S. M., Yu, Z., Dehority, B. a., and Tuovinen, O. H. (2011). Effect of external resistance on bacterial diversity and metabolism in cellulose-fed microbial fuel cells. *Bioresource technology*, 102(1):278–83.

[Roundy et al., 2004] Roundy, S., Steingart, D., Frechette, L., Wright, P., and J (2004). Power sources for wireless sensor networks. *Sensor Networks*, 2920:1–17.

[Rozendal et al., 2007] Rozendal, R. a., Hamelers, H. V. M., Molenkamp, R. J., and Buisman, C. J. N. (2007). Performance of single chamber biocatalyzed electrolysis with different types of ion exchange membranes. *Water research*, 41(9):1984–94.

[Sakai et al., 2009] Sakai, H., Nakagawa, T., Tokita, Y., Hatazawa, T., Ikeda, T., Tsujimura, S., and Kano, K. (2009). A high-power glucose/oxygen biofuel cell operating under quiescent conditions. *Energy & Environmental Science*, 2(1):133.

[Seeman, 2008] Seeman, M. (2008). Analysis and Optimization of Switched-Capacitor DC-DC converters. *Power Electronics, IEEE*, 23(2):841–851.

[Seiko, 2010] Seiko (2010). "Ultra-low voltage operation charge pump for step-up DC-DC converter startup," S-882Z Series datasheet.

[Shichman and Hodges, 1968] Shichman, H. and Hodges, D. (1968). Modeling and simulation of insulated-gate field-effect transistor switching circuits. *IEEE Journal of Solid-State Circuits*, 3(3):285–289.

[Shimizu et al., 2001] Shimizu, T., Hirakata, M., Kamezawa, T., and Watanabe, H. (2001). Generation control circuit for photovoltaic modules. *IEEE Transactions on Power Electronics*, 16(3):293–300.

[Sievers et al., 2010] Sievers, M., Schläfer, O., Bormann, H., Niedermeiser, M., Bahnemann, D., and Diller, R. (2010). Machbarkeitsstudie für die Anwendung einer mikrobiellen Brennstoffzelle im Abwasser- und Abfallbereich. *cutec.de*, 49(0):0–18.

[Siu and Chiao, 2008] Siu, C.-P.-B. and Chiao, M. (2008). A Microfabricated PDMS Microbial Fuel Cell. *Microelectromechanical Systems*, 17(6):1329–1341.

[Spies et al., 2007] Spies, P., Pollak, M., and Rohmer, G. (2007). Energy harvesting for mobile communication devices. In *Proceedings of INTELEC*, pages 481–488. IEEE.

[ST, 2011] ST (2011). "High efficiency solar battery charger with embedded MPPT", SPV1040 Datasheet.

[Stuart and Zhu, 2011] Stuart, T. A. and Zhu, W. (2011). Modularized battery management for large lithium ion cells. *Journal of Power Sources*, 196(1):458–464.

[Tartakovsky et al., 2011] Tartakovsky, B., Mehta, P., Santoyo, G., and Guiot, S. (2011). Maximizing hydrogen production in a microbial electrolysis cell by real-time optimization of applied voltage. *International Journal of Hydrogen Energy*, 36(17):10557–10564.

[Tewolde, 2010] Tewolde, G. (2010). Current trends in low-power embedded computing. In *Electro/Information Technology (EIT), 2010 IEEE International Conference on*, pages 1–6. IEEE.

[Thauer and Jungermann, 1977] Thauer, R. and Jungermann, K. (1977). Energy Conservation in Chemotrophic Anaerobic bacteria. *Bacteriological reviews*.

[The Nielsen Company, 2009] The Nielsen Company (2009). iPhone users watch more video... and are older than you think.

[TI, 2008] TI (2008). "LOW INPUT VOLTAGE SYNCHRONOUS BOOST CONVERTER WITH 1.3-A SWITCHES," TPS61200 datasheet.

[TI, 2011a] TI (2011a). "Low-cost, low-power 2.4GHz RF tranceiver", CC2500 datasheet.

[TI, 2011b] TI (2011b). "Ultra Low Power Boost Converter with Battery Management for Energy Harvester Applications," bq25504 datasheet.

[Torki (CMP), 2012] Torki (CMP), K. (2012). "Rép : Informations CMOS65 et CMOS40" E-mail communication - the 3rd of May 2012.

[Vighetti, 2010] Vighetti, S. (2010). *Systèmes photovoltaïques raccordés au réseau : Choix et dimensionnement des étages de conversion*. PhD thesis, Université de Grenoble.

[Vighetti et al., 2010] Vighetti, S., Lembeye, Y., Ferrieux, J., and Barbaroux, J. (2010). PHOTOVOLTAIC MODULE AND SHADOW: STUDY AND INTEGRATION OF A CURRENT BALANCING SYSTEM. In *Proceedings of EUPVSEC*, pages 4139 – 4143.

[Wei et al., 2011] Wei, J., Liang, P., and Huang, X. (2011). Recent progress in electrodes for microbial fuel cells. *Bioresource technology*, 102(20):9335–9344.

[Wikipedia, 2012] Wikipedia (2012). Bacteria.

[Win et al., 2011] Win, K., Dasgupta, S., and Panda, S. (2011). An optimized MPPT circuit for thermoelectric energy harvester for low power applications. In *Proceedings of ECCE Asia*, pages 1579–1584. IEEE.

[Winfield et al., 2012] Winfield, J., Ieropoulos, I., and Greenman, J. (2012). Investigating a cascade of seven hydraulically connected microbial fuel cells. *Bioresource technology*, 110:245–50.

[Woodward et al., 2010] Woodward, L., Perrier, M., Srinivasan, B., Pinto, R., and Tartakovsky, B. (2010). Comparison of Real-Time Methods for Maximizing Power Output in Microbial Fuel Cells. *AIChE Journal*, 56(10):2742–2750.

[Woodward et al., 2009] Woodward, L., Tartakovsky, B., Perrier, M., and Srinivasan, B. (2009). Maximizing power production in a stack of microbial fuel cells using multiunit optimization method. *Biotechnology Progress*, 25(3):676–682.

[Yu and Yue, 2011] Yu, H. and Yue, Q. (2011). Power management and energy harvesting for indoor photovoltaic cells system. *Mechanic Automation and Control*, pages 521–524.

[Zhang et al., 2011] Zhang, L., Zhu, X., Li, J., Liao, Q., and Ye, D. (2011). Biofilm formation and electricity generation of a microbial fuel cell started up under different external resistances. *Journal of Power Sources*, 196(15):6029–6035.

[Zhao et al., 2009] Zhao, F., Slade, R. C. T., and Varcoe, J. R. (2009). Techniques for the study and development of microbial fuel cells: an electrochemical perspective. *Chemical Society reviews*, 38(7):1926–39.

[Zhong et al., 2008] Zhong, Z., Huo, H., Zhu, X., Cao, G., and Ren, Y. (2008). Adaptive maximum power point tracking control of fuel cell power plants. *Journal of Power Sources*, 176(1):259–269.

[Zhuang and Zhou, 2009] Zhuang, L. and Zhou, S. (2009). Substrate cross-conduction effect on the performance of serially connected microbial fuel. *Electrochemistry Communications*, 11:937–940.